Structural and Thermal Controls on the Formation of the Hishikari Epithermal Gold Deposit, Japan

ギヨーム ドゥドゥ ファイ

Structural and Thermal Controls on the Formation of the Hishikari Epithermal Gold Deposit, Japan

By

Guillaume Doudou Faye

A thesis submitted in partial fulfillment of the requirements
for the degree of

Doctor of Engineering

Examination committee
Prof. Koichiro Watanabe
Prof. Akira Imai
Prof. Kazuya Idemitsu
Assoc. Prof. Kotaro Yonezu

Economic Geology Laboratory
Department of Earth Resources Engineering
Graduate School of Engineering
Kyushu University

July 2018

Abstract

Epithermal deposits form at shallow depths as a result of hydrothermal activity, which involves fluid circulation through fractures, powered by a heat anomaly. This makes the fluid paths a key factor in the formation process of this type of ore deposit. The heat source is the driving force of the system and in some cases, its emplacement creates the fractures that become fluid paths. Thus, it is also an important part of the system. Therefore, for a better understanding of the mineralization at the Hishikari deposit, it is important not only to investigate the paleostress and fluid pressure regimes, but also to study the actual effect of the basement uplift on the occurrence of the fractures hosting the veins. The latter requires to constrain the position, temperature, shape and overpressure of the heat source. In this thesis, I unravel the structural controls of the Hishikari low sulfidation epithermal deposit and I put constraints on the heat source of its mineralizing hydrothermal system.

Firstly, Chapter 1 introduces the deposit geology and provides all the background information on stress inversion and the methods used for the paleostress analysis. Hishikari is part of the Hokusatsu gold district, located in southern Kyushu (Japan) where previous research revealed that veins could be hosted in both conjugate faults (e.g. Kushikino) and tensile fractures (e.g. Hashima). In Hishikari, the presence

of ENE-WSW to NW-SE-trending normal faults were recognized in previous studies. Moreover, in the northern part of the Honko sub-deposit, fault gauge, pull-apart structures and drag folds were reported and the conclusion was further made that the local basement uplift was responsible for the formation of the veins. However, the reported structures placed only a weak constraint on the paleostress conditions as assumptions and particular situations were needed to explain their occurrence by normal faulting. On the other hand, horizontal strain rate calculation suggested that regional extensional movements in southern Kyushu were responsible for the mineralization at Hishikari; but the study did not further constrain the stress tensor. A question arises as to whether the veins at Hishikari resulted from local or regional movements and left hanging the topic of the paleostress conditions that prevailed during the mineralization. Moreover, the orientations of the veins show spatial variations between the Honko-Sanjin sub-deposit (N50°E-70°NW to 90°) and the Yamada sub-deposit (N50°E-70°NW to 90° and N30°E-80°NW to 90°). Furthermore, structural differences (strike, dip, and width) between early and late veins might suggested a temporal variation of the stress conditions. Thus, spatio-temporal variations of the paleostress conditions under which the Hishikari deposit formed are to be expected. The software GArcmB, implementing the method of Yamaji (2016) for fitting orientation data to a mixed

Bingham distribution is used in this study. The principles of stress inversion in general and of this technique in particular are also detailed in Chapter 1.

In Chapter 2, the results of the paleostress analysis of the Hishikari deposit are presented. Vein orientations (strike and dip) were collected at the Hishikari mine, along with their respective widths and gold grades. The results reveal that 98% of the veins at Hishikari were formed under extensional stress with a NW-SE-trending horizontal σ3-axis and a northeasterly-inclined σ1-axis with a relatively high stress ratio. The high stress ratio explains the ease of rotation of the σ1- and σ2-axes, leading to a mean stress regime intermediate between normal faulting and strike-slip faulting. This stress condition is consistent with the regional stress field that was present in southern Kyushu at the time of the mineralization, suggesting that regional tectonics controlled the deposition of almost all the veins in Hishikari. The remaining veins were formed under an axial compression stress condition that could be related to local perturbations.

Chapter 3 details the fluid pressure regimes in the Hishikari deposit during mineralization. The Driving Pressure Index (DPI) is defined as the 95 percentile point of normal stresses on the wall of the fracture. It is considered as the representative driving pressure ratio *p*. The calculation of *p* during the formation of the veins gives a result of ~0.2. Moreover, *p* is determined at various depths in the mine and its variation

with depth studied. Whereas it is demonstrated that *p* has a negative correlation with depth in hydrostatic pressure conditions regardless of the stress regime, a positive correlation between *p* and depth is found at Hishikari. This suggests that pressure compartmentalization occurred in Hishikari, with pressure compartments bound by pressure seals that were repeatedly broken and re-created. Moreover, the driving pressure ratio is higher in the Honko-Sanjin sub-deposits (0.24) than in the Yamada sub-deposit (0.19). This could be explained by a higher fluid pressure in the Honko-Sanjin sub-deposits, which is consistent with the fact that the main fluid conduit is located in Sanjin, suggested by previous research. Finally, it is found that in the Yamada sub-deposit, the veins having a gold grade higher than 100 g/t have higher driving pressure ratios (0.24) than the rest of the veins (0.19). This indicates that higher driving pressure was associated with higher gold grades during the mineralization at Hishikari, and that fluid pressure controlled gold grade.

In Chapter 4, physical and geometric constraints are put on the heat source of the Hishikari mineralizing hydrothermal system, by means of 1D steady-state heat conduction modeling. I use stratigraphic columns made from drillholes (outside the mine) and cross sections (inside the mine) taken from a geothermal research report by NEDO (1991). The depth of the heat source is varied between 2 km and 10 km with a

step of 1 km and the temperature of the heat source is varied between 250 °C and 1200°C with a step of 50 °C. Hence, 180 models are run for each stratigraphic column. The temperature is calculated along the stratigraphic column every 10 m using the software OpenGeoSys (OGS). The calculated temperatures are then compared to the fluid inclusion homogenization temperatures by the calculation of the root mean square error (RMSe) of each model, the best fit model being the one with the lowest RMSe. This gives the depth and the temperature of the heat source. Using the depth and rock densities, the lithostatic pressure (P_l) is calculated. On the other hand, the total pressure (P_t) is obtained using the temperature and Al-in hornblende geobarometer. The subtraction of P_l from P_t gives the overpressure in the magma chamber. From a discussion involving the Mogi spherical point source model, the tectonic regime and the absence of ring fault, the shape of the magma chamber is inferred. The depth of the Shishimano Dacite magma chamber, considered as the heat source, is estimated at ~9 km. The magma had a temperature of ~1075-1200°C at the onset of the mineralization, and seems to have cooled down to a temperature of ~300-500°C after the mineralization. The estimated excess pressure within the magma chamber is ~ 6.5 MPa and the shape of the magma chamber is likely prolate ellipsoidal.

Chapter 5 provides an overall discussion of my results that summarizes my

contribution to the understanding of the mineralization in Hishikari, as well as the remaining challenges. The potential contribution of the basement uplift to the mineralization is addressed and the hypotheses include the weakening of host rocks, the creation of faults, and the apparition of 5% of the veins in the Yamada sub-deposit. The other point of discussion is related to the possible causes of pressure sealing and the hypotheses include the self-sealing by the precipitation of the vein-forming minerals, sealing by the clay-rich alteration halo and capillary sealing by the gases released during boiling process.

Finally, in Chapter 6, I give a recapitulation of the main conclusions of my study.

Acknowledgements

This thesis came to completion thanks to the support of the people and institutions that were involved in my project and in my life.

My sincere gratitude goes to:

Prof. Koichiro WATANABE, for accepting me under his supervision, guiding me in my work, and for his constant support and his flexibility. Thank you also for all the advices provided on academic and non-academic matters;

Prof. Atsushi YAMAJI, for accepting to supervise the part of my work related to paleostress analysis and for teaching me a whole new world about structural geology;

Prof. Akira IMAI, for his availability and useful advices that significantly improved the second part of my study. Thank you also for being part of my examination committee;

Prof. Kazuya IDEMITSU, for having accepted to critically review my thesis and be part of my examination committee;

Associate Prof. Kotaro YONEZU, for his scientific advices and discussions as well as his support in all the aspects of my PhD. Thank you for being part of my thesis committee;

Assistant Prof. Thomas TINDELL, for being always ready to discuss and answer to questions related to my research. Thank you also for critically reviewing all my manuscripts;

Prof. Takeshi TSUJI, thank you for the useful discussions about my research project and interests and for having been very supportive despite your busy schedule.

My study was supported by a scholarship from MEXT, to which I am greatly indebted.

Special thanks go to Sumitomo Metal Mining Co. Ltd, for allowing me the access to the Hishikari mine site and to their data. I thank all the geologists who helped me in my data collection.

The Kyushu University Foundation (Kyudai Kikin) and the Geological Society of Australia are highly appreciated for providing me with conference funding.

To all the members of the Economic Geology Laboratory (those who already graduated and those who are still here), thank you for your comradeship and your cooperation.

To the Staff of the School of Engineering and that of the Department of Earth Resources Engineering, thank you for making my life as an international student a lot easier.

To all my friends, mentors, former teachers and supervisors, your encouragements and suggestions have helped me a great deal during this journey. Thank you!

At last, this achievement is dedicated to my family. No word is strong enough to tell you how grateful I am to have you. Your undying love, support, encouragements and prayers kept me going. Diokandial a paax!

Table of Contents

List of figures

List of Tables

1. Introduction

1.1 Background

The discovery of a world-class gold deposit, 60% of the reserves of which are hosted by the Shimanto Supergroup sedimentary rocks that were previously considered as barren (Izawa et al., 1990), together with the coherent trend of the veins not only in Hishikari but in all the epithermal deposits of the Hokusatsu gold province, strongly suggest a structural control on the mineralization. In southern Kyushu, Matsutoya (1967) assumed that conjugate faults and tensile fractures hosted the veins, and suggested a wide range of σ_{Hmin} orientations. A fault-slip analysis near the Yamagano Mine (Fig. 1-1) suggested the rotation of σ_1- and σ_3- axes of the strike-slip regime by ~90° at ~2 Ma (Hikichi and Yamaji, 2008). Morishita and Kodama (1986) performed structural simulations by means of finite element modeling to find that differential vertical movement of basement blocks created conjugate faults hosting the veins in the Kushikino deposit (Fig. 1-1). These experiments were revisited by Morishita and Nakano (2008) who concluded that the same phenomenon explains fracturing in the Hishikari deposit. Other elements strongly support the hypothesis of a structural control on the mineralization at Hishikari. Abe et al. (1986) described ENE-WSW to NW-SE-trending normal faults in the Hishikari area. Naito (1993) reported the presence of fault

gauge, pull-apart structures as well as drag folds in the northern part of the Honko sub-deposit. This led to the conclusion that the fractures in the Hishikari deposit were formed as a result of continuous uplift of the basement before, during and after the mineralization stage, causing a continuous opening of the fissures under a tensional stress field. However, the reported structures place only a weak constraint on the paleostress conditions as assumptions and particular situations were needed for normal faulting to explain their occurrence. On the other hand, horizontal strain rate calculation suggested that regional extensional movements in southern Kyushu are responsible for the mineralization at Hishikari (Uto et al., 2001); but the study did not further constrain the stress tensor. A question arose as to whether veins at Hishikari resulted from local or regional movements and left hanging the topic of the paleostress conditions that prevailed during the mineralization. Moreover, structural differences (strike, dip, and width) between early and late veins (Sekine et al., 2002) might suggest a temporal variation of the stress conditions in Hishikari deposit during mineralization. Also, the orientations of the veins show spatial variations between the Honko-Sanjin sub-deposit (N50°E - 70°NW to 90°) and the Yamada sub-deposit (N50°E - 70°NW to 90° and N30°E - 80°NW to 90°) (Ibaraki and Suzuki, 1993). Thus, spatio-temporal variations of the paleostress conditions under which the Hishikari deposit formed should be

expected. However, the scarcity of tectonic structures (due to the subsequent deposition of pyroclastic rocks covering up the Plio-Pleistocene rocks that contain evidence for paleostresses) as well as the generally coherent trend of the veins make it difficult to separate the potential different paleostress states and determine their characteristics. To overcome this difficulty, a stress inversion method may be utilized. Yamaji et al. (2010) successfully used this technique to determine paleostress conditions of Plio-Pleistocene epithermal gold and silver-mineralized veins of Hashima located in the same gold district in southern Kyushu as the Hishikari deposit (Fig. 1-1).

$^{40}Ar/^{39}Ar$ ages of adularia contained in successive growth bands of the Hosen-1 vein established that the shortest duration for an increment of vein formation is 30,000 years whereas the longest time interval is 110,000 years, thus demonstrating that vein formation occurred episodically at different intervals rather than at a constant rate (Sanematsu et al., 2006). This also emphasizes episodic fracturing and ascent of fluids for the formation of the veins, giving a primary importance to the fluid pressure regimes in the mineralization process.

Therefore, for a better understanding of the mineralization at the Hishikari deposit, it is important not only to investigate the paleostress and fluid pressure regimes, but also to study the actual effect of the basement uplift on the occurrence of the fractures

hosting the veins. The latter requires to constrain the position, temperature, shape and overpressure of the magma chamber related to the Shishimano Dacite, considered as responsible for the basement uplift.

In this thesis, I address the above questions. It is organized as follows:

- Chapter 1 is an introduction to the deposit geology and provides all the background information on stress inversion and the methods used for the paleostress analysis.
- Chapter 2 describes the results of the paleostress analysis and discusses their implications at a local (deposit) level and regional level.
- Chapter 3 details the method used to calculate the driving pressure ratio and discusses the fluid pressure regimes in Hishikari.
- Chapter 4 presents the thermal modeling carried out in order to estimate the depth, temperature and shape of the heat source and further discusses their implications in terms of magma chamber overpressure as well as its cooling history.
- Chapter 5 provides an overall discussion of my results that summarizes my contribution to the understanding of the mineralization in Hishikari, as well as the remaining challenges.
- Finally, in Chapter 6, I recapitulate the main conclusions of this study.

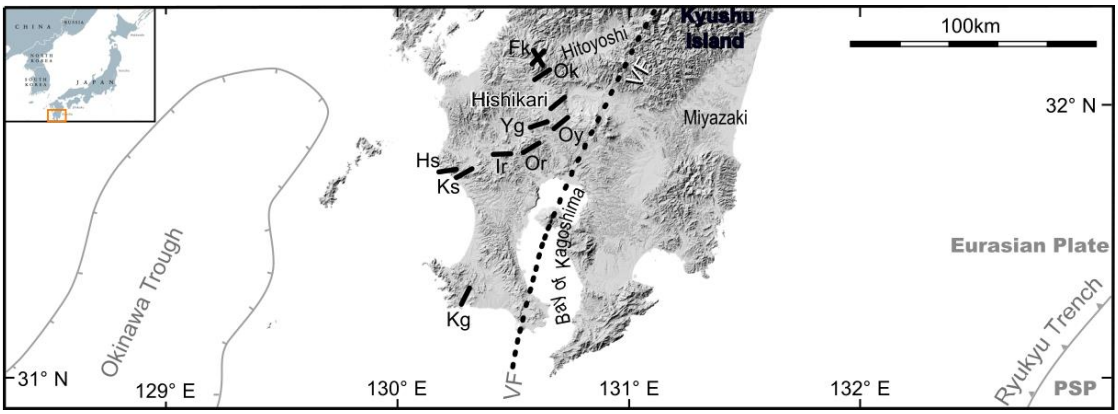

Fig. 1-1 Trends of representative ore veins (represented by bars) formed during the Plio-Pleistocene ore in southern Kyushu, Japan (Urashima et al., 1981; Izawa, 2004). Fk = Fuke Mine, Hs = Hashima Mine, Ir = Iriki Mine, Kg = Kago Mine, Ks = Kushikino Mine, Ok = Ohkuchi Mine, Or = Ohra Mine, Oy = Ohnoyama Mine, Yg = Yamagano Mine; PSP = Philippine Sea Plate; VF = Present volcanic front.

1.2 Tectonic setting of southern Kyushu

The subduction of the Philippine Sea Plate (PSP) beneath the Eurasian Plate and its directional changes and related volcanism over geological time paced the structural history of southern Kyushu (Fig. 1-2). During the Oligocene, the PSP subduction under Southwest Japan-Ryukyu Arcs was initiated (Honza and Fujioka, 2004). During the Early Pliocene, a change of the subduction direction from westward to north-northwestward is suggested (Watanabe, 2005). This change shifted the Kyushu-Palau Ridge northward, resulting in the underplating of the slab of Amami Basin at the place of the slab of Shikoku Basin beneath southern Kyushu (Yamaji, 2003). The slab of Amami Basin is old (85-60 Ma) and negatively buoyant whereas the slab of Shikoku Basin is young (27-15 Ma) and buoyant (Yamaji, 2003). As a result, the slab of Amami Basin sank during a process known as slab rollback (Yamaji, 2003). This slab rollback induced the trenchward migration of the volcanic front of southern Kyushu described by Izawa and Watanabe (2001) and the formation of the Kagoshima Graben (Watanabe, 2005). The area overlying the old slab of Amami Basin was subjected to extensional tectonics beneath southern Kyushu until 2 to 1 Ma; this resulted in rifting along the Kagoshima Graben (Watanabe, 2005). The volcanism coinciding with the rifting in the

back-arc was associated with widespread low-sulfidation epithermal mineralization in southern Kyushu, including the Hishikari deposit (Watanabe, 2005).

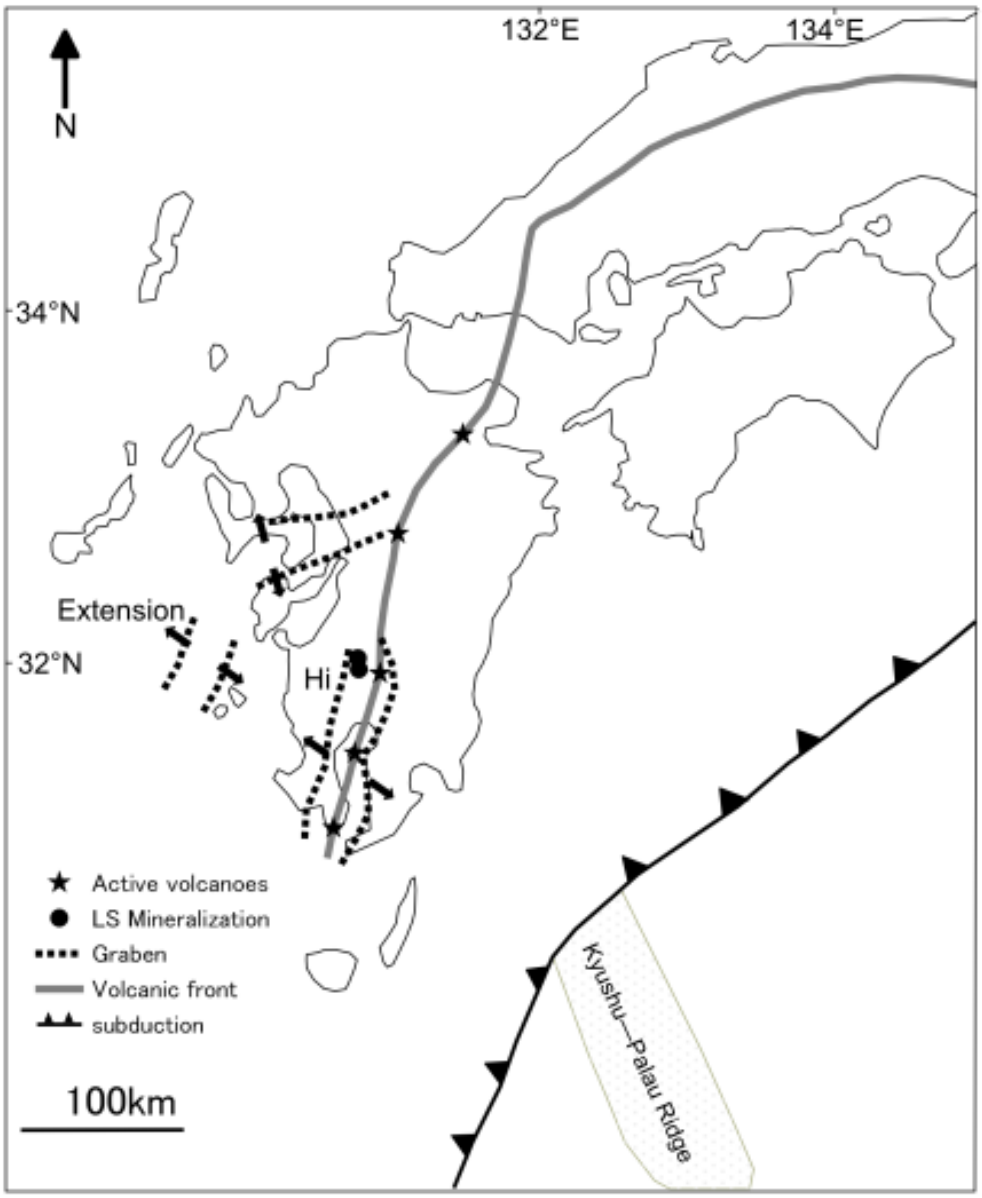

Fig. 1-2 Tectonic setting of southern Kyushu at 1 Ma (Watanabe, 2005); and locations of Hishikari (mineralization at 1.25-0.6 Ma) (Izawa et al., 1990; Sanematsu et al., 2006; Tohma et al., 2010) and Ohnoyama (mineralization at 0.55 Ma) (MITI, 2001). LS = Low Sulfidation.

1.3 Geology and mineralization

The Hishikari deposit is hosted by the Cretaceous Shimanto Supergroup and the Quaternary Hishikari Lower Andesites (Fig. 1-3). The Shimanto Supergroup is comprised of shale, sandstone as well as their alternations; tuffaceous shale and chert are also noticed in minor proportions (Izawa et al., 1990). The Hishikari Lower Andesites consist of augite-hyperstene andesite lava flows and andesitic pyroclastic rocks in the lower part of which thin intercalations of lava flows can be found; lacustrine sediments may be present locally (Izawa et al., 1990). The Hishikari Lower Andesites unconformably overlie the Shimanto Supergroup (Fig.1-3b).

Widths of major veins are 1-3 m in Honko-Sanjin and 2-5 m in Yamada (Uto et al., 2001). Horizontal lengths over 400 m are common with a maximum of about 1,100 m; branching, pinches and swells can be observed (Uto et al., 2001).

The ore mineral assemblage is made of pyrite, marcasite, chalcopyrite, argentite, electrum, naumannite-aguilarite (Izawa et al., 1990). Usually, gold appears in dark, sulfide-rich, electrum bands (ginguro containing 60 to 80% of gold according to Izawa et al. (1990) and Ibaraki and Suzuki (1993)) most frequently found in the outer early bands of monoaxial veins (Nagayama, 1993). Gangue minerals are dominantly quartz and adularia and less commonly truscottite, calcite, vermiculite and smectite. However,

the initial precipitated amount of calcite could be higher than observed presently (Imai and Uto, 2002). A precipitation sequence referred to as normal order and essentially consisting of adularia, adularia/quartz, quartz and/or smectite from the margin to the center of the vein is characteristic of the deposit (Nagayama, 1993).

K/Ar and $^{40}Ar/^{39}Ar$ age dating of the adularia-quartz veins of the Hishikari deposit shows that mineralization in the Hishikari area began at 1.25 Ma and lasted about 0.6 Ma, ending at 0.606 ± 0.009 Ma (Izawa et al., 1993a; Tohma et al., 2010). Two categories of veins (early and late) occur in the Hishikari deposit (Sekine et al., 2002). Age dating in the Honko-Sanjin sub-deposit assigned ages ranging from 1.11 to 0.86 Ma to early veins and 0.84 to 0.73 Ma to late veins (Sekine et al., 2002). Moreover, it was demonstrated that mineralization duration was longer in Yamada sub-deposit than in Honko-Sanjin sub-deposits (Sanematsu et al., 2006). Fukusen-1 vein ($^{40}Ar/^{39}Ar$ ages between 0.617 ±0.024 Ma and 0.606 ± 0.009 Ma) is one of the youngest veins of the Hishikari deposit (Tohma et al., 2010).

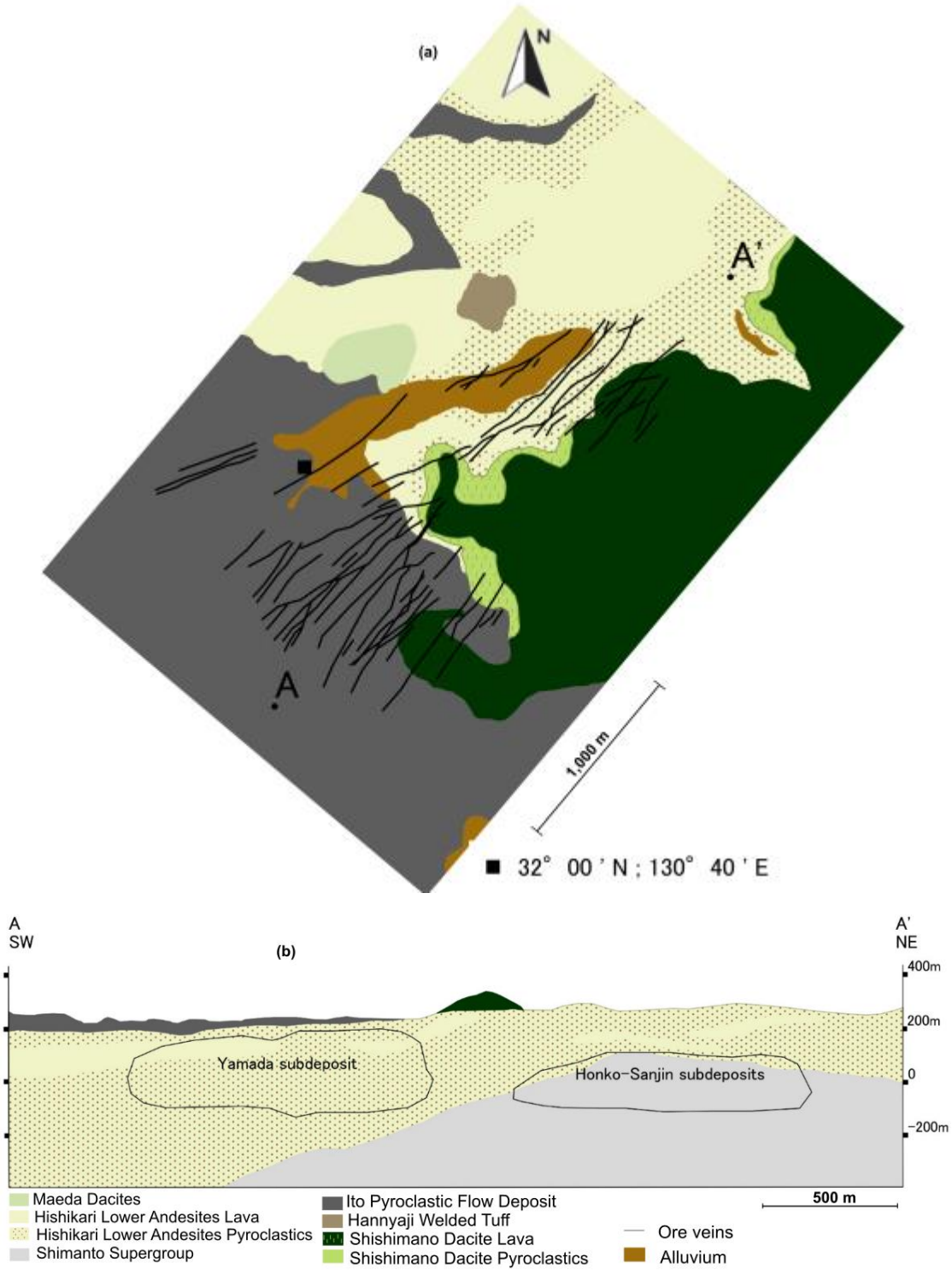

Fig. 1-3 (a) Geologic map of Hishikari deposit and its surroundings; (b) Cross-section A-A' from (a) (after Ibaraki and Suzuki, 1993).

1.4 Method

1.4.1 Stress inversion theoretical background

Stress is a second order tensor defined by a matrix that has six degrees of freedom: the directions of the three principal stress axes σ_1, σ_2 and σ_3 (eigenvectors) and the magnitudes of the three principal stress components (eigenvalues). If the aspect ratio of the principal stress magnitudes or stress ratio

$$\Phi = \frac{\sigma_2 - \sigma_3}{\sigma_1 - \sigma_3} \quad ,$$

is considered, it reduces the three last parameters to one. This stress ratio forms, together with the three principal stress axes orientations, the reduced stress tensor. Calculating the stress tensor responsible for observed structures is known as stress inversion (Carey and Brunier, 1974). In the case of fault-slip data, it consists of finding among all the stress tensors possibly responsible for the measured structures the one that minimizes the misfit angle between the maximum resolved shear stress and the slickenline vector, assuming after Wallace (1951) and Bott (1959) that the slip direction is parallel to the maximum resolved shear stress. Different approaches have been proposed to solve the inverse problem (Angelier, 1979, 1984; Armijo et al., 1982). The multiple inverse method, proposed by Yamaji (2000), was further improved by Sato and Yamaji (2006) and Otsubo and Yamaji (2006).

In the case of fractures caused by overpressured fluids (hydraulic fracturing) usually leading to the formation of veins or dykes, it is also possible to apply stress inversion. Here, the basic assumption is that a fracture opens when the fluid pressure exceeds the normal pressure on the walls of the fracture ($P_f > \sigma_n$) (Delaney et al., 1986). Baer et al. (1994) proposed an approach for the determination of paleostress axes orientations and stress ratio as well as the normalized driving pressure

$$R = \frac{P_m - \sigma_3}{\sigma_1 - \sigma_3}$$

(where P_m = magma pressure) in dykes resulting from dilation of prior cracks and applied it with good results to dykes in Timna, Israel. The technique is rooted in the fact that a dyke intruding a uniform rock creates a fracture perpendicular to the least compressive stress (Anderson, 1942) with the difference that it was considered not only for a single fracture but also for arrays of subparallel as well as randomly oriented cracks (Pollard et al., 1975; Baer and Beyth, 1990; Baer, 1991). The two latter configurations are more realistic. Jolly and Sanderson (1997) proposed a Mohr circle construction where the possibility of fracture opening is subject to the condition

$$R = \frac{P_f - \sigma_m}{\tau_{max}} \geq \cos 2\theta \ ,$$

R being termed driving stress ratio (Delaney et al., 1986); ($\sigma_m =$ mean stress and $\tau_{max} =$ maximum shear stress). The direction of opening could also be determined following the relationship:

$$\tan \mu = \frac{\tau}{P_f - \sigma_n} = \frac{\sin 2\theta}{R - \cos 2\theta}$$

(Delaney et al., 1986). If the ranges of θ angles utilized by the fractures are known, it is possible to retrieve the stress ratio, the driving pressure as well as principal stress axes orientations based on the construction and the following relationships:

$$\text{for } P_f < \sigma_2, \ \Phi = \frac{1+\cos 2\theta_2}{1+\cos 2\theta_1} \ ;$$

$$\text{for } P_f > \sigma_2, \ \Phi = \frac{1-\cos 2\theta_2}{1-\cos 2\theta_3} \ .$$

The driving pressure is given by

$$R' = \frac{1 + \cos 2\theta_2}{2}$$

(Jolly and Sanderson, 1997). Yamaji et al. (2010), Yamaji and Sato (2011) and Yamaji (2016) proposed a stochastic model for the fuzzy clustering and paleostress analysis of vein or dyke orientations data by fitting them to a mixed Bingham distribution. Four assumptions are made: 1) The state of far field stress did not change during the formation of the cluster (Yamaji et al., 2010) ; 2) The isotropy of the host rocks so that the vein orientations can inherit the orthorhombic symmetry from the stress (Baer et al., 1994); 3) Veins were formed in fractures only under the condition that the mineralizing

fluid pressure was greater than the normal stresses acting on the fractures (Fig. 1-4) (Delaney et al., 1986); 4) The cluster formation resulted from multiple events of thermal fluid ascent having various fluid pressures (Sekine et al., 2002; Sanematsu et al., 2006).

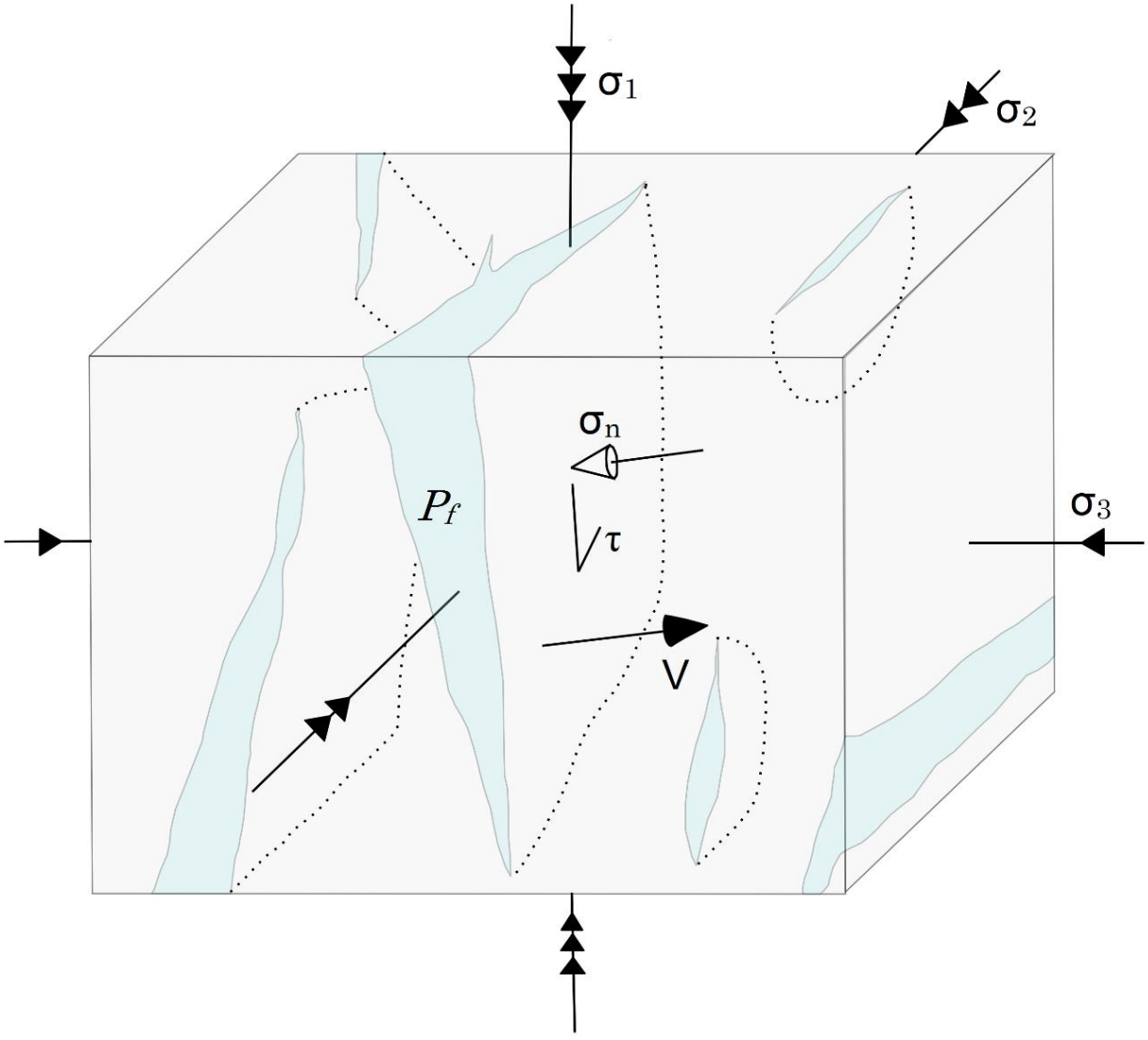

Fig. 1-4 Stress state around a dilatant fracture with fluid circulating inside (from Sato et al., 2013). The condition for vein formation is $Pf > \sigma_n$ (Delaney et al., 1986).

1.4.2 GArcmB

GArcmB is a computer program for fitting a mixed Bingham distribution to 3D orientation data (Yamaji, 2016). It is a genetic algorithm, meaning that it is grounded on the mechanics of biological evolution (Goldberg, 1989). Each mixed Bingham distribution *X*, expressed by a 5-dimensional vector, is considered as an individual with its fitness represented by the logarithmic likelihood function $L(X)$ (Yamaji, 2016). The laws of biological evolution apply to them and the population is maintained constant and improved iteratively (Yamaji, 2016). The algorithm calculates the membership of each datum to each of the clusters or the responsibility of each cluster for each datum by the means of the probability density function of the mixed Bingham distribution

$$m_n^k = \frac{P_B(v_n|x^k)}{\sum_{k=1}^{K} P_B(v_n|x^k)}$$

(where *v* is the unit vector representing an orientation, *x* the vector representing a single component or Bingham distribution, P_B the probability density of a Bingham distribution, and *K* the number of clusters) (Yamaji and Sato, 2011). The data are fitted to a mixed Bingham distribution by maximizing the logarithmic likelihood function

$$L(X) = \sum_{n=1}^{N} Log_e\ P_{mB}(v_n|X)$$

of the probability density

$$P_{mB}(v|\theta,\varpi) = \sum_{k=1}^{K} \varpi^k P_B(v|x^k)$$

of the mixed Bingham distribution with

$$P_B(v|K,E) = \frac{1}{A} exp(v^T E^T K E v) \quad ,$$

where *N* represents the number of data points, ϖ^k is the mixing coefficient of the *k*th Bingham component, θ the set of *K* vectors representing Bingham distributions, E the orthogonal matrix representing the symmetry axes of a Bingham distribution, and T a matrix transpose (Yamaji et al., 2010; Yamaji, 2016).

The partition *K* that optimally fits the data is chosen by finding the minimum of the Bayesian Information Criterion (*BIC*);

$$BIC = -2L\left(\hat{\theta},\hat{\varpi}\right) + (6K-1)log_e N$$

where $\hat{\theta}$ and $\hat{\varpi}$ are the optimal versions of are θ and ϖ (set of *K* mixing coefficients) (Bishop, 2006).

The termination condition of the genetic algorithm is either the reach of a chosen maximum number of iterations (100,000) or convergence which means that if a certain number of generations Δ_g passes without the $L(X)_{max}$ being updated, the computation stops. The condition for the algorithm to reach convergence is

$$g = g' + K\Delta_g \quad ,$$

Δ_g can be 100 or 1000, its value is changing according to the level of complexity of the dataset to be clustered; g' being the last generation for which $L(X)_{max}$ was updated and g the current generation (Yamaji, 2016).

The algorithm is run several times for each value of *K* between 1 and 5 to find the global maximum of *L*. Afterwards, the *BIC*s of the 5 runs representing global maxima are compared and the optimal *K* value is the one with the lowest *BIC* (Yamaji, 2016). The method gives, for each cluster:

- the principal stress axes orientations σ_1 , σ_2 and σ_3 that correspond respectively to the concentration axes of the poles to vein orientations e_1 , e_2 and e_3;
- the stress ratio that is approximated by the concentration parameters ratio

$$\boldsymbol{\kappa_2}/\boldsymbol{\kappa_1} \ ,$$

where the absolute values of $\boldsymbol{\kappa_1}$ and $\boldsymbol{\kappa_2}$ indicate the concentration of data points from e_3 to e_1 and from e_3 to e_2 respectively on a sphere, $0 \geq \boldsymbol{\kappa_2} \geq \boldsymbol{\kappa_1}$ (Fig. 1-5) (Yamaji et al., 2010);

Error analysis allows for the calculation of the 95% confidence ellipses for each cluster following

$$a_{ij}^k = \frac{2.45}{2\left|\left(K_i^k - K_j^k\right)\left(\tau_i^k - \tau_j^k\right)\right|}$$ (Tanaka, 1999);

where K_i^k is the *i*th concentration parameter of the of the *k*th cluster, τ_i^k the *i*th eigenvalue of the *k*th cluster, and a_{ij}^k the semi-axis of the *i*th error ellipse towards the *j*th concentration axis of the *k*th cluster) (Yamaji, 2016).

The robustness of the method has been tested by Yamaji et al. (2010) and the results prove to be stable as long as the number of data points is higher than or equal to 20. The method was successfully applied to veins at the Hashima mineral deposit in southern Kyushu by Yamaji and Sato (2011) and to veins at the Akenobe mine by Yamaji (2016).

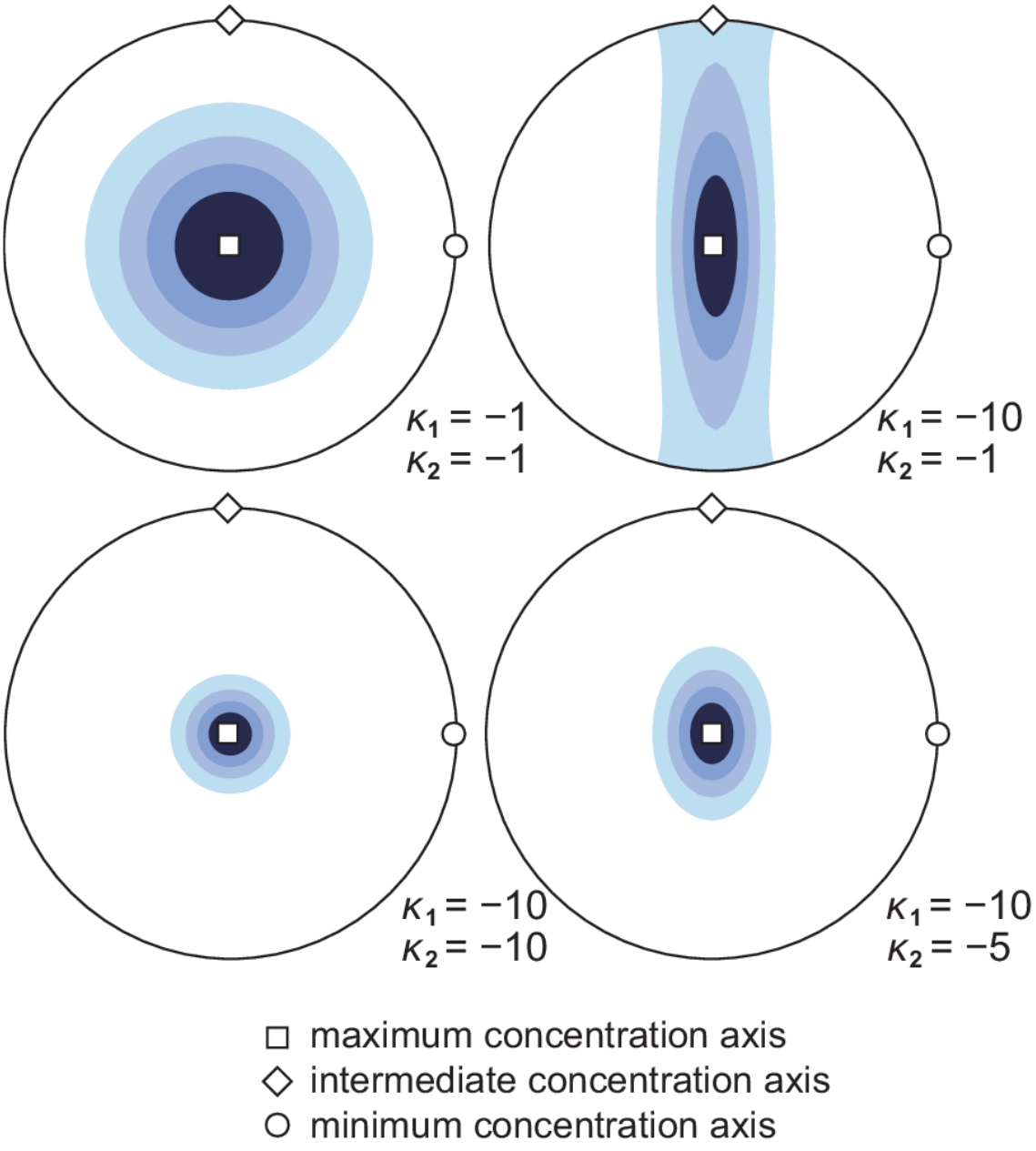

Fig. 1-5 Density contours of Bingham distributions having various concentration ratios, κ_1 and κ_2, which satisfy $0 \geq \kappa_2 \geq \kappa_1$, shown by equal-area projections.

1.5 Chapter 1 summary

In this section, the characteristics of the Hishikari deposit, as well as those of the Kushikino and Hashima deposits located in the same gold district and the structural controls of which were already studied, are summarized. Based on this overview, it is clear that the probability of a structural control on the mineralization in Hishikari is high. Moreover, a review of the stress inversion methods with an emphasis on the one used in the paleostress analysis of the veins at Hishikari is provided. The results of the above-mentioned analysis are presented in the next chapter.

2. Paleostress regimes during the mineralization at Hishikari

2.1 Data acquisition

The data to which this technique was applied are vein orientations data (strike and dip), collected from the Hishikari mine (Fig. 2-1). The veins at Hishikari are banded (Fig. 2-2), with each set of symmetrical bands representing a different episode of thermal fluid ascent. The majority of the veins at a given location display the same orientation. However, it is common to observe few veins with orientations different from the main orientation. Those veins were potentially formed under different stress states.

I collected 978 orientation data points on the veins wider than 1 cm at 653 different mining faces in different vein groups (Table 2-1). If all the veins display the same orientation, only one datum is collected from the mining face. If some veins show orientations different from the main orientation, those orientations are also measured and I collect as many data points as there are different orientations at the mining face (Fig. 2-3). Veins showing an orientation different from the main one at every mining face are very common. Indeed, 60% of the data come from a mining face where at least two data points have been collected (Fig. 2-4).

The method that I used only accommodates hydrofractures. This means that it wouldn't distinguish extensional shear veins if they existed in Hishikari. However, the presence of shear stress cannot be ruled out during the mineralization, especially since slickenlines have been reported by Sekine et al. (2002). Nevertheless, in the absence of significant displacement, I consider the veins in Hishikari as purely extensional.

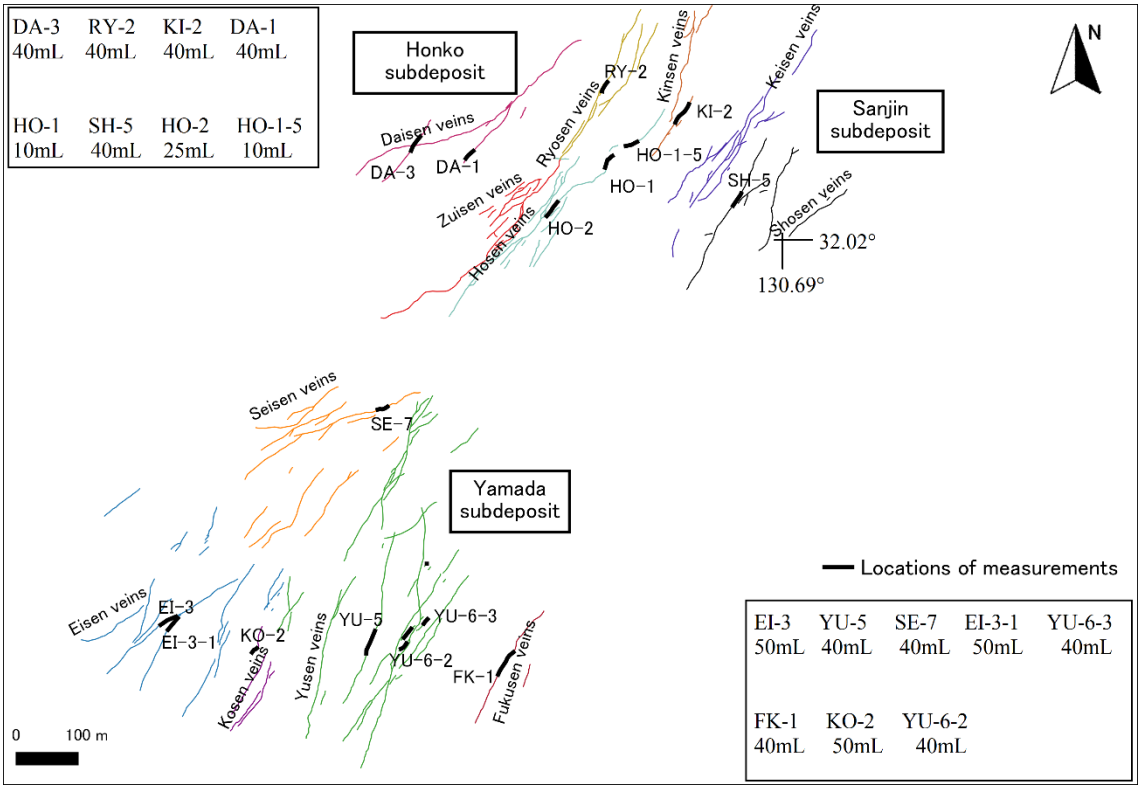

Fig. 2-1 Vein map of the Hishikari deposit; distinct vein groups are represented by different colours. The black solid lines indicate the sites where the orientation data of ore veins were collected. The elevations of the data collection sites (above the sea-level) are shown in the boxes; mL means meter level.

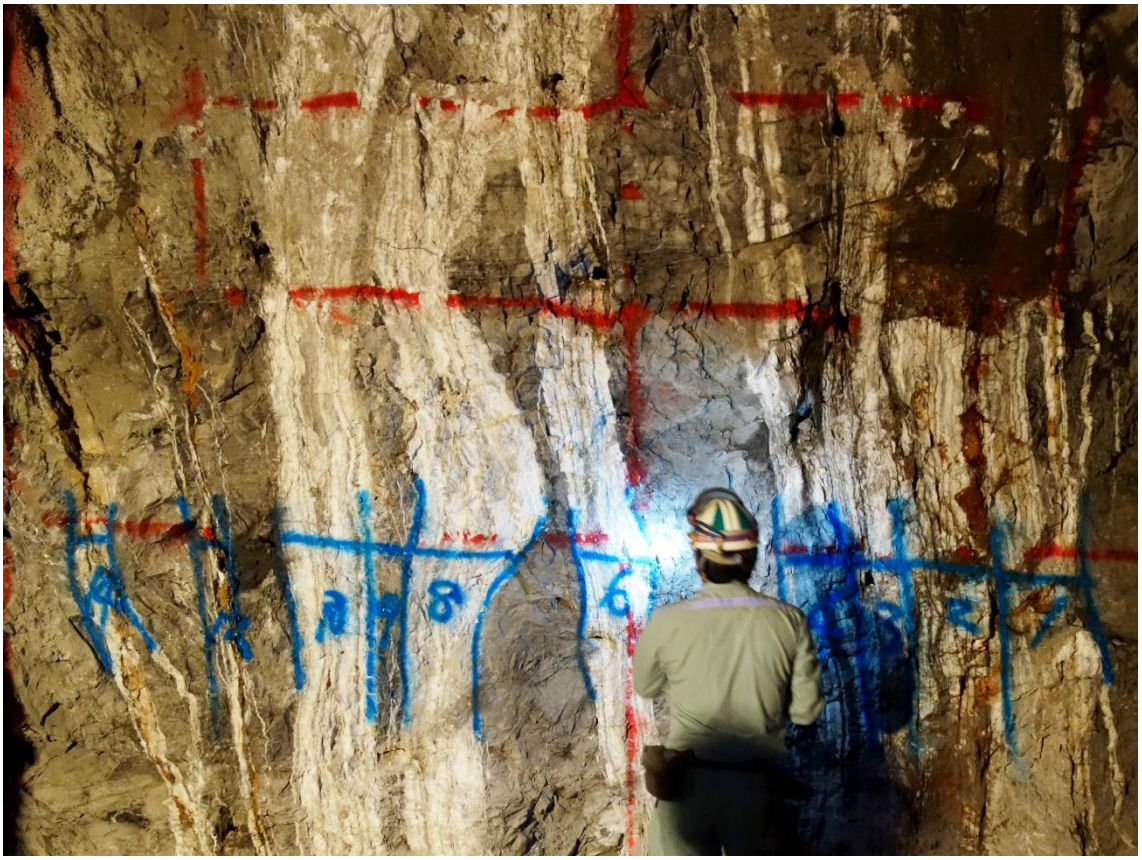

Fig. 2-2 Illustration of a mining face in the Hishikari mine (within the Yamada sub-deposit). The scale is provided by the person standing.

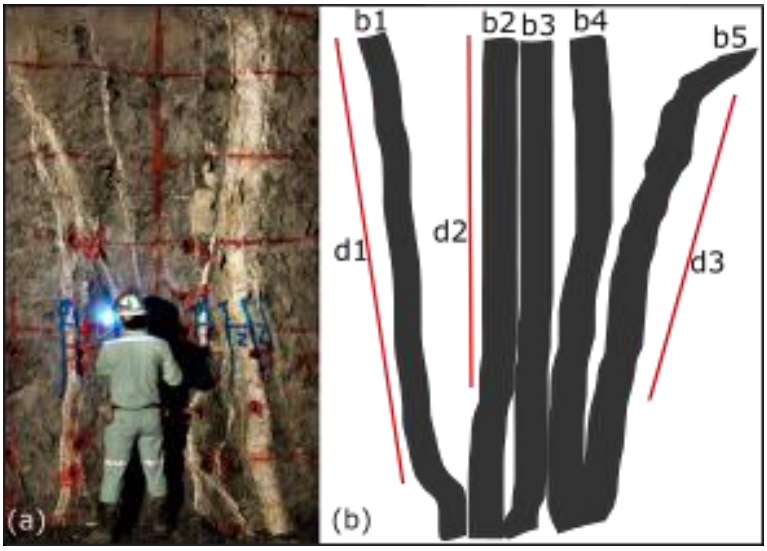

Fig. 2-3 (a) Mining face. The vein is comprised of several bands (sub-vertical white features) that display different orientations. (b) Schematic illustration of the veins and the data collection procedure. b1, b2, through to b5 represent the different veins. At a mining face with such a configuration, three data points will be collected as the veins generally displays three different directions. d1, d2 and d3 represent each an individual datum (strike, dip) that would be collected from this mining face following the procedure used in this study.

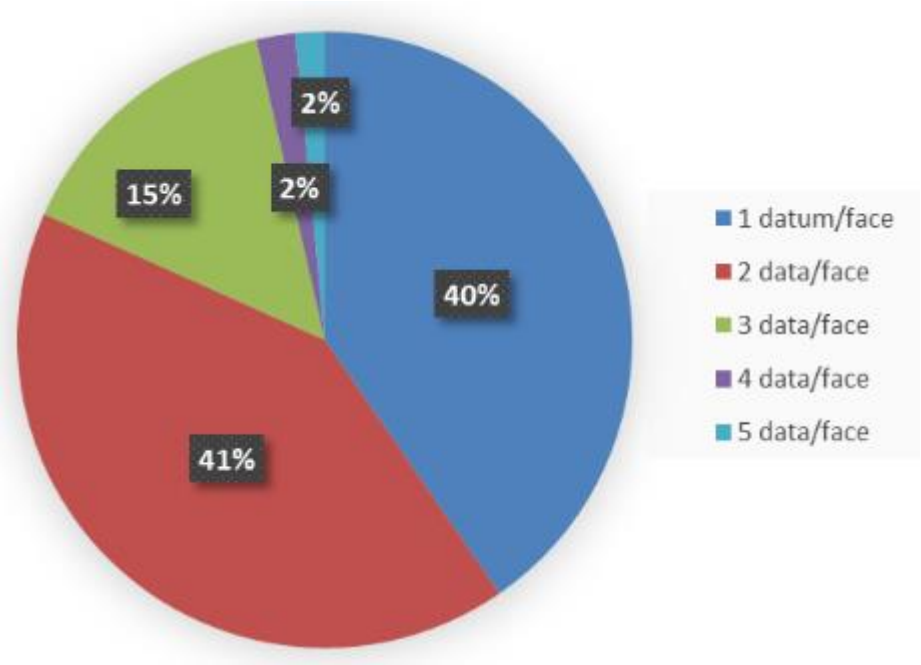

Fig. 2-4 Distribution of the measured veins by the number of data points collected per mining face.

Table 2- 1 Spatial quantitative distribution of measured veins.

Zone	Sub-deposit	Vein group	Subtotal			Total
Honko-Sanjin	Honko	Daisen	141	456	512	978
		Hosen	182			
		Kinsen	73			
		Ryosen	60			
	Sanjin	Shosen	56	56		
Yamada	Yamada	Eisen	96	466	466	
		Fukusen	53			
		Kosen	55			
		Seisen	25			
		Yusen	237			

2.2 Paleostress analysis in Honko-Sanjin

In total, 512 orientation data were collected from the Honko-Sanjin sub-deposits. The minimum BIC was found for $K = 1$ (Fig. 2-5a), which means that a single stress state was responsible for the formation of all the vein orientations making up the dataset. The optimal stress was of strike-slip regime with a σ_3-axis trending NW-SE and $\Phi = 0.79$ (Fig. 2-5b and c). It is called Stress HS. The Φ value indicates that $\sigma_1 \approx \sigma_2$, meaning that the σ_1- and σ_2-axes could relatively easily rotate about the σ_3-axis and swap their respective horizontal and vertical positions.

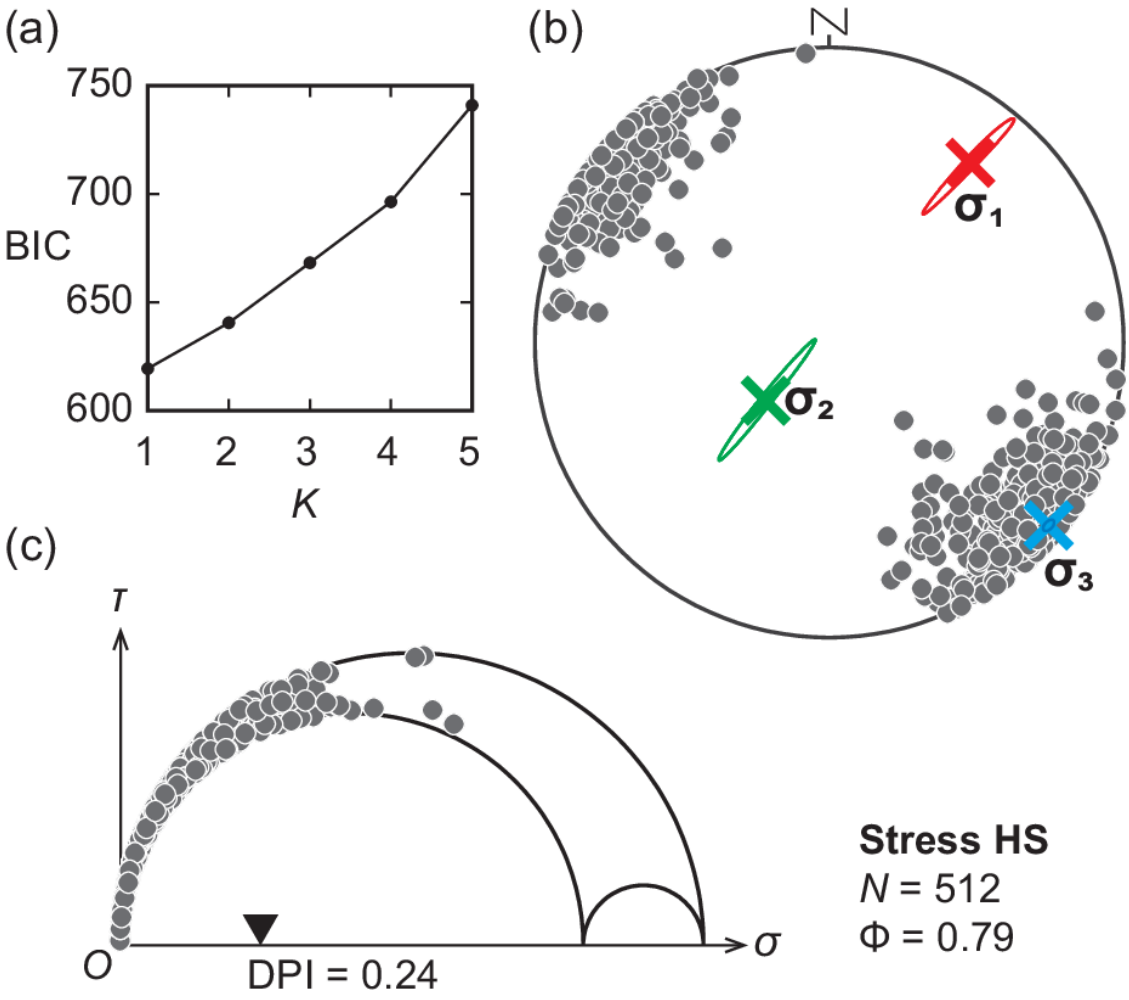

Fig. 2-5 Stress inversion results from the Honko-Sanjin sub-deposits. (a) *K* vs BIC curve showing a minimum BIC for *K* = 1, meaning that a single stress state (called HS) was responsible for the formation of all the veins. (b) Equal-area projection of the poles to the veins of the sub-deposit. Bold crosses represent the principal stress axes and are located at the center of their 95% error ellipses. The stress ratio was 0.79. (c) Mohr circles of the stress and non-dimensional normal and shear stresses on the vein walls.

2.3 Paleostress analysis in Yamada

I obtained 466 quartz vein orientation data points from the Yamada area, and two stress states were found from them (Fig. 2-6a and b). These stress states are termed Stresses YA and YB, and their ϖ values are respectively 0.95 and 0.05. This means that 95% of the veins were formed under Stress YA, and 5% of them were formed under Stress YB. The σ_3-axis of Stress YA and the σ_1-axis of Stress YB, respectively, were nearly horizontal, but their remaining stress axes were inclined. The colors of the data points in (Fig. 2-6b) indicate their memberships to YA and YB, each of which has a value between 0 and 1, and indicates the probability for Stress YA or Stress YB to be responsible for the formation of a vein defined by a datum point. In the stereogram, dark brown circles show the veins formed probably under Stress YA, whereas the veins formed probably under Stress YB are indicated by open circles. The stress axes have relatively small confidence regions due to the large number of data.

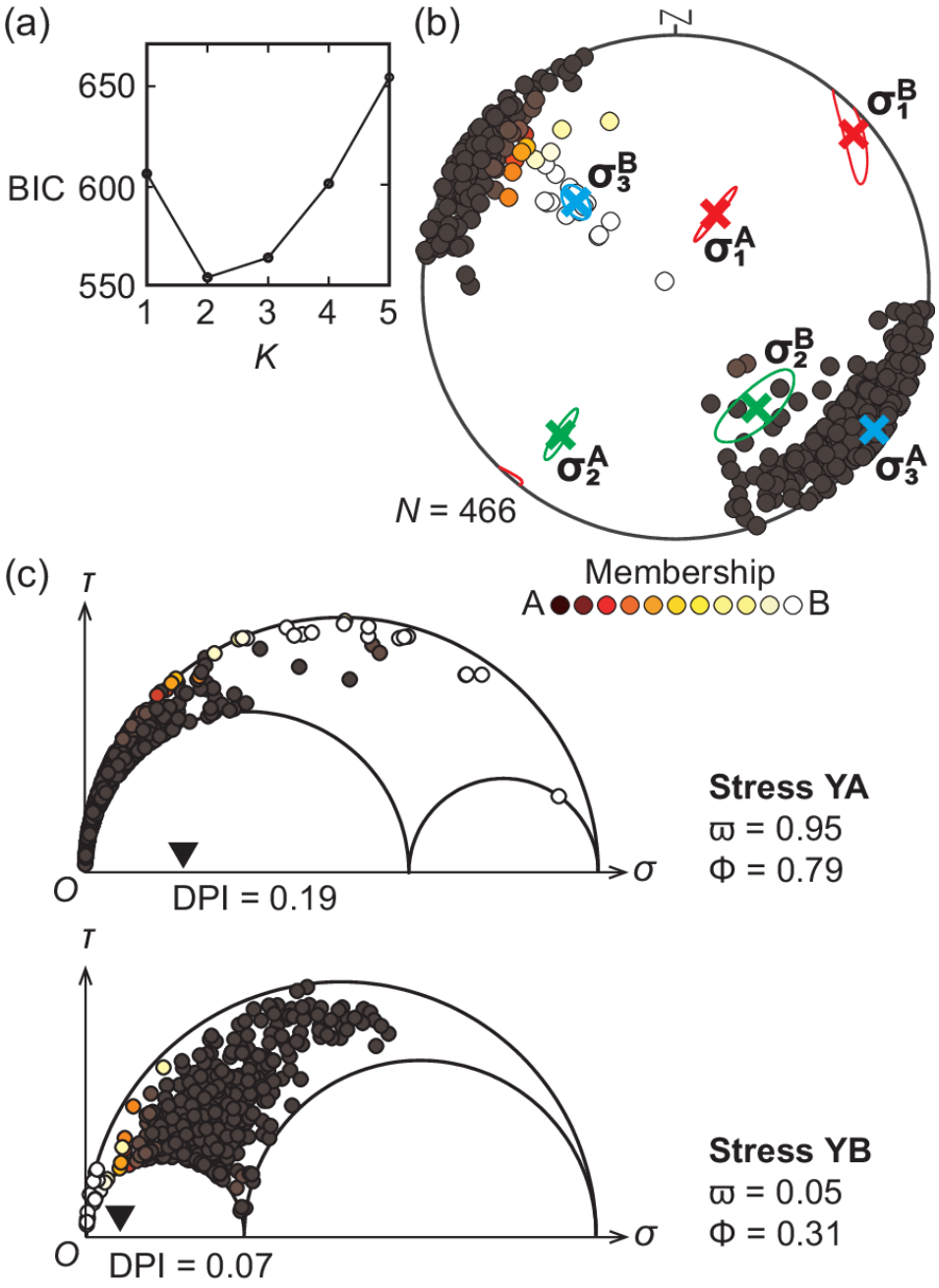

Fig. 2-6 Stress inversion results from the Yamada sub-deposit. (a) The *K* vs BIC curve reaches its minimum for $K = 2$, which means that the vein orientations should be divided in two clusters. The corresponding stresses are called Stresses YA and YB. (b) Equal-area projection of the poles to the veins of the sub-deposit. The membership of an orientation to one of the stress states is indicated by the color of the datum point representing that orientation. (c) Mohr circles of the stresses and the normalized normal and shear stresses on the vein walls exerted by the stress states.

2.4 Implications of the different stresses and mean stress M in Hishikari

Normal and strike-slip faulting stress regimes (Stresses HS and YA) were found from the Hishikari veins, and a minor part of the veins was formed under horizontal compression (Stress YB). The stress axes were inclined to some extent. The small depths of veining and growing volcanic loads around the mine during the formation of the veins qualitatively explain the inclined stress axes. Pleistocene andesitic lava and pyroclastic rocks accumulated in the area and had a thickness of a few hundred meters, simultaneously with the mineralization (1.25 to 0.6 Ma) (Izawa et al., 1993a; Tohma et al., 2010). These rocks are the Hishikari Lower Andesites (1.78 Ma to 0.98 Ma), the Hishikari Middle Andesites (0.79 Ma to 0.78 Ma), the Kurozonsan Dacites (1.56 Ma to 0.95 Ma) and the Shishimano Dacites (1.7 Ma to 0.5 Ma) (Izawa et al., 1990; Hosono and Nakano, 2003). Although the Yamada sub-deposit and Honko-Sanjin sub-deposits were formed more or less simultaneously, the mineralization started earlier in Yamada (Sanematsu et al., 2005). Stresses YA and HS have similar σ_3- axes and indicate high stress ratios $\Phi = 0.79$. Their high stress ratios indicate that the σ_1- and σ_2- axes were relatively easy to rotate about the σ_3- axis. Hence, I propose a primary normal faulting regime in the whole Hishikari deposit area at the beginning of the mineralization that has been transformed into a strike-slip faulting regime in Honko-Sanjin sub-deposits by

the rotation of the maximum and intermediate stress axes. The amplitude of the paleo-topographic undulations and the paleo-depths at which veins formed were comparable. According to Pan et al. (1994), stresses are affected by topographic loading down to depths similar to the amplitude of the loading. The topographic perturbation explains the difference in the stress conditions found in the Honko-Sanjin and Yamada sub-deposits.

On the other hand, the Stress YB in the Yamada sub-deposit was detected from veins located right beneath the lacustrine mudstone beds deposited in a hydrothermal eruption crater (Izawa et al., 1993b) (Fig. 2-7). The concerned vein goups are Yusen-5, Kosen-2, Yusen-6-3 and Fukusen-1. However, the same vein groups also contain veins formed under Stress YA, which suggests that Stress YB is coeval to Stress YA. Stress YB could represent a local perturbation. Stress YB is intermediate between strike-slip faulting regime and reverse faulting regime, whereas Stress YA is of normal faulting regime. Horizontal slickenlines denoting a strike-slip motion have been reported in the Yusen veins in the Yamada sub-deposit (Sekine, 2002). These slickenlines are likely to be resulting from the strike-slip component of Stress YB. Since the slickenlines are found on veins, it is likely that the motion happened after those veins were already formed. Given that the majority of the veins in Yamada were formed under the Stress YA, a

chronological relationship can be drawn between Stress YA and Stress YB. This latter, although it was simultaneously active with YA, would have appeared later than YA.

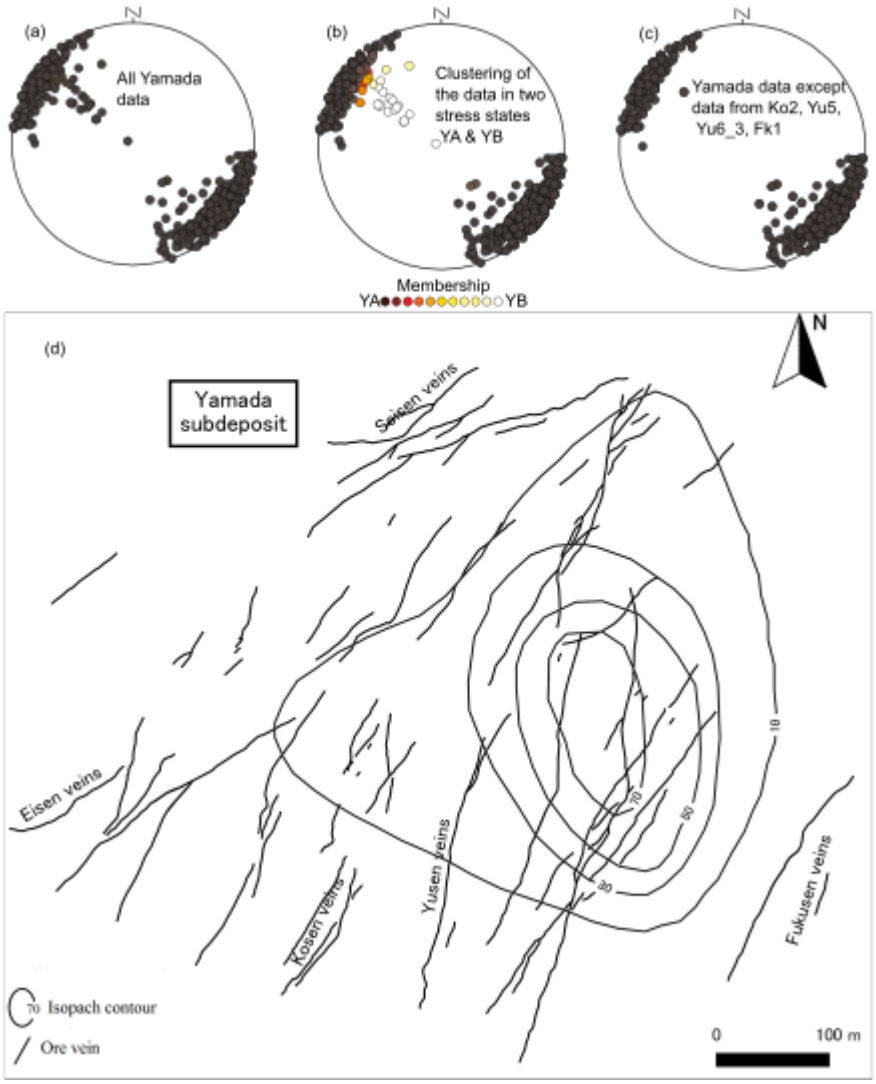

Fig. 2-7 (a) Equal-area projection of all the poles to vein orientations collected from the Yamada sub-deposit. (b) Result of the clustering of the orientation data from Yamada (Fig. 2-6b). (c) Equal-area projection of all the orientation data from Yamada except those from Yu-5, Ko-2, Yu-6-3 and Fk-1. Stress YB appears to be active only in the previously cited vein groups. (d) Isopachs of the lacustrine beds thickness in the Yamada area from Izawa et al. (1993b) are overlain on the vein map of Yamada sub-deposit. There is a close spatial relationship between the mudstone beds and Stress YB.

All the three stress states HS, YA and YB found in Hishikari have σ_3-axes trending NW-SE. The 95% confidence regions of the principal axes orientations of the stresses HS and YA don't intersect one another (Fig. 2-8a). Nevertheless, these two stress states are not significantly different, as demonstrated in the following argument. On a hypersphere, S_5, in a 5-dimensional space, a reduced stress tensor is represented by a point; and the angular distance that separates the points on S_5 representing the tensors is a measure of the dissimilarity between the reduced stress tensors (Yamaji and Sato, 2006). This dissimilarity measure is represented by the symbol Θ and it is termed angular stress distance. Fig. 2-8b indicates the Θ values between the stress states HS, YA and YB. HS and YA have the smallest distance between them. Given two randomly oriented fault planes, created by two different stresses, the mean angular difference between their slip directions is approximated by the angular stress difference of the two stresses (Yamaji and Sato, 2006). A convention in fault-slip analysis establishes that the difference between reduced stress tensors is considered insignificant if the differences between the slip directions of faults formed under those stresses are smaller than 20–30° (Angelier, 1990; Žalohar and Vrabec, 2007). In this regard, the difference between Stresses HS and YA (Θ = 15°) is not significant. However, Stress YB is significantly different from HS and YA (Θ = 59° and Θ = 74°, respectively). It is worth mentioning that the error ellipses denote the precision of each of the detected principal stress axes orientations. The convention, which only deals with the mechanics of faulting, is not extended to this precision.

The difference between Stresses HS and YA having been proven to be insignificant, their mean Stress M is used in the following discussions. The mean is the centroid of the points representing Stresses HS and YA on S_5. The principal axes orientations of

Stress M are shown in Fig. 2-8a; the stress ratio Φ is equal to 0.83. The value of the stress ratio is slightly greater than both the Φ values of Stresses HS and YA. This is explained by the fact that iso-Φ lines do not correspond to great circles on S_5 (Fig. 2-8b) except for the lines of Φ = 1/2 (Yamaji and Sato, submitted). Given two random points on S_5, they are always aligned with their centroid on a great circle. Stress M has an approximately horizontal σ_3-axis, but its σ_1-axis has a plunge of 44°, denoting a stress state intermediate between the normal and strike-slip faulting regimes. The relatively high stress ratio indicates that the σ_1- and σ_2-axes could be easily rotated about the σ_3-axis by perturbations.

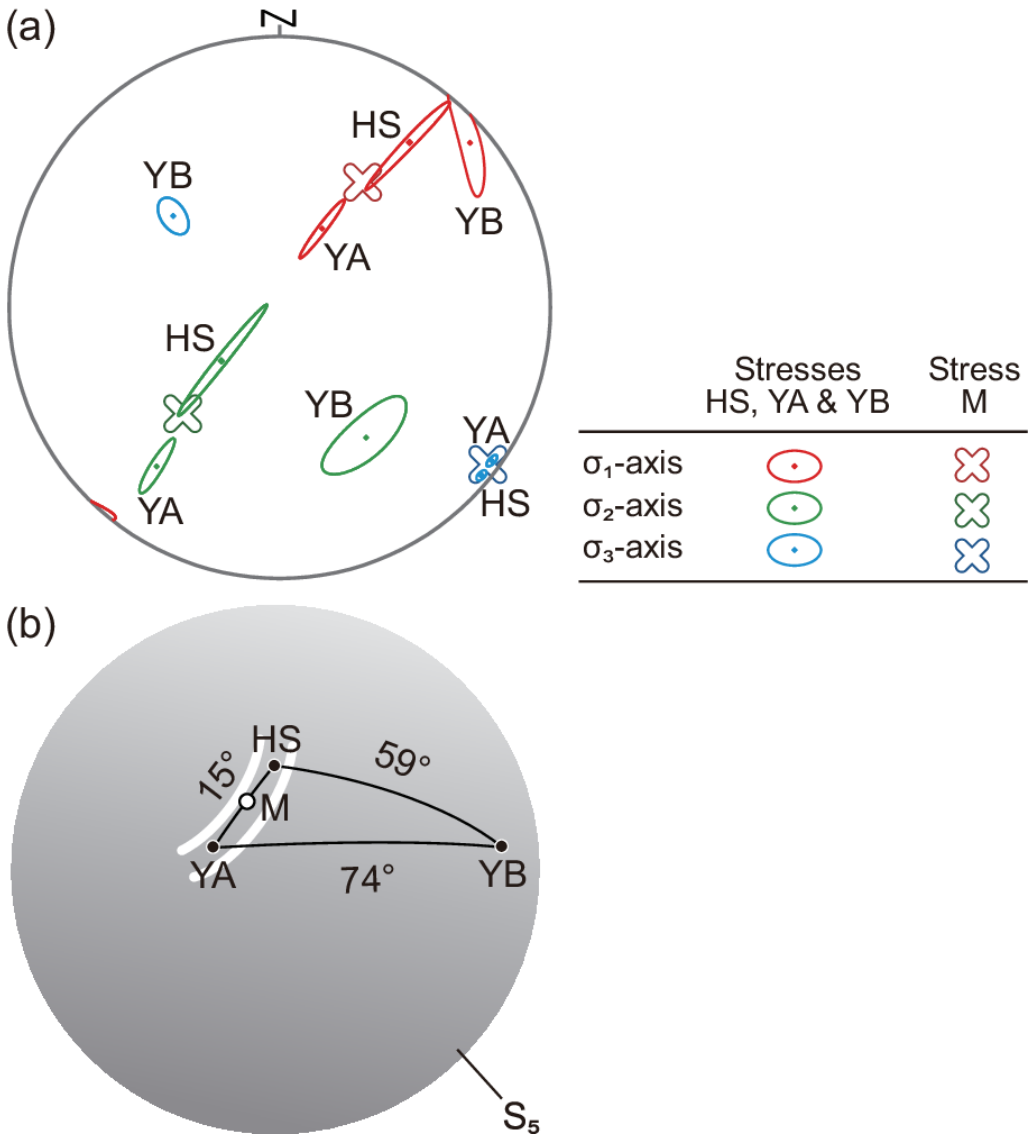

Fig. 2-8 (a) Principal axes of the Stresses HS, YA, YB found in Hishikari and of the Stress M that is the mean of HS and YA shown by a lower-hemisphere, equal-area projection. 95% confidence regions are depicted by ovals (Figs. 2-5 and 2-6). (b) Schematic illustration of the unit hypersphere, S_5, in 5-dimensional space (Sato and Yamaji, 2006), on which the three points represented by closed circles correspond to Stresses HS, YA and YB. The angular distance between HS and YA is 15°; the angular distance between HS and YB is 59°; and that between YA and YB is 74°. The open circle shows the centroid between the points of HS and YA; it represents Stress M. White lines are the contour lines of the stress ratio Φ.

2.5 Outlook on the regional scale: stress history of southern Kyushu

Low-sulfidation epithermal gold veins are thought to be formed from near-hydrostatic fluids under a mildly extensional stress state (Sillitoe and Hedenquist, 2003; Simmons et al., 2005). Low stress magnitude was suggested also from other gold deposits in southern Kyushu. High differential stress favors shear fracturing rather than the opening of tensile fractures, and this leads to pervasive fault activities. The rarity of faults around the mid Pliocene veins in the Hashima deposit (Fig. 2-9) to the southwest of Hishikari is consistent with the low stress hypothesis (Yamaji et al., 2010). However, the existence of map-scale (Izawa et al., 1990) and mesoscale faults (Abe et al., 1986; Naito, 1993; Sekine et al., 2002) in and around the Hishikari deposit suggest that the differential stress magnitude during the mineralization was not as low as previous researchers had envisaged for this type of deposits.

The K-Ar age of epithermal veins in the Fuke deposit (Fk in Fig. 2-9) to the north of Hishikari is 1.4 Ma (Urashima and Ikeda, 1987). Unstable near-surface stress conditions are suggested by the bimodal (normal faulting and strike-slip faulting stress regimes) trends of these epithermal veins (Muto, 1952). The stress inversion of mesoscale faults near the Yamagano mine in lower Pleistocene formations (Fig. 2-9) indicates a variable stress condition (Hikichi and Yamaji, 2008).

The deposition of low-sulfidation epithermal veins is known to be associated with rifting (Sillitoe and Hedenquist, 2003; Simmons et al., 2005). Southern Kyushu was subjected to extensional stress since 5 Ma (Yamaji, 2003). In the lower and middle parts of the Miyazaki Group, mesoscale faults are common. However, they are rare in the upper part. This suggests a waning of fault activity in the Miyazaki area during late Pliocene (Fig. 2-9). A strike-slip faulting stress regime prevails in southern Kyushu today as evidenced by seismic focal mechanisms, except for the Kagoshima Rift (Fig. 2-9) and its northern extension (Matsumoto et al., 2015). Nakamura (1977) suggested a σ_{Hmax}-axis trending WNW-ESE in southern Kyushu, based on the arrays of young volcanic craters around Kirishima, Sakurajima and Kaimondake (Fig. 2-9). However, the distribution of volcanic craters of Kirishima was reinterpreted by Kagiyama (1994) as an accidental alignment of dilational jogs accompanied by strike-slip faulting, based on focal mechanisms and the distribution of hypocenters of crustal earthquakes.

Intra-arc extensional deformation became localized into the Kagoshima Rift, with a rapid subsidence beginning at ~1 Ma (Uchimura et al., 2014), although slow rifting had started in the Okinawa Trough backarc basin at ~2 Ma (Fig. 1-1) (Sibuet et al., 1995). In southern Kyushu, strike-slip faulting seems to be dominant during the early Pleistocene whereas earlier ore veins appear to have formed under normal faulting stress

regime (Fig. 2-9). However, there are the NE-SW-trending Inabazaki normal faults that exist nearby Hishikari and that cut the Shishimano Dacite (age: 1.7-0.5 Ma). Moreover, seismologically active faults exist in Izumi. This suggests that, although the change of stress regime between normal faulting to strike-slip faulting from the Pliocene to the Pleistocene indicates a reduction of the extensional stress in southern Kyushu, this extensional stress has continued prevailing until the present day.

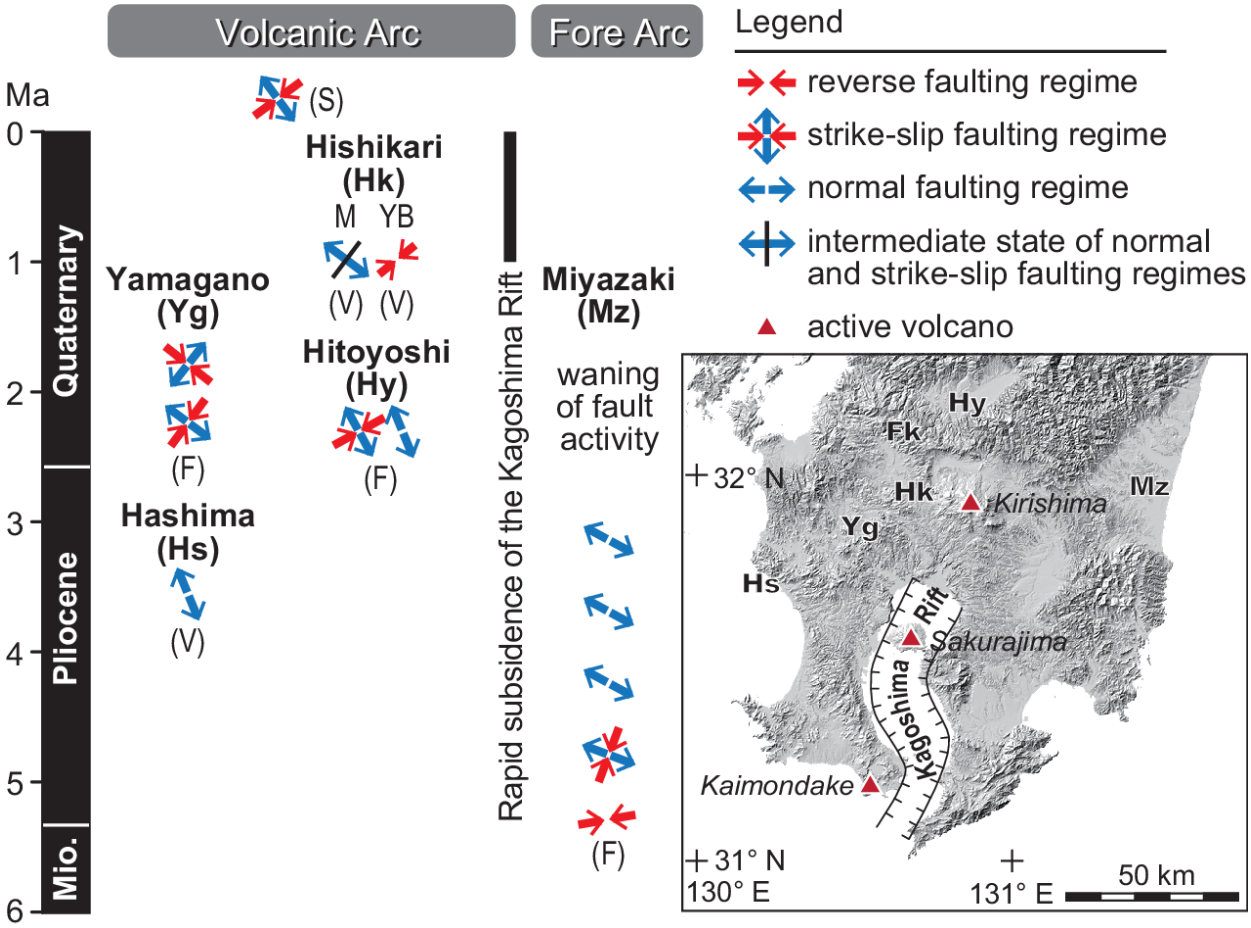

Fig. 2-9 Stress history of southern Kyushu. Results of stress analyses that could determine stress regimes are shown. Parenthesized letters F, S and V respectively indicate mesoscale faults, seismic focal mechanisms and ore veins used for the determination of paleostresses. In the Yamagano and Miyazaki areas, mesoscale faults were used to infer paleostresses; a change in the paleostresses correlated with the stratigraphy suggested a change in the stress condition at ~2 Ma. Paleostresses determined from mesoscale faults in the Hitoyoshi basin have an age that remains unclear. Paleostress data sources include: Hishikari (this study), Yamagano (Hikichi and Yamaji, 2008), Hitoyoshi (Yamaji et al., 2003), Miyazaki (Yamaji, 2003), and focal mechanisms (Matsumoto et al., 2015).

2.6 Chapter 2 summary

In this chapter, the stress conditions under which Hishikari deposit formed were unveiled. Almost all the veins formed under an extensional stress with a σ_3-axis trending NW-SE and a σ_1-axis inclined to the NE. This stress state is consistent with stresses found elsewhere in southern Kyushu, including in other low-sulfidation epithermal veins, meaning that regional tectonics controlled the mineralization in Hishikari. However, a minor amount of veins formed under axial compression could have resulted from local factors. The relatively low differential stress magnitude suggested by the rarity of faults in the epithermal deposits of southern Kyushu increase the importance of understanding the fluid pressure regimes during the mineralization. In the next chapter, this aspect and its relationship to the mineralization are discussed.

3. Fluid pressure regimes during the mineralization at Hishikari

3.1 Fluid pressure and epithermal gold mineralization

The driving pressure ratios (*p)* associated with low-sulfidation epithermal gold deposits are generally low (Sillitoe and Hedenquist, 2003; Simmons et al., 2005). However, other vein-type ores yielded higher *p* value estimates (Zachariáš, 2016; Lahiri and Mamtani, 2016).

3.2 Driving pressure index

The progress made in the techniques for stress inversion of dilational fractures makes it possible to determine the stress condition, as well as the driving pressure ratio,

$$p = (p_f - \sigma_3) / (\sigma_1 - \sigma_3), \quad (1)$$

from the orientations data of dilational fractures, p_f being fluid pressure, and σ_1, σ_2 and σ_3 representing the principal stresses. Compressive stress is seen as positive, and the inequality $\sigma_3 \leq \sigma_2 \leq \sigma_1$ is satisfied.

The method used in the paleostress analysis (Chapter 2) can determine stresses from a mixture of orientation data created by different stress conditions. The fundamental assumption is that an array of veins forms intermittently when p_f exceeds σ_3 (Fig. 3-1), while the principal stress axes orientations and the stress ratio, $\Phi = (\sigma_2 -$

$\sigma_3)/(\sigma_1 - \sigma_3)$, remain unchanged. The term "a stress condition", refers to the states of stress having the same principal axes and stress ratio, regardless of their stress magnitudes. When the magnitudes are neglected, a stress condition is denoted by the reduced stress tensor,

$$\boldsymbol{S} = \boldsymbol{Q}^{\mathrm{T}}\mathrm{diag}(1, \Phi, 0)\boldsymbol{Q}, \quad (2)$$

where $\boldsymbol{Q}$ is the 3 × 3 orthogonal matrix indicating the principal stress orientations, and $\mathrm{diag}(1, \Phi, 0)$ stands for the diagonal matrix with the components, 1, Φ and 0.

Veins are formed only along the fractures with normal stress, σ, satisfying $\sigma < p_{\mathrm{f}}$ because fluid pressure overcomes the normal stress to open the fractures. The plane perpendicular to the σ_3-axis will have the minimum normal stress σ, acting on it. Therefore, fluids with $p_{\mathrm{f}} < \sigma_3$ will not form veins. Hence, the condition about the driving pressure ratio (Eq. 1), $p > 0$, should be met for veins to be formed. The fractures that are nearly perpendicular to the σ_3-axis readily satisfy the condition, $\sigma < p_{\mathrm{f}}$, meaning that they are favourably oriented to be dilated by overpressured fluids (Fig. 3-1). Conversely, the fractures nearly perpendicular to the σ_1-axis are the least favourably oriented ones to be dilated.

During the formation of the veins at Hishikari, which lasted for 6×10^5 years (Izawa et al., 1993a; Sanematsu et al., 2005; Tohma et al., 2010), fluid pressure is assumed to

have fluctuated while the stress condition remained the same (Fig. 3-1a). The favourably oriented fractures had a higher probability of forming veins than the unfavourably oriented fractures (Figs. 3-1b and c). As a result, the poles to veins make an elliptical cluster centered on the σ_3-axis upon an equal-area projection, and the cluster is elongated along the great circle defined by the σ_3- and σ_2-axes (Fig. 3-1). Poles to the veins formed under axial compression ($\Phi = 0$) are scattered along this great circle to make a girdle pattern, because σ_2- and σ_3-axes are indistinguishable for this stress condition. In contrast, poles to veins formed under axial tension ($\Phi = 1$) make a circular cluster, σ_2- and σ_1-axes being indistinguishable. The cluster shape indicates Φ (Jolly and Sanderson, 1997). Such clusters and girdles can be represented by the Bingham distribution (Borradaile, 2003), which has the probability density function,

$$\mathrm{P_B}(\boldsymbol{x}) = \frac{1}{A}\exp[\boldsymbol{x}^{\mathrm{T}}\boldsymbol{Q}^{\mathrm{T}}\mathrm{diag}(\kappa_1, \kappa_2, 0)\boldsymbol{Q}\boldsymbol{x}], \quad (3)$$

where $\boldsymbol{x}$ is the unit vector indicating an orientation, A is the normalizing factor, κ_1 and κ_2 are concentration parameters ($\kappa_1 \leq \kappa_2 \leq 0$), and $\boldsymbol{Q}$ is the orthogonal matrix that indicates the minimum, intermediate and maximum concentration axes. Uniform distribution has the parameters, $\kappa_1 = \kappa_2 = 0$; and smaller clusters have larger $|\kappa_1|$ and $|\kappa_2|$ values. $\boldsymbol{\theta}$ represents κ_1, κ_2 and $\boldsymbol{Q}$, collectively. Bingham distributions with various concentration parameters are shown in Fig. 1-5. The aspect ratio of a

cluster is denoted by κ_2/κ_1.

It follows from Eq. (2) that normal stress upon the plane normal to $\boldsymbol{x}$ is written as

$$\sigma = \boldsymbol{x}^{\mathrm{T}}\boldsymbol{Q}^{\mathrm{T}}\mathrm{diag}(1, \Phi, 0)\boldsymbol{Q}\boldsymbol{x}, \tag{4}$$

where $\boldsymbol{Q}$ is the orthogonal matrix standing for the stress axes. The exponential function in Eq. (3) is a monotonously increasing function. Hence, Yamaji et al. (2010) pointed out that the contour lines of $\mathrm{P_B}(\boldsymbol{x})$ are identical with those of σ (Fig. 3-1) when the minimum, intermediate and maximum concentration axes are parallel to the σ_1-, σ_2- and σ_3-axes, respectively, and

$$\Phi = \kappa_2/\kappa_1. \tag{5}$$

Therefore, the stress axes and stress ratio are determined from vein orientations if a Bingham distribution is fitted to the orientations.

If veins were formed under different stress conditions, each condition may have had different values of representative driving pressure ratios. A group of veins may have been formed from highly overpressured fluids, while others originate from mildly overpressured ones. The representative value of the driving pressure ratios of the ore fluids can be determined for each of the clusters as follows. Noting the negative signs of κ_1 and κ_2, and combining Eqs. (3)–(5), it is possible to write:

$$\mathrm{P_B}(\boldsymbol{x}) \propto \exp(-|\kappa_1|\sigma). \tag{6}$$

The left-hand side of this equation approximates the frequency distribution of the poles to veins, whereas the right-hand side is the frequency distribution of the normal stresses at the vein walls. The right-hand side is a decreasing function of σ (Fig. 3-1d). If highly overpressured fluid was supplied frequently, the slope of the function is gentle. Thus, the frequency of the σ values is a proxy for the frequency distribution of driving pressure ratios (Fig. 3-1b and c). DPI (driving pressure index) is referred to as the 95 percentile point of the σ values, and is used as the representative value of p for the fluctuating pressure. From Eq. (6), it follows:

$$\frac{\int_0^{\mathrm{DPI}} \exp(-|\kappa_1|\sigma)\,\mathrm{d}\sigma}{\int_0^{\infty} \exp(-|\kappa_1|\sigma)\,\mathrm{d}\sigma} = 0.95.$$

Solving this equation, the following formula is obtained:

$$\mathrm{DPI} \approx 3.00/|\kappa_1|.$$

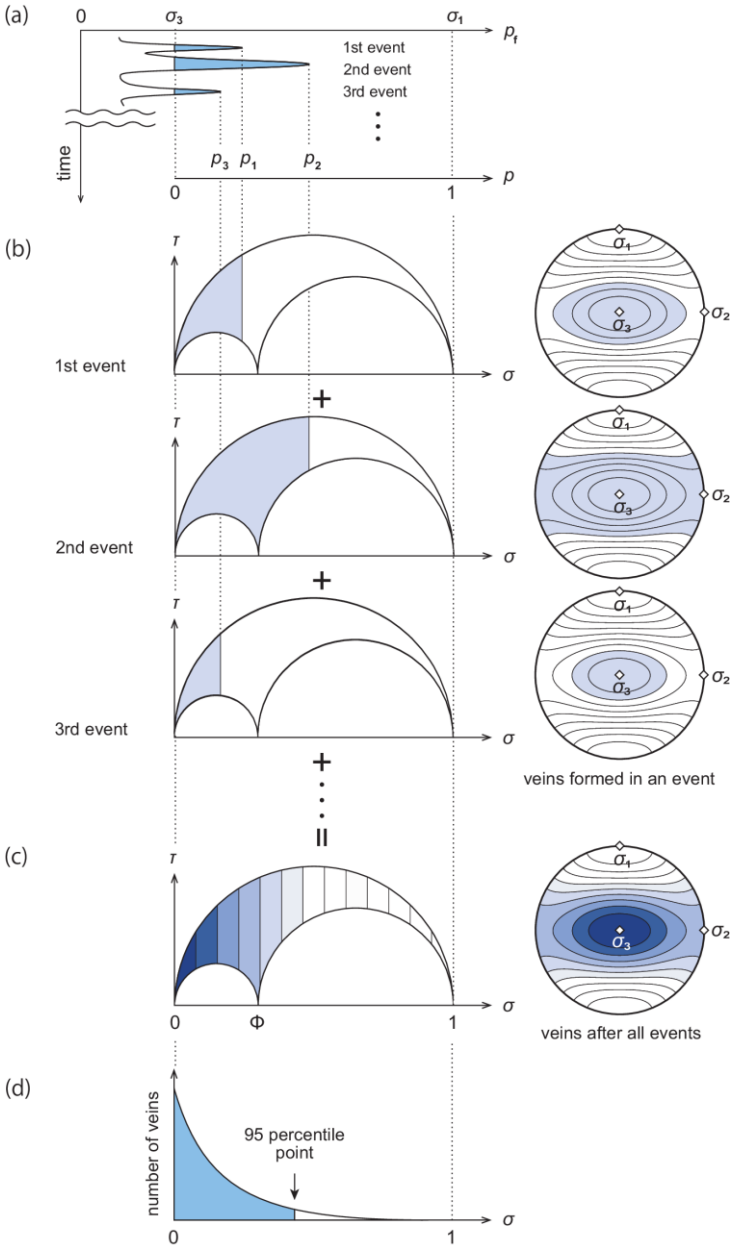

Fig. 3-1 Illustrations of the stochastic model (Yamaji et al., 2010) used in the present study. (a) Fluctuation of the pressure of ore fluid, p_{f}, through time. Ore veins are formed when the condition, $p_{\mathrm{f}} > \sigma_3$, is satisfied. The symbols, p_1, p_2, p_3, etc., denote the peak driving pressure ratios of the series of events when it is satisfied. (b) The filled areas in Mohr diagrams depict the regions where veins can be formed in each of the events. Equal-area projections show the contours of normal stresses, σ, and the possible areas for the poles to the veins formed in each of the events. (c) Observed veins at present are the summation of the veins formed in a great number of such events. (d) Schematic illustration of the frequency distribution of veins corresponding to the gradation in the Mohr diagram in (c).

3.3 Depth vs DPI

3.3.1 Concept of the analysis

Principal stresses tend to be proportional to overburden pressure, because brittle strength of the upper crust is controlled by friction in the shallow part of the crust (Goetze and Evans, 1979; Brace and Kohlstedt, 1980; Turcotte and Schubert, 2014, §8.4). It follows that differential stress can be approximated as:

$$\Delta\sigma \equiv \sigma_1 - \sigma_3 = \alpha z \tag{7}$$

where z is depth, and α is the constant of proportionality ($\alpha > 0$) (Fig. 3-2). Overburden pressure is equal to σ_1 in the normal faulting regime;

$$\sigma_1 = \rho_\mathrm{r} g z, \tag{8}$$

where ρ_r is the mean density of rocks, and g is the gravitational acceleration. Combining this equation and Eq. (7), the following equation is obtained:

$$\sigma_3 = \rho_\mathrm{r} g z - \alpha z. \tag{9}$$

Hydrostatic pressure gradient can be expected to approximate the gradient of p_f in a network of open fractures,

$$p_\mathrm{f} = \rho_\mathrm{w} g z + p_0, \tag{10}$$

where ρ_{w} is water density, and p_0 is the fluid pressure at the surface. Since overpressured fluids are assumed to have existed at depths, p_0 is expected to be positive in sign. Combining Eqs. (1) and (7)–(10), the following equation is obtained:

$$p = -\frac{p_0}{\alpha z} - \frac{(\rho_{\mathrm{r}} - \rho_{\mathrm{w}})g}{\alpha} + 1.$$

It follows that the gradient of driving pressure ratio is negative in sign because

$$\frac{\mathrm{d}p}{\mathrm{d}z} = -\frac{p_0}{\alpha z^2} < 0. \tag{11}$$

In case of the strike-slip faulting regime, the intermediate stress axis is vertical and overburden pressure is equal to σ_2:

$$\sigma_2 = \rho_{\mathrm{r}} g z \tag{12}$$

Instead of Eq. (8). It follows from $\Phi = (\sigma_2 - \sigma_3) / (\sigma_1 - \sigma_3)$ that $\sigma_2 = (\sigma_1 - \sigma_3)\Phi + \sigma_3$. Replacing σ_2 by its expression in Eq. (12), the following equation is obtained:

$$\sigma_3 = \rho_{\mathrm{r}} g z - \Phi \alpha z. \tag{13}$$

Using Eq. (13) instead of (9), Eq. (11) is obtained again. It can be seen by replacing Eq. (9) with $\sigma_3 = \rho_{\mathrm{r}} g z$ that Eq. (11) holds for the reverse faulting regime of stress as well. Consequently, driving pressure ratio decreases with depth irrespective of stress regimes as long as overpressured ore fluid has a hydrostatic pressure gradient (Eq. 9).

However, this trend is disturbed by the compartmentalization of overpressured fluid by impermeable layers (Fig. 3-2). Just like the difficulty of predicting the leak of oil

from a reservoir, it is difficult to recognize the layers that effectively worked as seals during ancient vein formation.

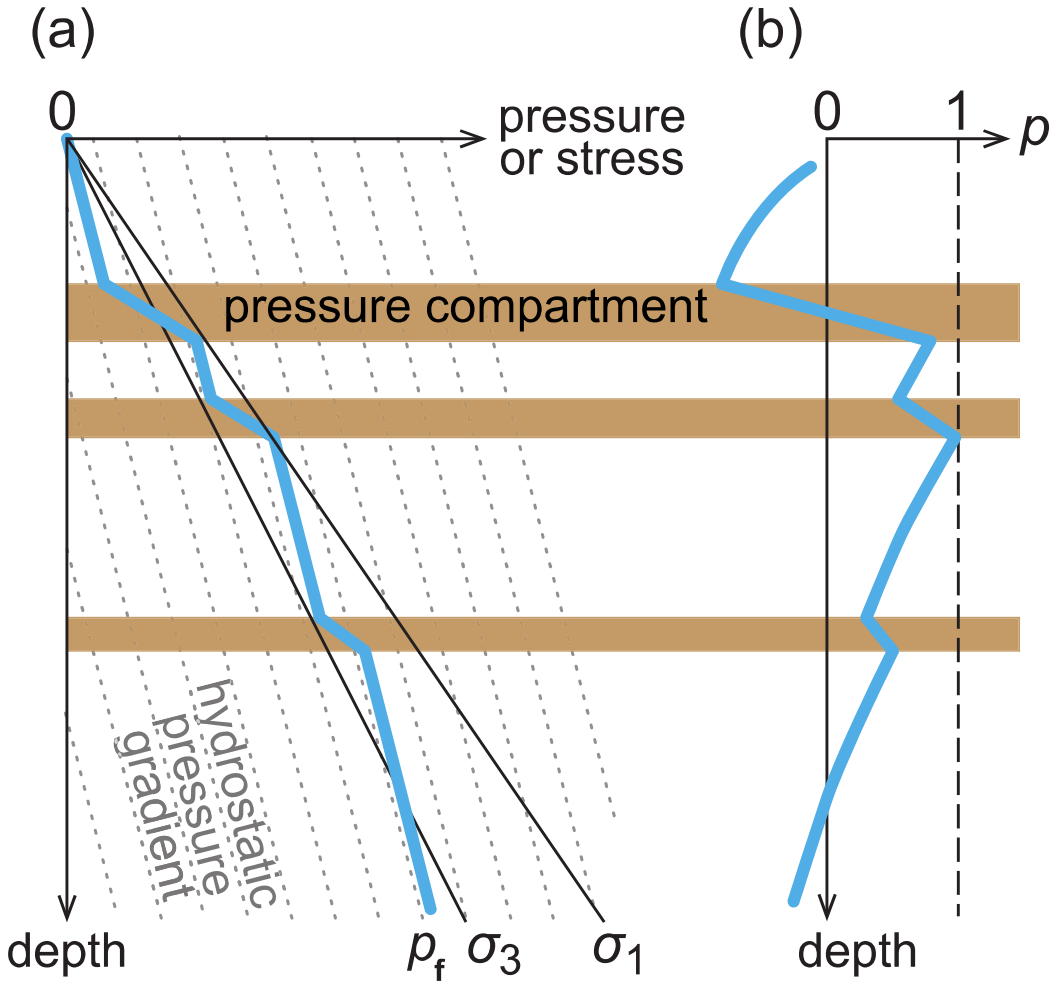

Fig. 3-2 Schematic illustrations of (a) the evolution of principal stresses and fluid pressure, p_f, with depth, z and (b) the driving pressure ratio, p, with depth. In a network of open fractures, the pressure gradient is hydrostatic and p has a negative correlation with z. However, when impermeable units acting as pressure seals surround an area, that area forms an abnormal pressure compartment within which fluid supra-hydrostatic fluid pressure gradient prevails and p has a positive correlation with z.

3.3.2 Results

Veins orientation data were collected from mining faces at the levels of 10 m, 25 m, 40 m and 50 m above the present sea-level and this allowed the investigation of the depth dependence of the driving pressure ratio in Hishikari. The DPIs at these levels are shown in Fig. 3-3. Stresses HS and YA were detected at different levels, but Stress YB was determined only at the 50 m level. The trends of the DPI for the cases of HS and YA were opposite to the expectation that p should have negative correlations with the paleo-depth (z) of veins or a positive correlation with the height above the present sea-level if ore fluid had a hydrostatic pressure gradient (Eq. 11, Fig. 3-2). The positive correlations with paleo-depths suggest the existence of pressure seals between the levels, and overpressured ore fluids were compartmentalized during mineralization.

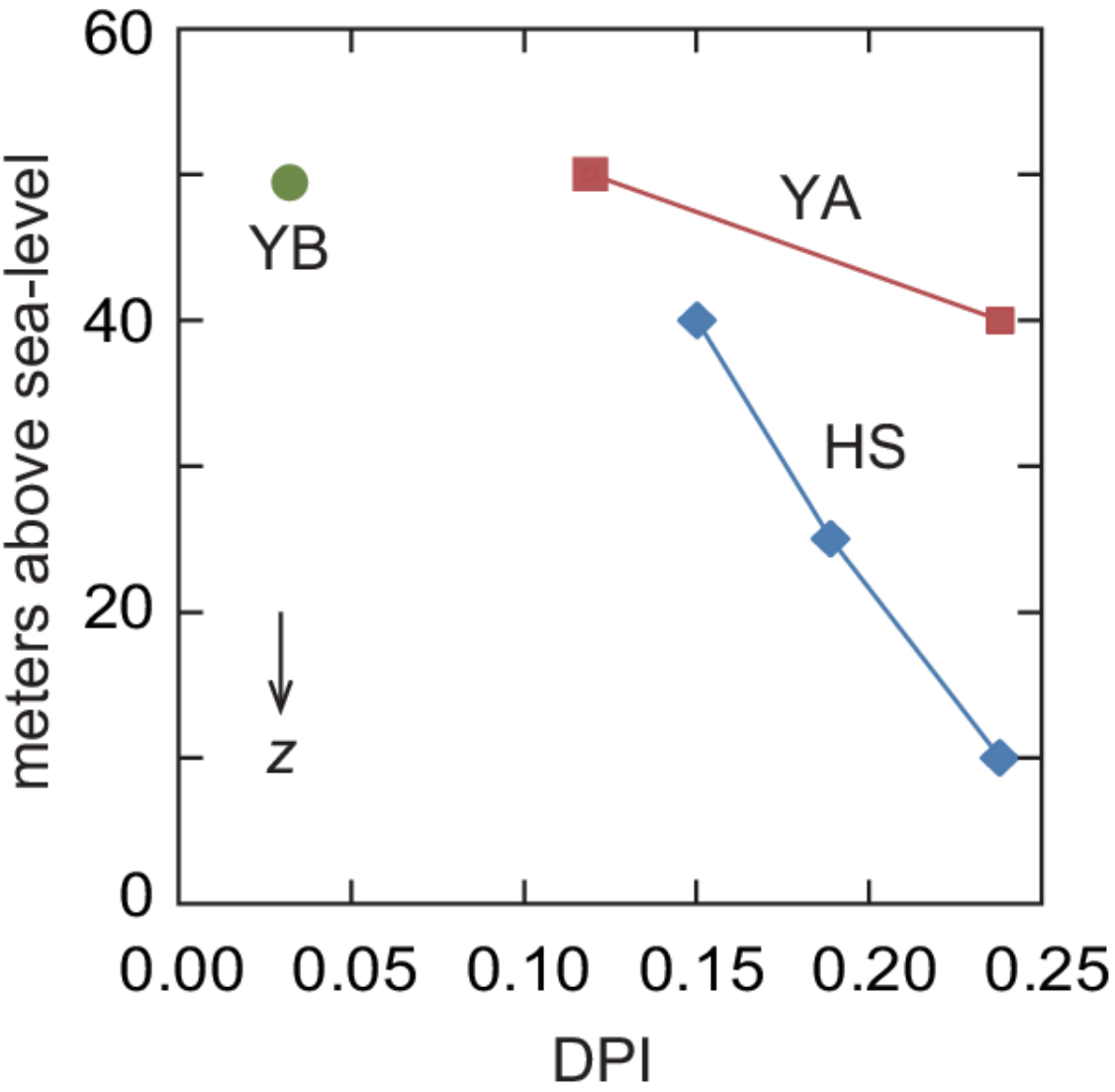

Fig. 3-3 Diagram showing the variation of the driving pressure index (DPI) with depth in the Honko-Sanjin and the Yamada sub-deposits. The *z*-axis points downward.

3.3.3 Existence of pressure seals in Hishikari

The depth dependence of p in Fig. 3-3 suggests that the ore fluids that formed the veins between 10 and 50 m levels in the Hishikari mine were compartmentalized by pressure seals that existed during the mineralization. The formation of the Hishikari deposit was the result of repeated upwelling of ore fluids during geological time. Therefore, the pressure seals were likely formed and broken repeatedly by overpressured ore fluids during the mineralization that lasted for 6×10^5 years. The overpressured fluids and faulting may have broken the seals, and mineralization may have healed fractures to recreate them.

This interpretation appears to be inconsistent with the fact that thick veins penetrate different levels. However, these comprise composite veins, taking thousands of years to add lamellas intermittently and to form eventually wide veins (Sanematsu et al., 2006). Moreover, only 1/4 of the orientation data collected are from meter-scale veins, the majority being decimeter-scale and a few being centimeter-scale (Fig. 3-4). Additionally, the veins do not cluster by thickness, as it can be seen in Fig. 3-4, meaning that they were formed under the same stresses, regardless of their thicknesses.

The heights of the pressure compartments are at least equal to the depths intervals (10-15 m). There is a possibility that the pressure compartments extend to greater heights, but in the absence of data over greater intervals, this cannot be proven.

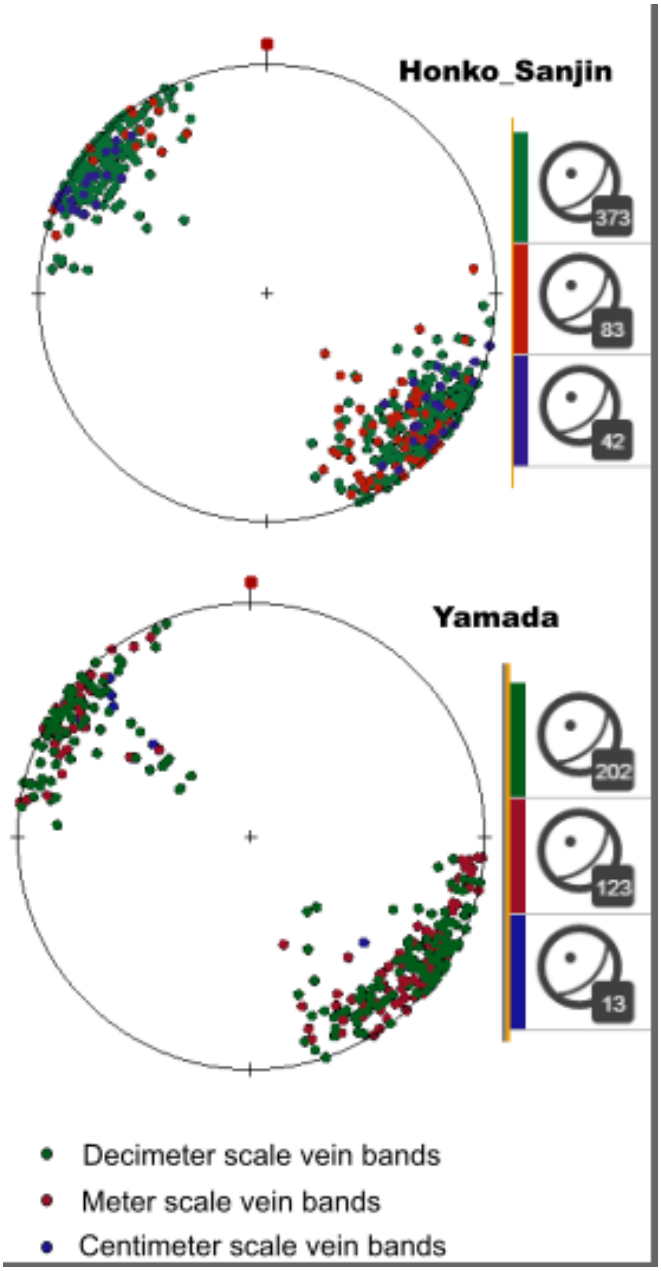

Fig. 3-4 Equal-area projection of the measured veins by width. Decimeter-scale veins make up the majority of the veins in Hishikari.

3.4 Variations of the DPI between the Honko-Sanjin and the Yamada sub-deposits

The driving pressure ratio in the Honko-Sanjin sub-deposits (0.24) is higher than that in the Yamada sub-deposit (0.19). This could be due to fluid pressure differences between the two areas or to variable differential stress. However, the consistency of the stress state M throughout the Hishikari deposit suggests that the differential stress was roughly the same everywhere. Thus, the spatial variation of the driving pressure ratio could mean that the fluid pressure was higher in Honko-Sanjin than in Yamada. This is consistent with the fact that Keisen veins, part of the Honko-Sanjin sub-deposit, were the main fluid conduit during mineralization (Sanematsu et al., 2005).

3.5 DPI vs Au grade in the Yamada sub-deposit

Alongside orientation data, I could collect the gold grades of the vein bands. I classified the veins in four groups based on their gold grades: <=10 g/t; 10 to 40 g/t; 40 to 100 g/t; and >=100 g/t Au. A frequency analysis of the different groups showed that the last group (Au>= 100 g/t) has the lowest frequency, far behind the other groups. A bar graph illustrating this analysis is shown in Fig. 3-5. Since highly overpressured ore fluids ascends less often than slightly overpressured ones during vein formation, I

suspected a possible correlation between the lowest frequency group (having the highest gold grade, Fig. 3-5) and higher driving pressures.

I obtained and analyzed orientation data from 22 veins with Au grades greater than or equal to 100 g/ton from the Yamada sub-deposit. Hexagons with blue contours in Fig. 3-6 indicate their orientations. The data points representing poles to veins with high Au grade are scattered over the clusters of dark and white data points, showing that both clusters, corresponding respectively to Stresses YA and YB, include data with Au grades greater than or equal to 100 g/ton. This means that a difference in DPI between the two groups (veins with Au grade >= 100 g/t and veins with Au grade <100 g/t) couldn't be related to the difference of stress states under which the veins formed. The DPI of the high-grade veins is at 0.24, higher than that of the other Yamada veins (0.19), thus indicating that very rich veins were formed from ore fluids with higher driving pressures in the Yamada sub-deposit.

This is further supported by the fact that the veins in the Honko-Sanjin sub-deposits have generally higher Au grades compared to the veins in the Yamada sub-deposit; and the veins in Honko-Sanjin sub-deposits also have a higher driving pressure (0.24) compared to the veins in Yamada sub-deposit (0.19). This result suggests that the gold grade was controlled by fluid pressure.

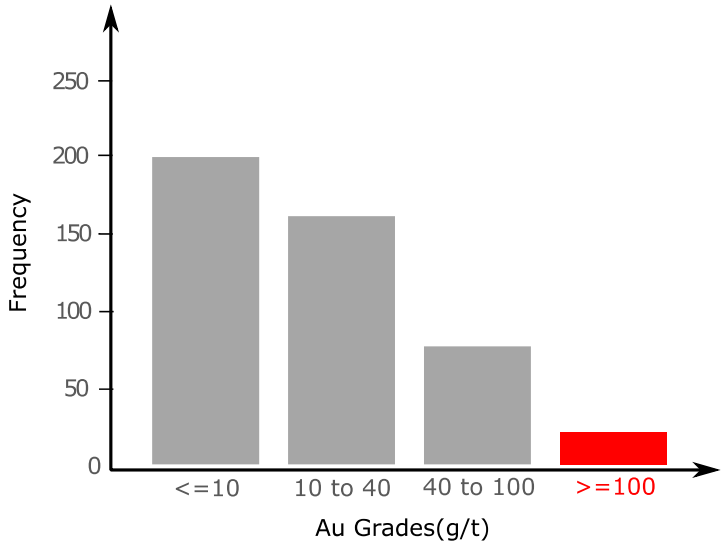

Fig. 3-5 Frequencies of the measured veins by gold grade ranges

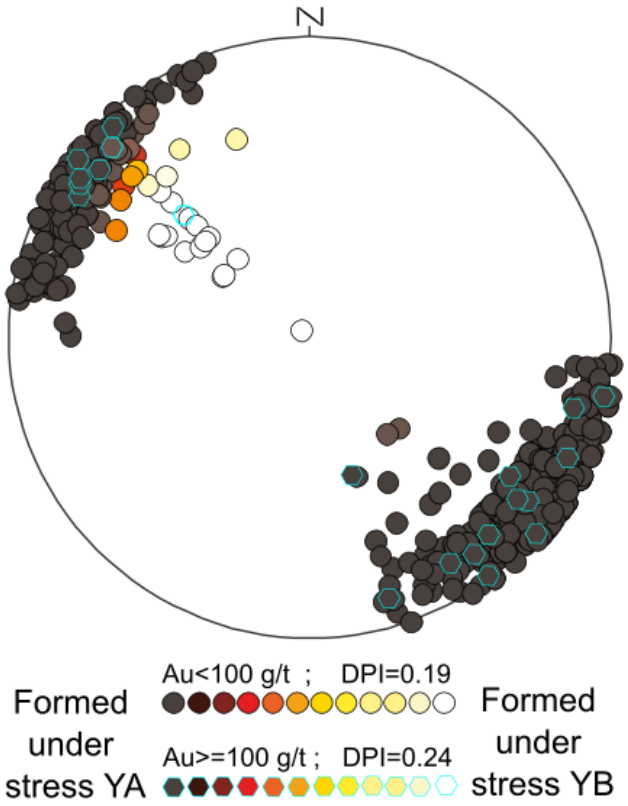

Fig. 3-6 Lower-hemisphere, equal-area projection of the orientations of the veins from the Yamada sub-deposit. The hexagons with blue contours indicate the veins with Au grades >= 100g/t. The veins with very high grades are found in both Stresses YA and YB. So their DPI is independent from the stress state. The DPI of the very high-grade veins appears to be higher than that of the rest of the veins in Yamada.

3.6 Chapter 3 summary

In this chapter, the Driving Pressure Index has been defined. The main information is the occurrence in Hishikari of pressure compartments bound by pressure seals. They were episodically broken and re-created, following the intermittent mechanics of vein formation.

Moreover, the high-grade veins are associated with higher fluid pressures, suggesting that fluid pressure controlled gold grade during the mineralization.

Fluid flow is a consequence of the existence of a hydraulic potential gradient, which the emplacement of a heat anomaly can cause (among other factors) (Chi and Xue, 2011).

The next chapter presents the physical and geometric characteristics of the heat source in Hishikari.

The main results in Chapter 2 and Chapter 3 have been published as an original research article entitled ‘’Paleostress and fluid-pressure regimes inferred from the orientations of Hishikari low sulfidation epithermal gold veins in southern Japan’’ in the Journal of Structural Geology with the DOI: https://doi.org/10.1016/j.jsg.2018.03.002 .

4. Geometric and physical constraints on the heat source of the Hishikari mineralizing hydrothermal system

4.1 Background

Epithermal deposits typically form at shallow depths < 1 km (Sillitoe, 2015) from hydrothermal activity. As such, their occurrence is owed to the interplay between structural, thermal as well as fluid circulation processes (Cox, 2005). A heat anomaly (heat source) creates fluid circulation cells that drive fluid flow through permeable layers, pre-existing fractures and/or fractures generated by the fluid circulation itself (hydrofractures) (Cox and Etheridge, 1989; Chi and Xue, 2011). At locations where boiling triggered by pressure drop and/or fluid mixing with meteoric water occurs, the fluids deposit metal-rich hydrothermal minerals inside the open spaces (Fig. 4-1) (Hedenquist and Henley, 1985; Matsuhisa and Aoki, 1994; Takahashi et al., 2017). In some cases, the heat anomaly, which is usually a magma intrusion, is also instrumental in creating the fluid circulation paths and controlling the localization of ore deposits (Koide and Bhattacharji, 1975; Sasada, 2000) as it is the case in the Kushikino deposit (Fig. 1-1) (Morishita and Kodama, 1986; Morishita and Nakano, 2008).

Therefore, it is important for a better understanding of such mineralizations to physically and geometrically constrain the heat source (temperature, depth, shape, excess pressure). The aforementioned constraints will improve the accuracy of the coupled modeling of ore deposits that take into account deformation, fluid flow, thermal and chemical processes (Hobbs et al., 2000).

Geothermal systems are modern analogues of paleo-hydrothermal systems that formed epithermal deposits (Hedenquist and Lowenstern, 1994). Hence, the same

methods used in geothermal studies can be used to determine the conditions under which epithermal deposits were formed. Some of those methods include thermal modeling to estimate the bottom temperature of a geothermal reservoir, using known thermal properties of country rocks and reference temperature data from geothermal wells for the choice of the best-fit models. Few examples include the study of the Larderello geothermal field in Italy (Della Vedova et al., 2008) and that of the Wairakei-Tauhara geothermal system in New Zealand (Mannington et al., 2004).

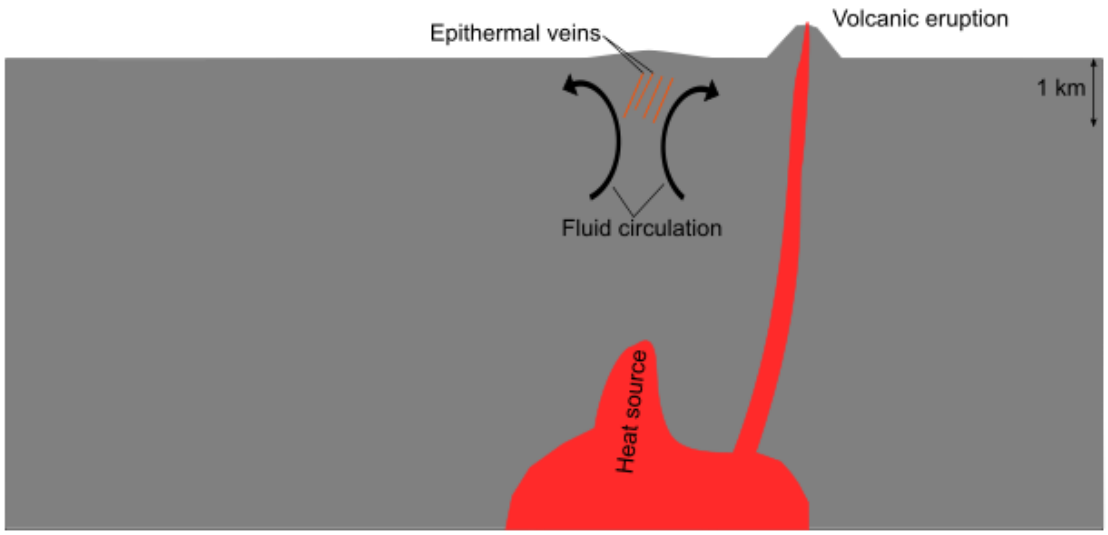

Fig. 4-1 Simplified schematic illustration of epithermal deposits and the elements that lead to their formation.

Thermal modeling can be used to estimate the depth and temperature of the heat source in epithermal deposits, provided that reference data are available for comparison. Fluid inclusion homogenization temperatures are reference data suitable for the choice of the best-fit models. Moreover, if the composition of the magma is known, it is

possible to subsequently calculate the pressure using geobarometers (Hammarstrom and Zen, 1986; Anderson and Smith, 1995) and derive the overpressure from it.

The heat source of the mineralization at Hishikari is thought to be a magma chamber from which originates the Shishimano Dacite (1.7-0.5 Ma). According to Hosono and Nakano (2003), the Shishimano Dacite is spatially and temporally related to the Hishikari deposit. The Shishimano Dacite is comprised of clots of plagioclase, hornblende and magnetite (Hosono and Nakano, 2003). So I assume that the heat source magma has the same mineralogical and chemical composition as the Shishimano Dacite.

In this chapter, I run several 1D vertical thermal models over stratigraphic columns obtained from boreholes (NEDO, 1991) or cross-sections (Etoh et al., 2002; Etoh, 2002) respectively around and in the Hishikari mine (Fig. 4-2). For each model, the depth and temperature of the heat source were chosen and the temperature over the stratigraphic column was calculated every 10 m. I compared the calculated temperatures to the fluid inclusion homogenization temperatures (NEDO, 1991; Etoh et al., 2002; Etoh, 2002; Sanematsu et al., 2006; Sanematsu, 2007) by calculating the Root Mean Square error (RMSe) of each model. The best-fit models were the ones that minimized the RMSe. I further proposed a cooling history for the heat source. Finally, I discussed the shape of the magma chamber and estimated its excess pressure.

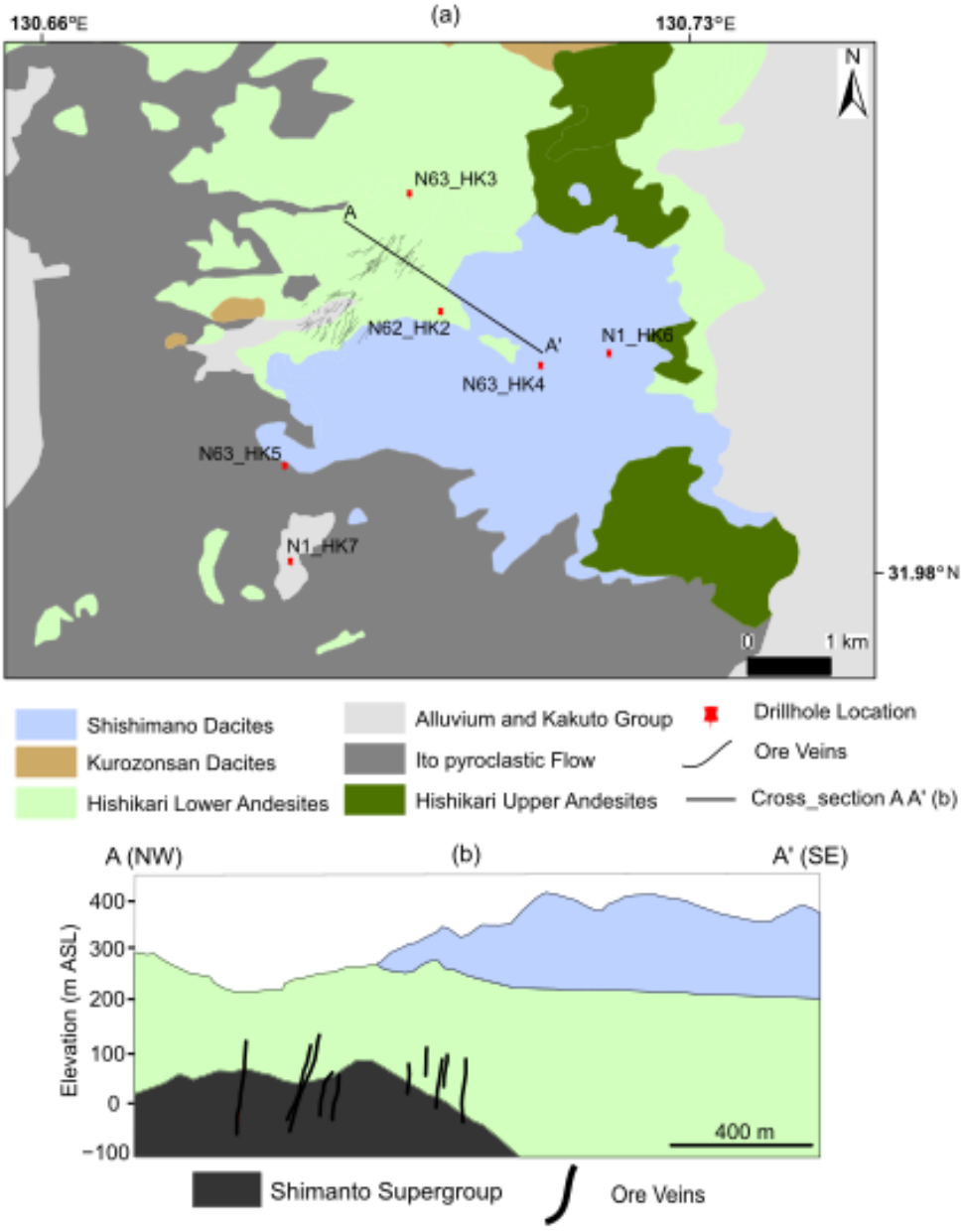

Fig. 4-2 Geology of the Hishikari deposit and surroundings. Widespread volcanism occurred in the area prior to, during and after the mineralization. The location of the drillholes and the cross-section used to make stratigraphic columns for the temperature modeling are also indicated (NEDO, 1991).

4.2 Method

In this study, 1D vertical heat conduction is modeled with the finite element method. I consider the propagation of heat from the heat source (bottom of the model) to the top of a stratigraphic column obtained from drillholes in the vicinity of the mine or cross-sections inside the mine.

In the case of heat propagation by conduction, the heat equation in three dimensions is:

$$\frac{\partial T}{\partial t} = \frac{k}{\rho C_p} * \left(\frac{\partial^2 T}{\partial^2 x} + \frac{\partial^2 T}{\partial^2 y} + \frac{\partial^2 T}{\partial^2 z} \right)$$

Where T = temperature, t = time, k = thermal conductivity, ρ = density, C_p = Specific heat capacity.

Assuming no lateral variation of the temperature and steady-state heat conduction (no temperature variation over time), the equation becomes:

$$\frac{\partial^2 T}{\partial^2 z} = 0$$

This equation can be solved if values at the boundaries are known. It is a boundary value problem that can be numerically solved by using the finite element method. The finite element method consists of discretizing a domain (geometry) into finite elements and calculating an unknown parameter for each element by solving partial differential equations. I used the open source finite element software Open Geo Sys (OGS)

(Watanabe et al., 2012; Böttcher et al., 2016; Kolditz et al., 2015). Steady-state heat conduction in a layered geological system using OGS is detailed by Böttcher et al. (2016).

Three parameters are particularly important in this model (i.e. the geometry of the model, the boundary conditions and the thermal properties of the rocks). The thermal properties of the rocks are known from NEDO (1991) (Table 4-1). The surface boundary condition is also fixed at a temperature of 15°C after Bottcher et al. (2016). The procedure consists of varying the bottom boundary condition (heat source temperature) from 250°C to 1200 °C with a step of 50 °C. The lower bound of the temperature range is justified by the fact that the highest average fluid inclusion homogenization temperature recorded in the mineralized veins is 230 °C (Sanematsu et al., 2005), although temperatures as high as 300 °C were recorded in the drillholes outside the mine (NEDO, 1991). The upper bound of the temperatures is taken from Francis (1993). According to this author, temperatures of dacitic magmas range between 800°C and 1100°C, whereas andesitic magmas can range between 950°C and 1200°C. There is abundant andesitic and dacitic volcanism in the Hishikari area throughout the mineralization time (Izawa et al., 1990). I thus took the maximum of the two (1200 °C)

to test all the possibilities, although Hosono and Nakano (2003) suggested that the heat source is related to the dacitic volcanism.

Concurrently, the geometry is varied by changing the bottom depth (heat source depth) from 2 km to 10 km with a step of 1 km. The lower limit of the depth range is set at 2 km because drillholes that reached 1.5 km depth in and around the mine did not intersect Shishimano Dacites beneath the Shimanto Supergroup (NEDO, 1991). The upper limit is justified by the fact that a magneto-telluric survey located a molten zone at a depth of 10 km in the Hishikari area (Izawa et al., 1990).

Table 4-1 Thermal properties of the different rock units used in this modeling.

Material	Rock Unit		Thermal conductivity ($W.m^{-1}.K^{-1}$)	Heat Capacity ($J.kg^{-1}.K^{-1}$)	Density ($kg.m^{-3}$)	Porosity
		Shishimano Dacite	1.24	810	2330	0.064
		Yotsueda Andesite	1.37	810	2490	0.099
		Goshiki Andesite	0.55	795	1680	0.379
		Shinkawa Andesite	1.23	810	2240	0.144
		Yamadagawa Andesite	1.92	810	2270	0.166
		Kusumoto Andesite	1.97	815	2620	0.035
		Shinkawa Conglomerate	0.83	795	1680	0.261
		Shimanto Supergroup	3.23	775	2640	0.028

Specific heat capacity data are from Waples and Waples (2004) assigned to each of the Hishikari rock types as described by NEDO (1991). The rest of the data are from NEDO (1991).

Each bottom-depth-temperature pair is considered as a model for which the temperature is calculated every 10 m. Locally, the mesh resolution is refined around depths for which fluid inclusion homogenization temperatures are available. Hence, 180 models were obtained for each stratigraphic column. Each model is then compared to the fluid inclusion homogenization temperatures through the calculation of the Root Mean Square error (RMSe). The model with the minimal RMSe is the best-fit for the fluid inclusion data (reference data). Therefore, the heat source depth of that model and its heat source temperature are considered as the optimal parameters for that stratigraphic column (Fig. 4-3).

This procedure was applied to eight stratigraphic columns (six drillholes outside the mine (Fig. 4-2a; Fig. 4-4) and two columns inferred from a cross-section in the mine for the Honko and Sanjin sub-deposits (Fig. 4-2b; Fig. 4-4)).

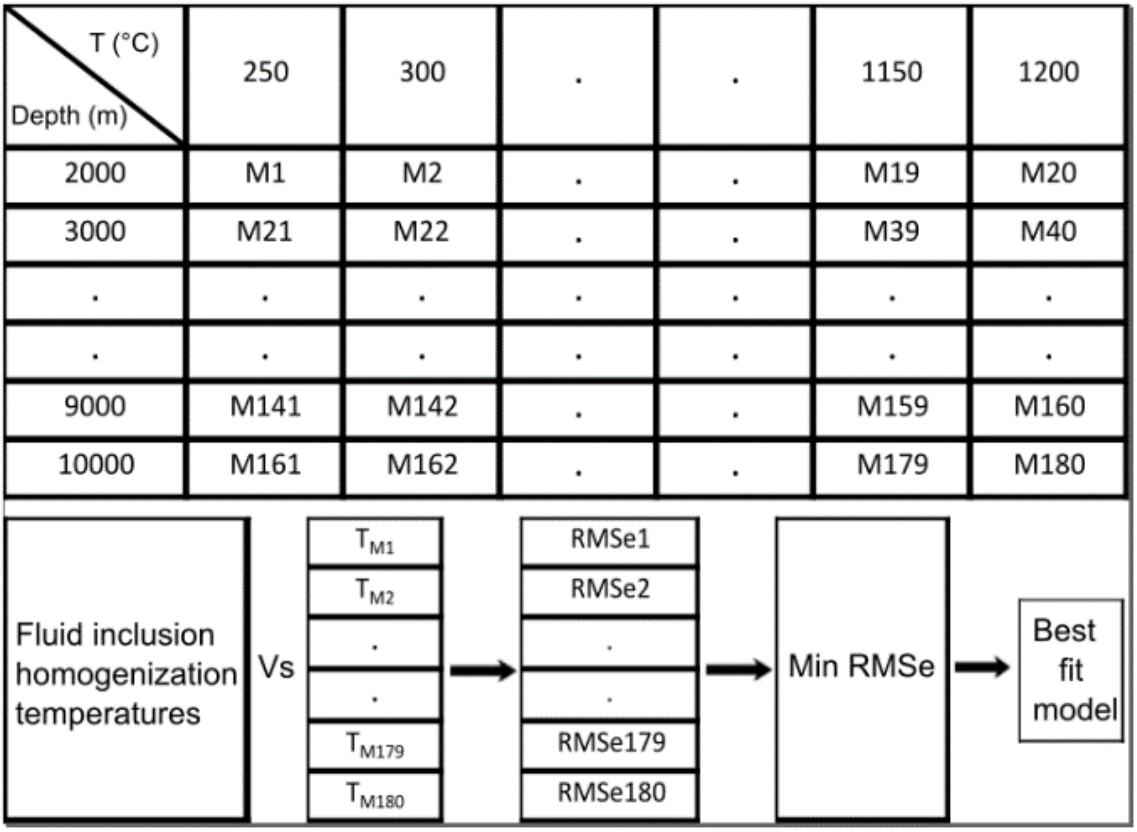

Fig. 4-3 Procedure used in this study for the evaluation of the depth and temperature of the heat source. The depth has been varied from 2 km to 10 km with a step of 1 km and for each depth, the temperature has been varied from 250°C and 1200°C with a step of 50°C. The computed temperature for each model is then compared to the fluid inclusion homogenization temperatures by calculating the Root Mean Square error. The model showing the minimum RMSe is chosen as the best-fit model.

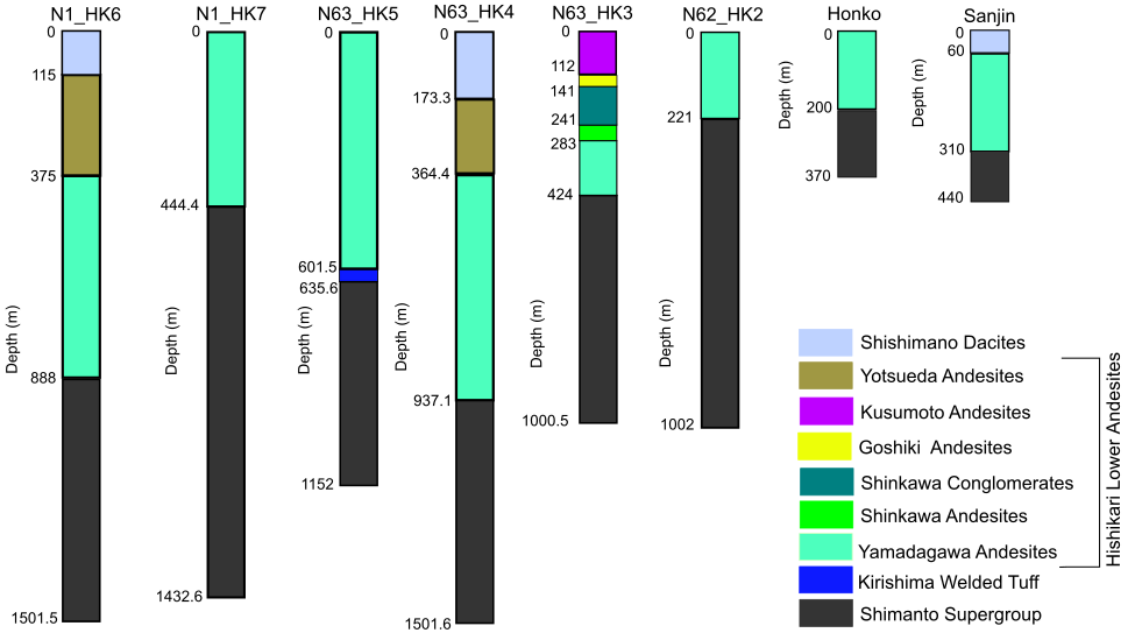

Fig. 4-4 Stratigraphy in the drillholes N62_HK2, N63_HK3 and N63_HK4, and of the the location of which are indicated in Fig. 4-2a (NEDO, 1991); the stratigraphy in Honko and Sanjin sub-deposits inferred from the cross-section shown in Fig. 4-2b is also indicated. In the modeling procedure, it is considered that the Shimanto Supergroup continues beyond the maximum depth reached by the drillhole or the cross-section until the depth of the heat source for each model.

4.3 Results

4.3.1 N62_HK2

For the drillhole N62_HK2, the best-fit 1D vertical heat conduction model is the one with a bottom (heat source) temperature of 1150 °C at a depth of 9 km (Fig. 4-5). The RMS error is 46°C. The reference data available for this drillhole were 20 fluid inclusion homogenization temperatures at depths ranging from 227.6 m to 927.9 m.

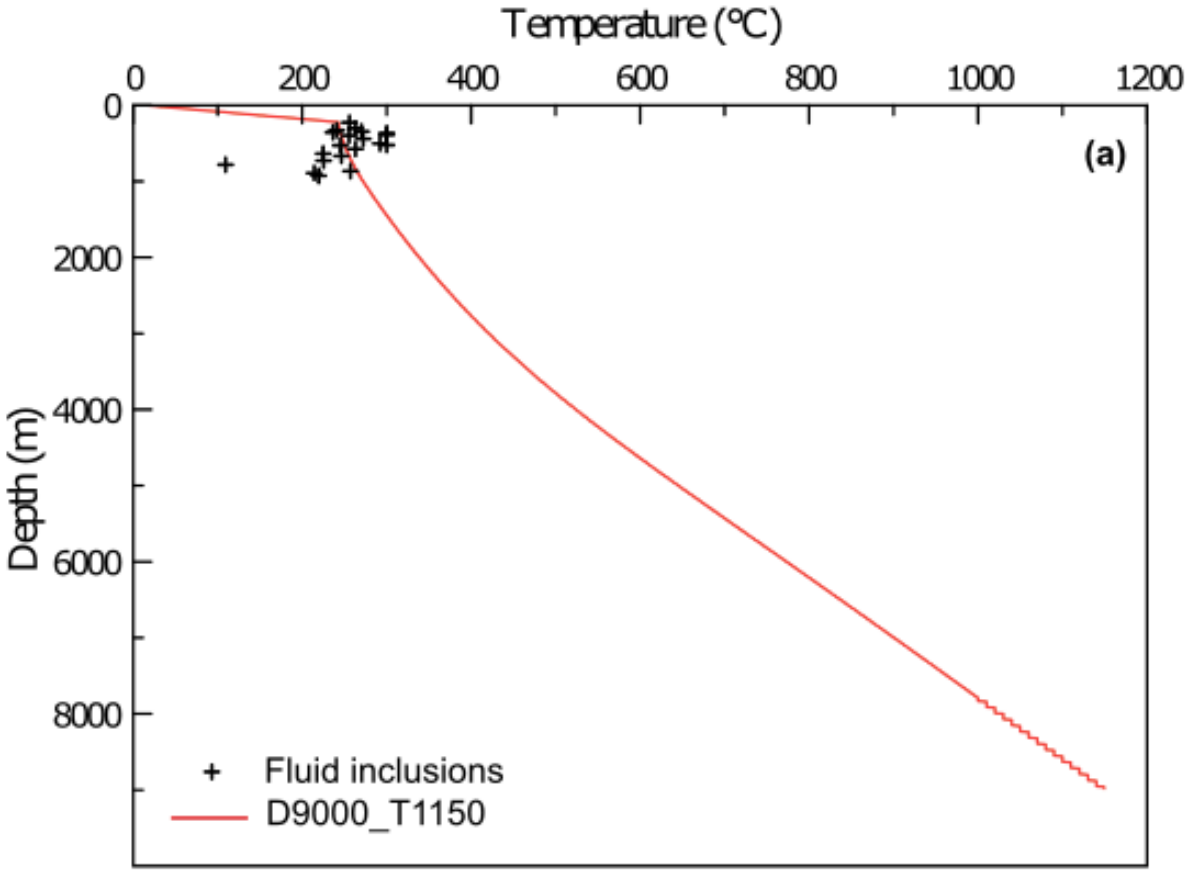

Fig. 4-5 Computed Temperature-Depth profiles from the best-fit models for N62_HK2. Fluid inclusion homogenization temperatures that served as reference data are also plotted.

4.3.2 N63_HK3

The best-fit 1D vertical heat conduction model for this drillhole located the heat source at 9 km but with a temperature of 500 °C (Fig. 4-6). The RMS error was very low (1.32 °C) but this could be due to the low number of fluid inclusion homogenization temperatures (two) and their relatively narrow depth range (609.3 m to 649.5 m).

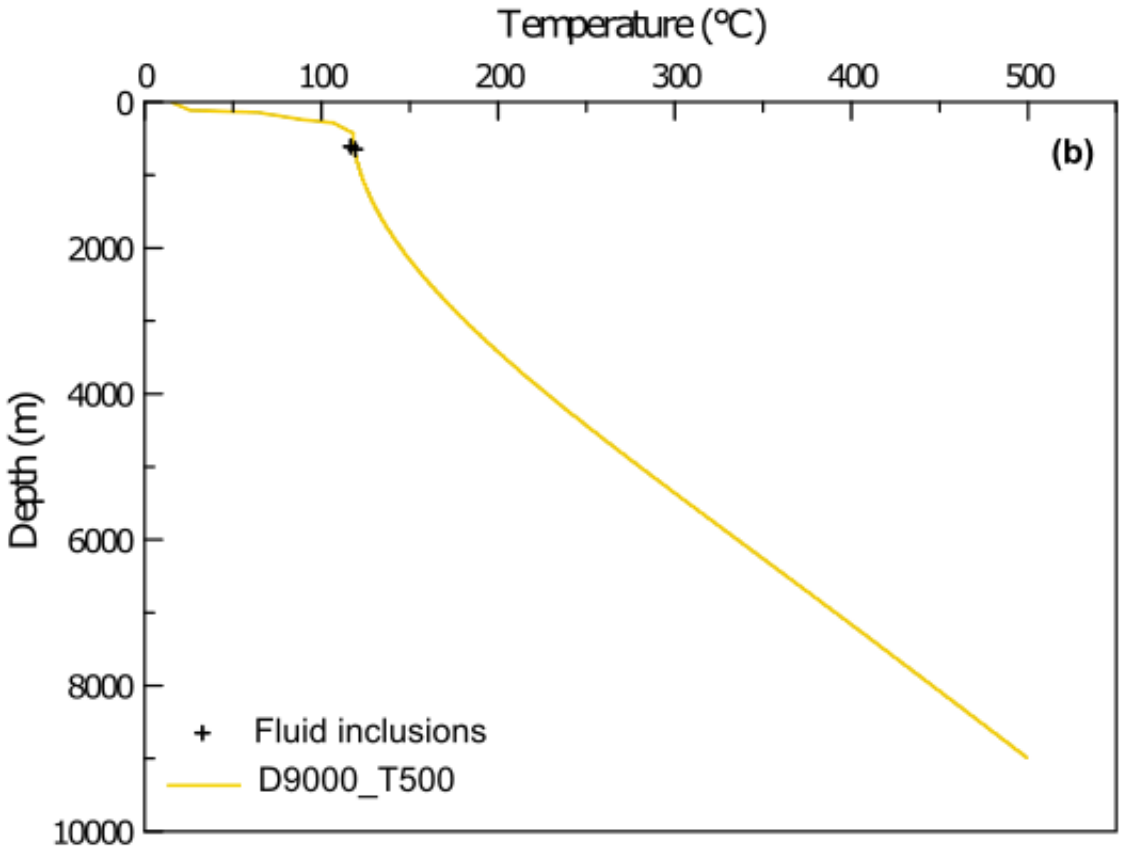

Fig. 4-6 Computed Temperature-Depth profiles from the best-fit models for N63_HK3. Fluid inclusion homogenization temperatures that served as reference data are also plotted.

4.3.3 N63_HK4

The optimal 1D vertical heat conduction model for the last drillhole is that which located the heat source at 9 km with a lower temperature of 300°C (Fig. 4-7). The error is 23.64 °C and the computed temperatures were compared to eight fluid inclusion homogenization temperatures found between 719 m and 1474.8 m.

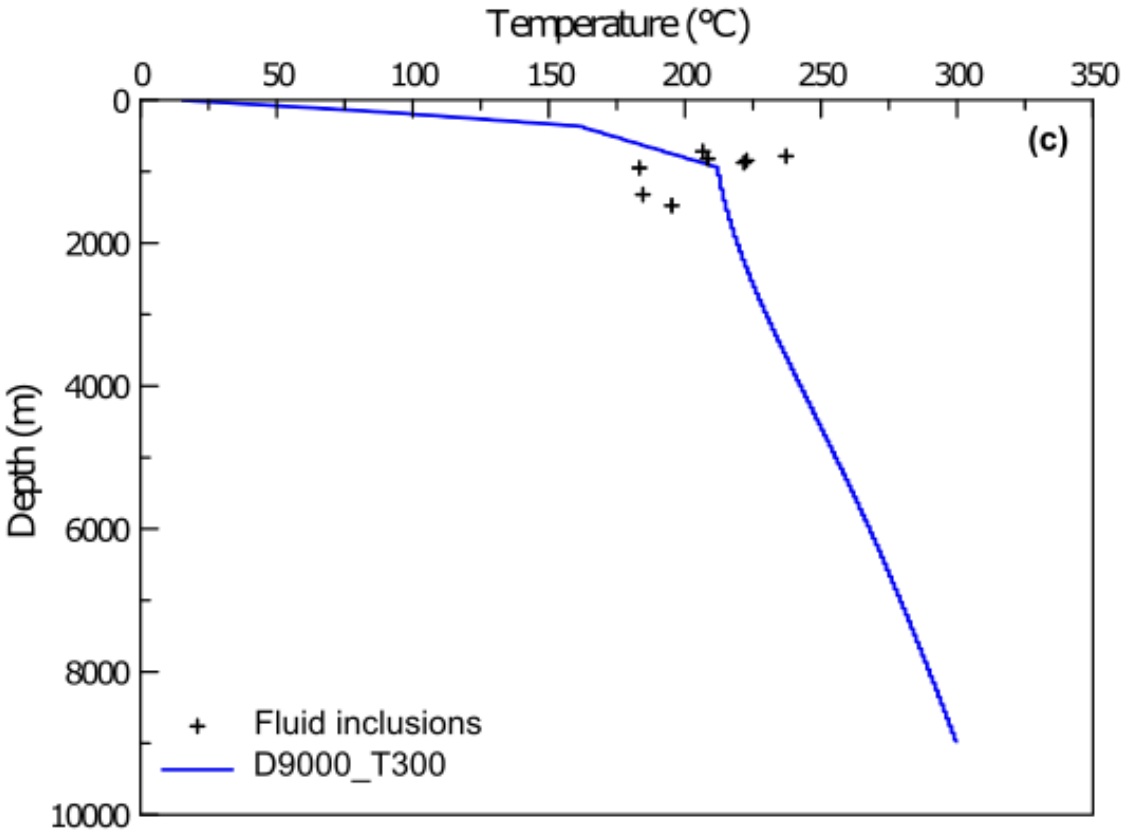

Fig. 4-7 Computed Temperature-Depth profiles from the best-fit models for N63_HK4. Fluid inclusion homogenization temperatures that served as reference data are also plotted.

4.3.4 Honko

The calculations on the stratigraphic column representing the center of the Honko sub-deposit gave a bottom temperature of 1150 °C and a bottom depth of 9 km for the best-fit 1D vertical heat conduction model (Fig. 4-8).

Reference data were separated in two subsets. Homogenization temperatures of fluid inclusions from columnar adularia (thought to be from early mineralization stage) were distinguished from those obtained from later quartz (Etoh, 2002). The former represent ten inclusions from depths between 185 m and 320.5 m and the latter represent four inclusions over the same depth range. The error against inclusions in columnar adularia is 28.65°C while that against inclusions in quartz is 21.02 °C.

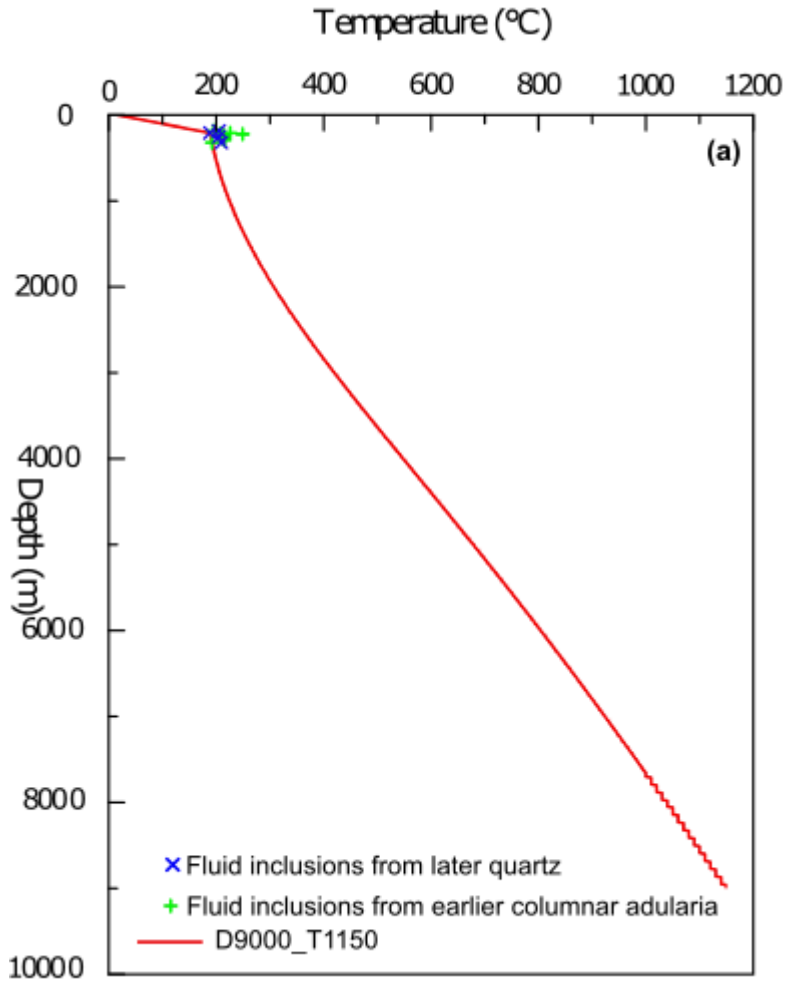

Fig. 4-8 Calculated Temperature-Depth profiles inside the mine for the Honko sub-deposit. The fluid inclusion homogenization temperatures from earlier columnar adularia are distinguished from fluid inclusion homogenization temperatures from later quartz (Etoh, 2002).

4.3.5 Sanjin

The best-fit 1D vertical heat conduction model for the stratigraphic column representing the Sanjin sub-deposit is that with a bottom depth of 9 km and a bottom temperature of 750 °C (Fig. 4-9). The fluid inclusion homogenization temperatures used for the comparison are three, over a depth range from 315 m to 345 m. The error is 8.22°C.

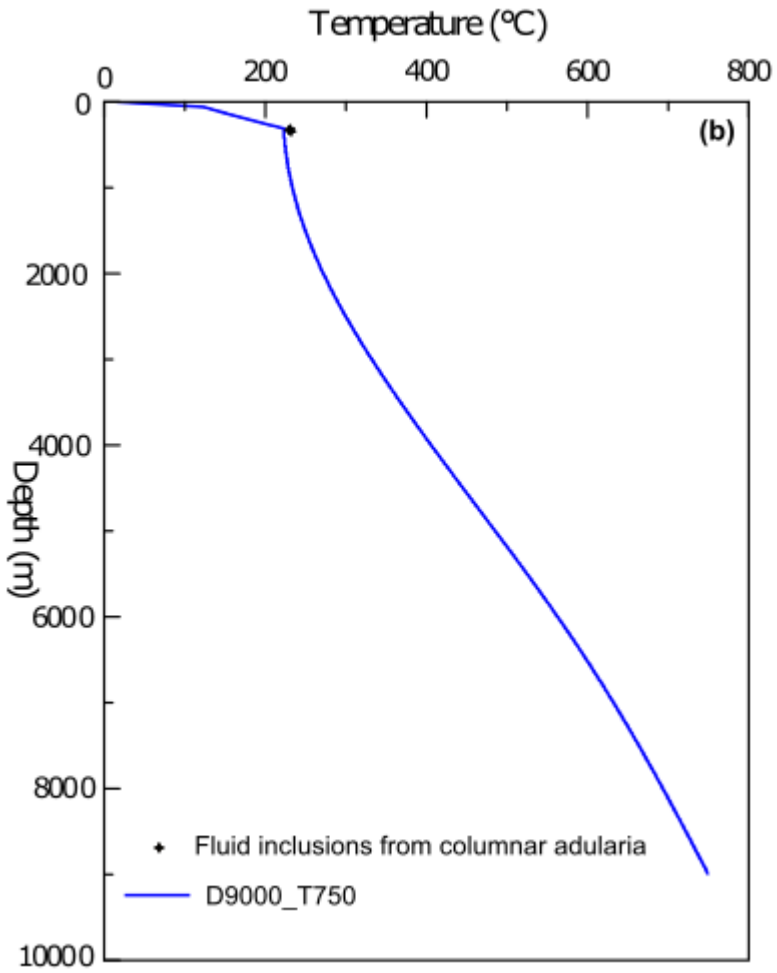

Fig. 4-9 Calculated Temperature-Depth profiles inside the mine for the Sanjin sub-deposit. The fluid inclusion homogenization temperatures are also plotted.

4.3.6 N63_HK5

For the drillhole N63_HK5, the best-fit 1D vertical heat conduction model is the one with a bottom temperature of 450 °C and a depth of 9 km (Fig. 4-10). However, the RMSe is higher than for any other drillhole, it is 127.59 °C. The reference data available for this drillhole were 12 fluid inclusion homogenization temperatures at depths ranging from 211.3 m to 932.3 m.

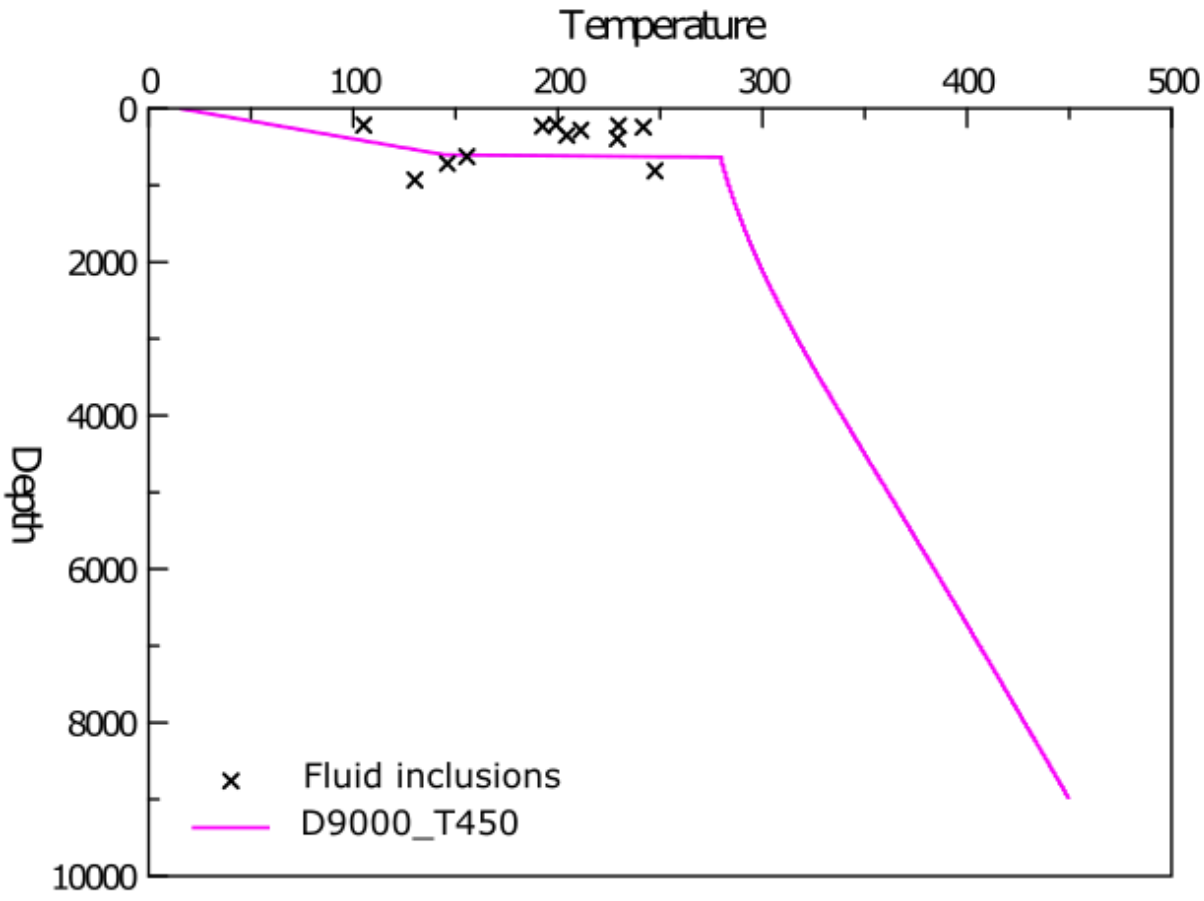

Fig. 4-10 Computed Temperature-Depth profiles from the best-fit models for N63_HK5. Fluid inclusion homogenization temperatures that served as reference data are also plotted.

4.3.7 N1_HK6

In the calculation performed on the stratigraphic column from the drillhole N1_HK6, the best-fit 1D vertical heat conduction model is the one with a bottom temperature of 1100 °C at a depth of 9 km (Fig. 4-11). The RMS error is 27.65 °C. The reference data available for this drillhole were 10 fluid inclusion homogenization temperatures at depths ranging between 645 m and 1451.5 m.

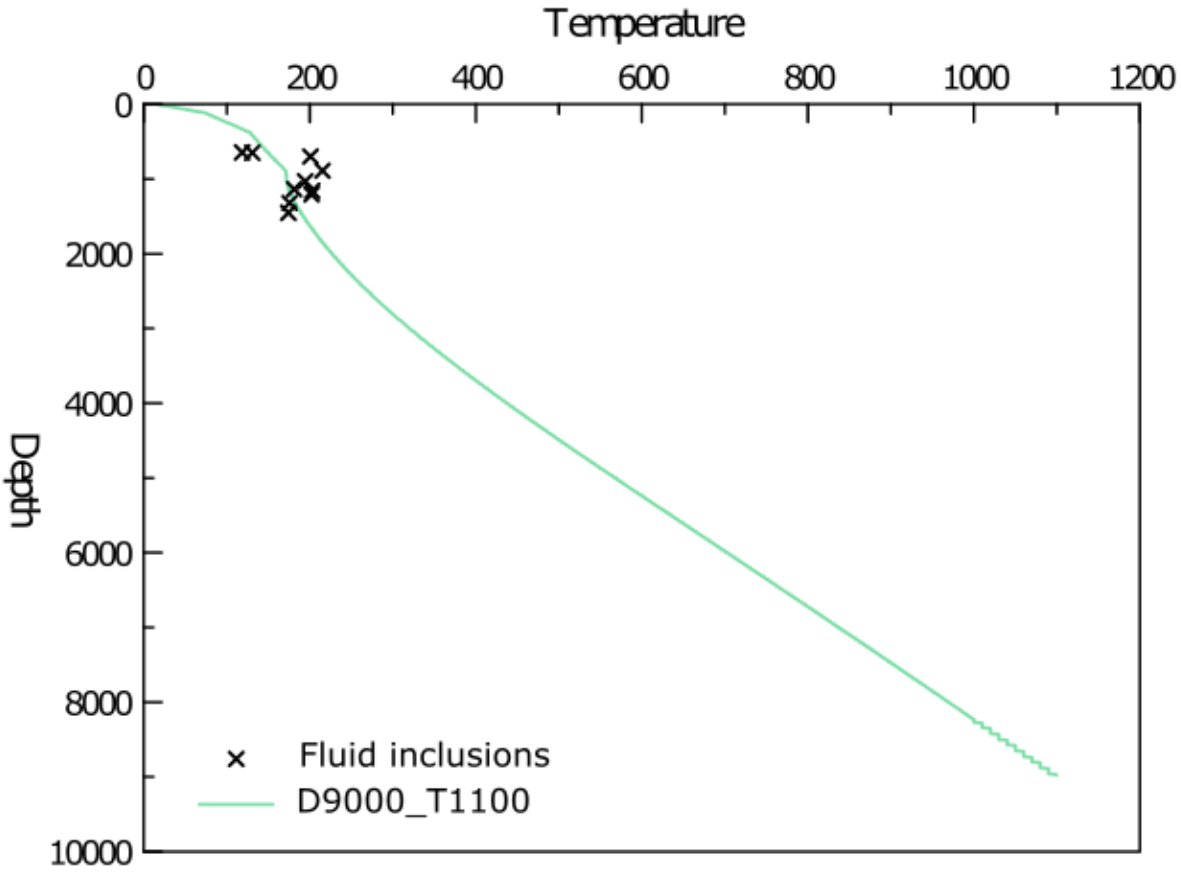

Fig. 4-11 Computed Temperature-Depth profiles from the best-fit models for N1_HK6. Fluid inclusion homogenization temperatures that served as reference data are also plotted.

4.3.8 N1_HK7

In the last drillhole, N1_HK7, the best-fit 1D vertical heat conduction model is the one with a heat source temperature of 1150 °C and a heat source depth of 9 km (Fig. 4-12). The RMSe is 55.58 °C. The reference data available for this drillhole were 17 fluid inclusion homogenization temperatures at depths ranging from 150 m to 1008.6 m.

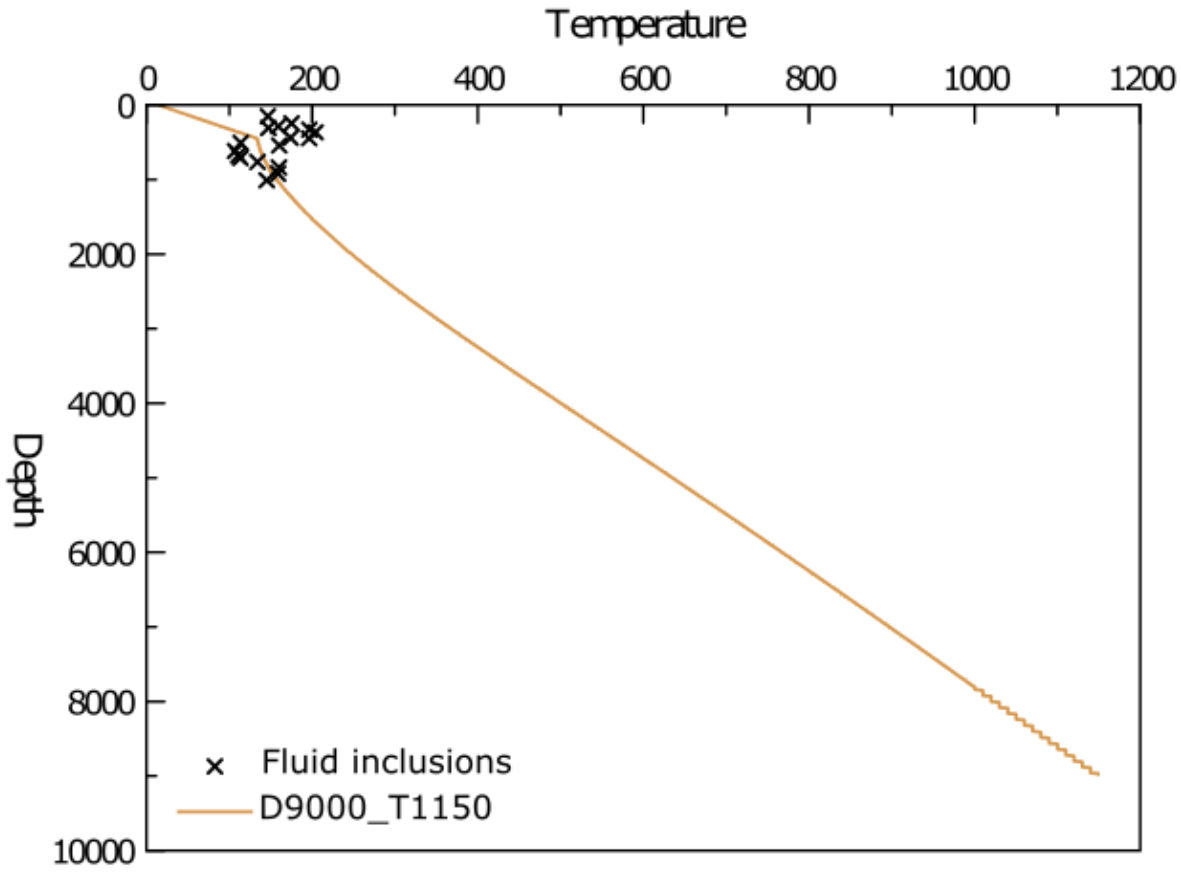

Fig. 4-12 Computed Temperature-Depth profiles from the best-fit models for N1_HK7. Fluid inclusion homogenization temperatures that served as reference data are also plotted.

4.4 Discussion

4.4.1 Depth of the heat source and heat distribution

The depth of the heat source for all the models matching the reference fluid inclusion homogenization temperatures is consistently situated at 9 km. This depth is consistent with the presence of a molten zone at 10 km (Izawa et al., 1990). The heat distribution along a NW-SE cross-section shows a correlation between the rock type variation and the temperature variation (Fig. 4-13). This is explained by the notable difference in thermal conductivity between the upper Hishikari Lower Andesites (HLA) (with an average thermal conductivity of 1.33 $W.m^{-1}.K^{-1}$) and the lower Shimanto Supergroup (SSG) sediments (with an average thermal conductivity of 3.23 $W.m^{-1}.K^{-1}$).

In the upper 1.5 km of the profile, a comparison between the calculated temperatures and the fluid inclusion homogenization temperatures shows that the former are generally higher (Fig. 4-13c, Fig. 4-14 and Fig. 4-15). The difference could be explained by the presence of a layer acting as a thermal seal between the two main rock units. Such a layer could be one with a much lower thermal diffusivity than the upper HLA and Lower SSG. Kirishima Welded Tuff is recognized to the south-east of the Hishikari deposit at a depth of 900 m and has a thermal conductivity (0.85 $W.m^{-1}.K^{-1}$) an order of magnitude lower than those of the surrounding layers.

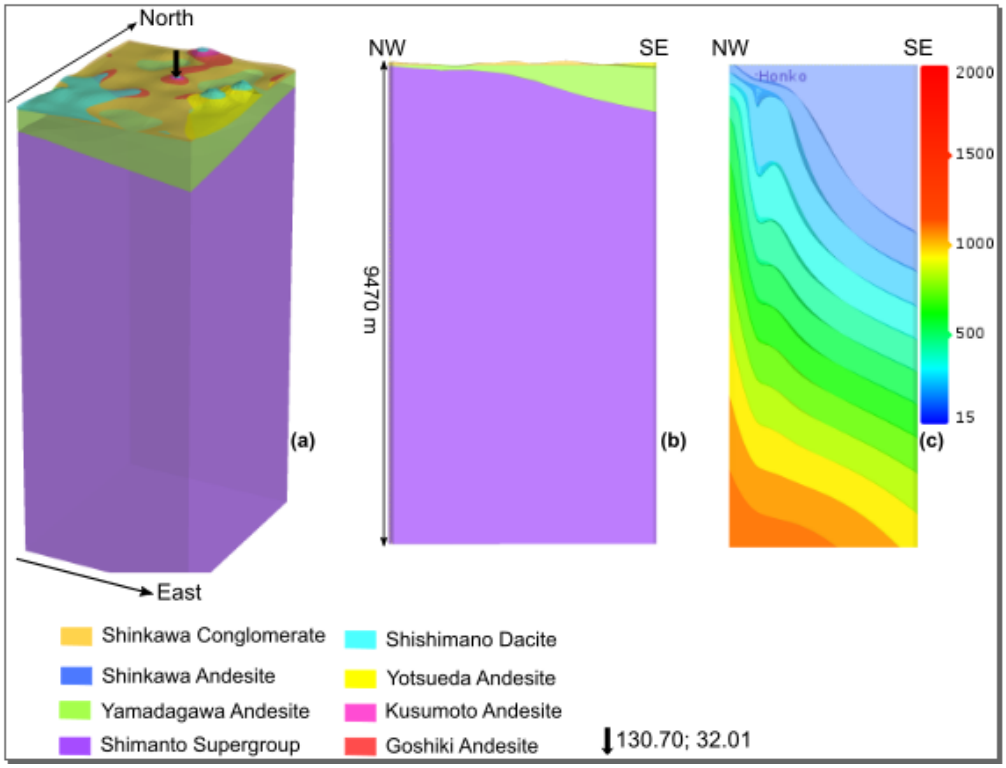

Fig. 4-13 (a) 3D Geological model of the Hishikari area; (b) NW-SE slice of the 3D model; (c) (computed) temperature distribution over the slice shown in (b). A correlation between the temperature variation and the lithology variation can be noticed, which is coherent as the thermal conductivity of the rocks controls heat conduction.

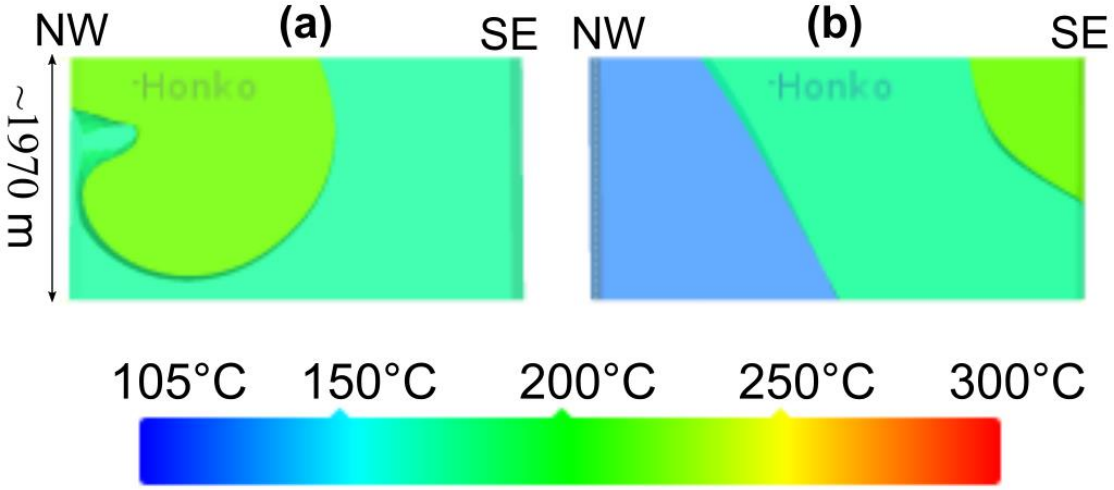

Fig. 4-14 Fluid inclusion homogenization temperature distribution in the upper 1.5 km of the NW-SE profile. (a) represents the homogenization temperatures that match a heat source temperature of 1150°C (early mineralization stage; see section 4.4.2); (b) represents the homogenization temperatures that match a heat source temperature of 500°C (post-mineralization stage; see section 4.4.2).

4.4.2 Temperature and cooling history of the heat source

The temperature of the heat source given by the calculations in Honko and N62_HK2 is 1150°C (Fig. 4-13c, Fig. 4-15a). Within error margins, this temperature is consistent with dacitic magma temperatures (Francis, 1993). In Honko, the distinctive evaluation of the model against fluid inclusions from columnar adularia and fluid inclusions from quartz gave the same temperature. This suggests that the temperature of the heat source remained constant throughout the mineralization time. However, the result in Sanjin gave a lower temperature of 750°C. Knowing that Sanjin has the highest fluid inclusion homogenization temperatures of all the sub-deposits in Hishikari (Sanematsu et al., 2005), this lower temperature is unlikely. The result for Sanjin could thus be unreliable due to the small number of fluid inclusion homogenization temperatures available as reference data (three).

The calculation in drillholes N1_HK6 and N1_HK7 (Fig. 4-11; Fig. 4-12), located respectively at 2 km to the south-east and 3.5 km to the south-west of the mine gave the same temperature of 1150 °C for the heat source. This not only confirms the heat source temperature during mineralization, but also suggests that the fluids were flowing in a SW-NE direction. It is consistent with the fact that the mineralization in Hishikari

started earlier in Yamada sub-deposit (located to the south-west of the Honko sub-deposit) (Sanematsu et al., 2005).

The results in N63_HK3 gave a heat source temperature of 500 °C (Fig. 4-15b). This drillhole is located outside the mine, and the veins from which the fluid inclusions were taken are likely to have formed after the main mineralization phase as no gold content were reported in them (NEDO, 1991). This suggests a cooling tendency of the heat source after mineralization. However, the number of reference data for the above-mentioned model was small (two), making the result unreliable. Therefore, other evidences are necessary. The calculation in the drillhole N63_HK5 (Fig. 4-10) located 3.5 km to the south-west of N63_HK3 gave a bottom temperature of 450°C. Moreover, the calculation in the drillhole N63_HK4 reveals a heat source temperature of 300 °C. This supports the hypothesis of a heat source temperature decrease after mineralization. The relative positions of drillholes N63_HK3, N63_HK4 and N63_HK5 and their similar temperatures (within error margins) also supports the hypothesis of a fluid flow pattern in a SW-NE direction, even after mineralization.

Based on the heat source temperatures yielded by the thermal modeling and discussed above, I propose a cooling history of the heat source of the Hishikari mineralizing hydrothermal system (Fig. 4-15). The temperature of the heat source

during mineralization was at 1075-1200°C and it cooled down to a temperature of 300-500°C after mineralization.

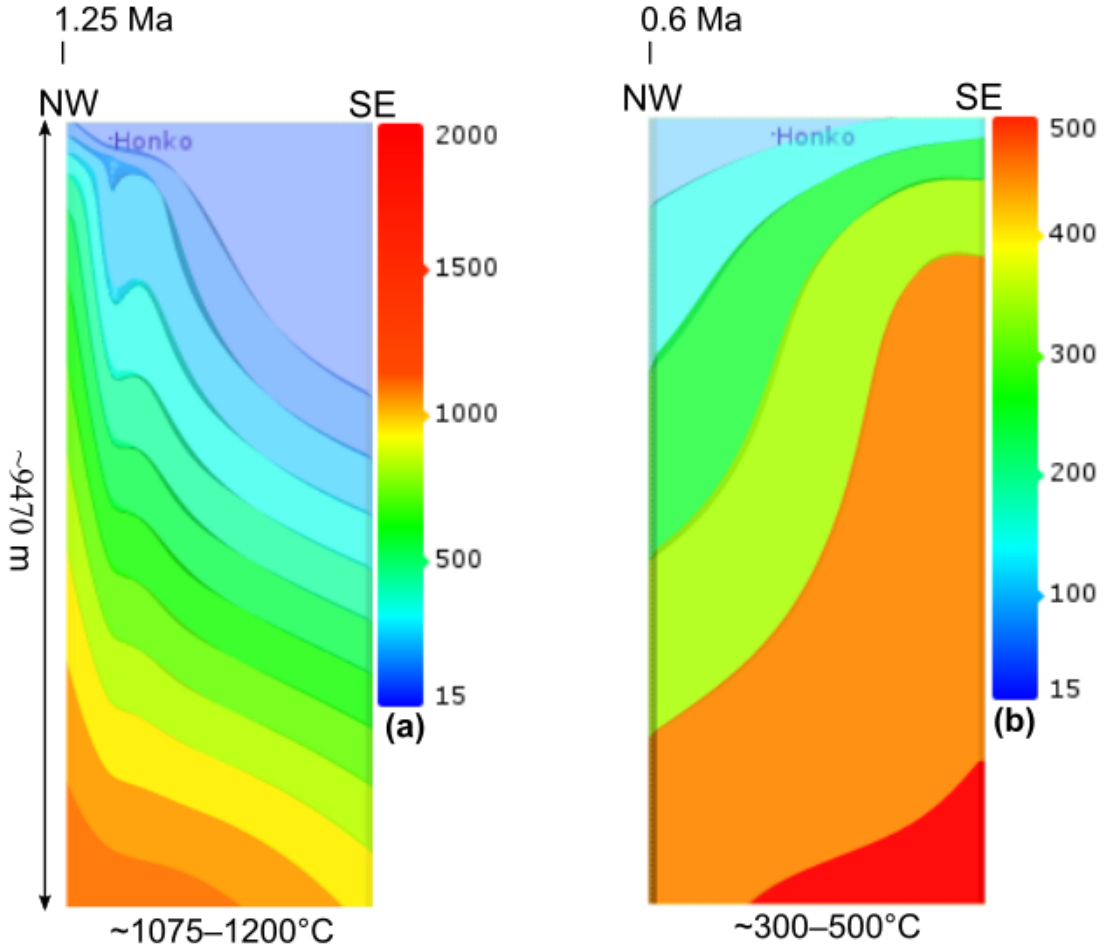

Fig. 4-15 Proposed cooling history of the heat source of the Hishikari mineralizing hydrothermal system. The heat source had a temperature of 1075-1200°C during mineralization stage then dropped to 300-500°C after the mineralization.

4.4.3 Implications on the overpressure and shape of the magma chamber

There is a basement uplift in Hishikari area, with a topographic high of the Shimanto Supergroup roof centered on the Honko sub-deposit (Izawa et al., 1990). This basement high has been discovered through a gravity survey that recognized a 1 km-wide gravity high extending over a length of 3 km in a NE-SW direction. The basement high has later been confirmed from exploration drilling and trenching (Izawa et al., 1990). For Naito (1993), the basement uplift is due to the emplacement of a magma chamber related to the Shishimano Dacite volcanic activity and has played a role in the faulting that provided paths for the fluids circulation. Thus, it is important to constrain the pressure regimes within the magma chamber that led to the uplifting.

The pressure within a magma chamber prior to eruption can be determined as the pressure at the time of hydrofracturing (the opening of the fracture through which the magma will ascend to the surface). It is known that the Shishimano Dacite erupted between 1.7 and 0.5 Ma (Hosono and Nakano, 2003), which spans over the mineralization time in Hishikari (1.25 to 0.6 Ma) (Sanematsu et al., 2006; Izawa et al., 1990; Sekine et al., 2002; Tohma et al., 2010) and beyond. So the pressure at the time of the first eruption can be considered as the maximum pressure within the magma chamber.

It was possible to estimate the pressure in the magma chamber from the Al-in-hornblende geobarometer. I used the model of Anderson and Smith (1995) which takes into account the effect of temperature. The pressure is given by the expression:

$$P(\pm 0.6) = 4.76 * Al - 3.01 - \left\{\frac{[T - 675]}{85}\right\} * \{0.530 * Al + 0.005294 * [T - 675]\}$$

Where P = pressure (kbar); T = temperature (°C); Al = Aluminum in hornblende (wt %).

The average Al-content of hornblende in the Hishikari Volcanic Rocks (HVR) is equal to 1.34 wt % in average (Hosono and Nakano, 2003). Hence, although this value was determined from a sample from the Kurozonsan Dacite, it is representative of the Al-content of hornblende of the Shishimano Dacite, because the Shishimano Dacite is part of the HVR (Hosono and Nakano, 2003). Since it is assumed that the heat source magma has the same chemical and mineralogical composition as the Shishimano Dacite (section 4.1), the Al-in-hornblende content of the heat source magma is also 1.34 wt %. I took the temperature as the one that prevailed towards the end of the Shishimano Dacite activity period, which was after the mineralization stage. The reason for this choice is that the samples from which the hornblende Al-content were measured were taken from outcrops (Hosono and Nakano, 2003), and there is no significant erosion due to the young age of the deposits. The late activity of Shishimano Dacite produced

lavas that covered up earlier pyroclastics (NEDO, 1991; Hosono and Nakano, 2003). Therefore, it is reasonable to think that the hornblende in the HVR that erupted at that time formed after the mineralization stage (between 0.6 and 0.5 Ma), when the magma chamber temperature was transitioning from 1075-1200°C to 300-500°C. The average of these temperature ranges is ~750°C; I used it in the calculation of the pressure in the magma chamber.

From the above parameters, the estimated pressure in the magma chamber was 238.63 MPa.

However, not all the pressure is responsible for deformations; the excess pressure or overpressure is the part of the pressure that leads to uplifting (Ellis et al., 2007) and/or to fracturing and dyke injection, which can result in an eruption if the magma reaches the surface (Gudmundsson, 2011). According to the same author, the total pressure is equal to the sum of the lithostatic pressure (overburden pressure) and the excess pressure:

$$P_t = P_l + P_e$$

Where P_t = total pressure, P_l = lithostatic pressure, P_e = excess pressure.

It follows that

$$P_e = P_t - P_l$$

The overburden pressure is calculated following the formula:

$$P_l = \rho g z,$$

ρ being the density, g the gravity acceleration and z the vertical extent of the rock column (depth).

The rock column is taken as the one in the Honko sub-deposit (Fig. 4-4) extended to the calculated depth of the magma chamber (9km). The calculated overburden pressure is equal to 232.09 MPa.

The pressure calculated from Al-in-hornblende geobarometer represents P_t. It follows from this that the overpressure or excess pressure in the magma chamber amounts to 6.54 MPa. This is consistent with the known values of excess pressures in magma chambers which range between 0.5 and 6 MPa with a maximum at 9 MPa and a usual value of 3 MPa (Gudmundsson, 2011).

There are three main ideal shapes for magma chambers: sphere, prolate ellipsoid and oblate ellipsoid (sill-like) (Gudmundsson, 1998 a, b, 2002). I calculated the radius of the magma chamber, assuming that it is spherical and using the Mogi point source model (Mogi, 1958). The result gives a radius an order of magnitude larger than the depth, which is in total contradiction with the condition for the Mogi model to apply to

a magma chamber: the radius of the magma chamber must be much smaller than its depth (Mogi, 1958). Thus, the magma chamber is non-spherical.

On the other hand, Gudmundsson and Nilsen (2006) indicate from numerical modelling that a sill-like magma chamber subject to tension may generate a ring fault and often a ring dyke. In the chapter 2 of this thesis, it was highlighted that the area was mainly subjected to extensional stress following previous authors (Naito, 1993; Uto et al., 2001). However, there is no record of a ring fault that formed during the mineralization which is more or less coincident with the eruption of the Shishimano Dacite. The earliest record of a caldera formation in the Hishikari area is at 0.3 Ma with the apparition of the Kakuto caldera whereas the mineralization as well as the Shishimano Dacite volcanic activity ended at 0.6-0.5 Ma. Hence, the likelihood that the magma chamber had an ellipsoidal oblate shape is low.

Therefore, a prolate ellipsoidal shape seems more probable for the magma chamber. Fig. 4-16 summarizes the geometric and physical characteristics of the heat source magma chamber during the main mineralization as proposed in this study.

4.5 Chapter 4 summary

In this chapter, the depth of the Shishimano Dacite has been estimated at ~9 km while its temperature was ~1075-1200°C. A cooling history of the intrusion has been proposed and the overpressure in the magma chamber calculated to be ~6.54 MPa. The volcano-tectonic history of the area suggests that the magma chamber was prolate ellipsoidal.

In the next chapter, I discuss the meaning of my study to the general understanding of the mineralization in Hishikari, as well as the remaining challenges.

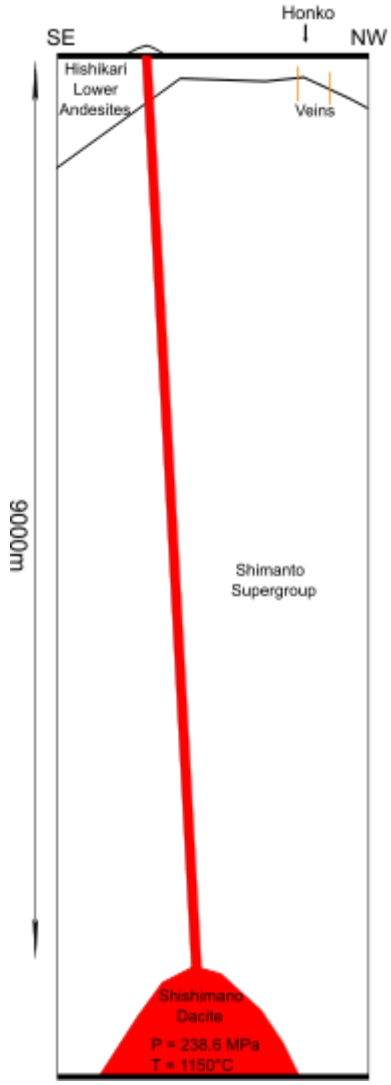

Fig. 4-16 Scaled representation of the Hishikari mineralizing hydrothermal system and the physical and geometric constraints put on it from this study (depth, pressure, temperature and shape of the magma chamber that acted as a heat source for the mineralization). The size of the magma chamber remains unknown.

5. General discussion

From the results of my study, arise two fundamental questions:

What was the exact role played by the basement uplift on the mineralization process?

Beyond the intermittent mechanics of epithermal vein formation, what caused/favored the occurrence of pressure seals?

5.1 The role of the basement uplift

Previous studies (Naito, 1993; Sanematsu et al., 2006; Morishita and Nakano, 2008) had suggested that the mineralization at Hishikari was mainly due to extension and fault movements resulting from the basement uplift. However, my results indicate that the quasi-totality of the veins in Hishikari formed under a stress state consistent with the regional tectonics of southern Kyushu during mineralization. It supports the conclusions of Uto et al. (2001) who reported that the strain rate in Hishikari was similar to that in southern Kyushu during mineralization.

Nevertheless, it is difficult to imagine that a basement uplift of at least 700 m (from the drillholes in NEDO, 1991) did not contribute anything to the mineralization. It could be responsible for the apparition of the axial compression under which 5% of the veins in Yamada were deposited. The mechanism through which this could happen is not

understood.

Also, the basement uplift could have contributed to weakening the rocks, allowing the fluids to fracture them more readily and precipitate gold-bearing veins. These hypotheses can be tested using the finite element method. A major difficulty to do so was related to the uncertainties on some aspects of the magmatic intrusion acting as the heat source (depth, overpressure, shape) that are critical to setup a realistic model. The second part of my study (Chapter 4) contributed to solving this problem by providing physical and geometric constraints on the heat source that can be used in future modeling attempts.

5.2 The probable causes of pressure compartmentalization

The pressure seals in Hishikari that led to pressure compartmentalization could result from the episodic veining process itself (Sanematsu et al., 2006). A fracture is progressively sealed as minerals precipitate, creating a pressure build-up that culminates in a subsequent fracturing of the deposited vein and follows another precipitation round (Cox, 2005). However, does this process necessarily lead to a positive correlation between driving pressure ratio and depth? Depth-dependent driving pressure ratios calculations in other epithermal deposits will clarify this question. If the answer is NO,

what was the factor in Hishikari that triggered the apparition of pressure seals?

The occurrence of overpressured compartments elsewhere in the earth crust is well known, especially in sedimentary basins hosting oil and gas resources. It usually has a sealing mechanism that creates low permeability zones at the boundaries of the compartments.

The first idea that comes in mind is the occurrence of lower permeability rocks that would act like sealing mechanisms to block the fluid flow and allow a pressure build-up in the pressure compartment. In Hishikari, the alteration zones immediately surrounding the veins are made of chlorite-illite zone and interstratified clay minerals zones (Murakami, 2008), that is clay-rich. However, the most argillaceous media have permeabilities greater than 10-20 m^2 (Neuzil, 1994), which doesn't allow them to maintain abnormal fluid pressures for 100 Ma (Deming, 1994). Nevertheless, for shorter time periods, it could be enough (Hishikari mineralization lasted 0.6 Ma).

Capillary gas sealing has been proposed as a suitable mechanism that has the advantage of accounting for the lateral sealing as well as achieving permeabilities low enough to maintain abnormal pressures by Revil et al. (1998). This could have occurred in Hishikari, especially considering the fact that boiling is recognized as a process that played a major role in the mineralization (Nagayama, 1993; Matsuhisa and Aoki, 1994;

Imai and Uto, 2002). It is known that boiling in epithermal environments releases gases, mostly CO_2 and H_2S. The trapping of these gases in the open spaces of the surrounding rocks by capillary forces could thus create momentary seals, allowing the fluid pressure to build up and maintain an abnormal level over a certain amount of time.

6. Conclusions

The main conclusions of this PhD thesis are summarized as follows:

- The mineralization is mainly controlled by regional tectonics with a stress state having a NW-SE-trending horizontal σ_3 axis and intermediate between normal faulting and strike-slip faulting regimes.
- A minor amount of veins was formed under an axial compression stress regime that appeared later than the main stress state.
- High-grade veins are associated with higher driving pressures, suggesting that fluid pressure controls gold grade.
- Pressure compartmentalization occurred during mineralization in Hishikari.
- The heat source was a ~9 km-deep likely prolate ellipsoidal magma chamber marked by a cooling trend from an onset temperature of ~1075-1200°C.
- The magma overpressure was high (6.5 MPa).

References

Abe, I., Suzuki, H., Isogami, A., Goto, T., 1986. Geology and development of the Hishikari mine. Min. Geol. 36, 117–130.

Anderson, E.M., 1942. The dynamics of faulting and dyke formation with applications to Britain. Oliver and Boyd, Edinburgh; London.

Anderson, J.L., Smith, D.R., 1995. The effects of temperature and fO2, on the Al-in-hornblende barometer. Am. Mineral. 80, 549–559. doi:10.1016/0031-9201(95)03018-R

Angelier, J., 1990. Inversion of field data in fault tectonics to obtain the regional stress-III. A new rapid direct inversion method by analytical means. Geophys. J. Int. 103, 363–376. doi:10.1111/j.1365-246X.1990.tb01777.x

Angelier, J., 1984. Tectonic analysis of fault slip data sets. J. Geophys. Res. Solid Earth 89, 5835–5848. doi:10.1029/JB089iB07p05835

Angelier, J., 1979. Determination of the mean principal directions of stresses for a given fault population. Tectonophysics 56, T17–T26. doi:10.1016/0040-1951(79)90081-7

Armijo, R., Carey, E., Cisternas, A., 1982. The inverse problem in microtectonics and the separation of tectonic phases. Tectonophysics 82, 145–160. doi:10.1016/0040-1951(82)90092-0

Baer, G., 1991. Mechanisms of dike propagation in layered rocks and in massive, porous sedimentary rocks. J. Geophys. Res. 96, 11911. doi:10.1029/91JB00844

Baer, G., Beyth, M., 1990. A mechanism of dyke segmentation in fractured host rock.

Baer, G., Beyth, M., Reches, Z., 1994. Dikes emplaced into fractured basement, Timna Igneous Complex, Israel. J. Geophys. Res. Solid Earth 99, 24039–24050. doi:10.1029/94JB02161

Borradaile, G., 2003. Statistics of Earth Science Data. Springer Berlin Heidelberg,

Berlin, Heidelberg. doi:10.1007/978-3-662-05223-5

Bott, M.H.P., 1959. The Mechanics of Oblique Slip Faulting. Geol. Mag. 96, 109–117. doi:10.1017/S0016756800059987

Böttcher, N., Watanabe, N., Gorke, U.-J., Kolditz, O., 2016. Geoenergy Modeling I: Geothermal Processes in Fractured Porous Media.

Brace, W.F., Kohlstedt, D.L., 1980. Limits on lithospheric stress imposed by laboratory experiments. J. Geophys. Res. Solid Earth 85, 6248–6252. doi:10.1029/JB085iB11p06248

Carey, M.E., Brunier, M.B., 1974. Analyse theorique et numerique d'un modele mecanique elementaire applique a l'etude d'une population de failles. C. R. Hebd. Seances Acad. Sci. 279, 891–894.

Chi, G., Xue, C., 2011. An overview of hydrodynamic studies of mineralization. Geosci. Front. 2, 423–438. doi:10.1016/j.gsf.2011.05.001

Cox, S.., Etheridge, M.., 1989. Coupled grain-scale dilatancy and mass transfer during deformation at high fluid pressures: examples from Mount Lyell, Tasmania. J. Struct. Geol. 11, 147–162. doi:10.1016/0191-8141(89)90040-0

Cox, S.F., 2005. Coupling between deformation, fluid pressures, and fluid flow in ore-producing hydrothermal systems at depth in the crust, Economic Geology 100th Anniversary Volume.

Delaney, P.T., Pollard, D.D., Ziony, J.I., McKee, E.H., 1986. Field relations between dikes and joints: Emplacement processes and paleostress analysis. J. Geophys. Res. 91, 4920–4938. doi:10.1029/JB091iB05p04920

Della Vedova, B., Vecellio, C., Bellani, S., Tinivella, U., 2008. Thermal modelling of the Larderello geothermal field (Tuscany, Italy). Int. J. Earth Sci. 97, 317–332. doi:10.1007/s00531-007-0249-0

Deming, D., 1994. Fluid flow and heat transport in the upper continental crust, in: Parnell, J. (Ed.), Geofluids: Origin, Migra Tion and Evolution of Fluids in

SedimentaryBasins. Geological Society Special Publications, pp. 27–42.

Ellis, S.M., Wilson, C.J.N., Bannister, S., Bibby, H.M., Heise, W., Wallace, L., Patterson, N., 2007. A future magma inflation event under the rhyolitic Taupo volcano, New Zealand: Numerical models based on constraints from geochemical, geological, and geophysical data. J. Volcanol. Geotherm. Res. 168, 1–27. doi:10.1016/j.jvolgeores.2007.06.004

Etoh, J., 2002. Fluid Inclusion Study on Boiling Phenomena in Hydrothermal Systems with Reference to Gold Mineralization of the Hishikari Deposit. Kyushu University.

Etoh, J., Izawa, E., Taguchi, S., 2002. A Fluid Inclusion Study on Columnar Adularia from the Hishikari Low - Sulfidation Epithermal Gold Deposit, Japan. Resour. Geol. 52, 73–78.

Francis, P., 1993. Volcanoes: a planetary perspecive. Calrendon Press; New York: Oxford University Press, Oxford.

Goetze, C., Evans, B., 1979. Stress and temperature in the bending lithosphere as constrained by experimental rock mechanics. Geophys. J. Int. 59, 463–478. doi:10.1111/j.1365-246X.1979.tb02567.x

Goldberg, D.E., 1989. Genetic Algorithms in Search, Optimization, and Machine Learning. Addison-Wesley.

Gudmundsson, A., 2011. Extension fractures and shear frractures, in: Rock Fractures in Geological Processes. Cambridge University Press, pp. 233–254. doi:10.1017/CBO9780511975684

Gudmundsson, A., 2002. Emplacement and arrest of sheets and dykes in central volcanoes. J. Volcanol. Geotherm. Res. 116, 279–298. doi:10.1016/S0377-0273(02)00226-3

Gudmundsson, A., 1998a. Formation and development of normal-fault calderas and the initiation of large explosive eruptions. Bull. Volcanol. 60, 160–170. doi:10.1007/s004450050224

Gudmundsson, A., 1998b. Magma chambers modeled as cavities explain the formation of rift zone central volcanoes and their eruption and intrusion statistics. J. Geophys. Res. Solid Earth 103, 7401–7412. doi:10.1029/97JB03747

Gudmundsson, A., Nilsen, K., 2006. Structures , models , and stress fields of ring faults in composite volcanoes 1–32.

Hammarstrom, J.M., Zen, E., 1986. Aluminum in hornblende: an empirical igneous geobarometer. Am. Mineral. 71, 1297–1313.

Hedenquist, J.W., Henley, R.W., 1985. Hydrothermal eruptions in the Waiotapu geothermal system, New Zealand; their origin, associated breccias, and relation to precious metal mineralization. Econ. Geol. 80, 1640–1668. doi:10.2113/gsecongeo.80.6.1640

Hedenquist, J.W., Lowenstern, J.B., 1994. The role of magmas in the formation of hydrothermal ore deposits. Nature 370, 519–527. doi:10.1038/370519a0

Hikichi, G., Yamaji, A., 2008. Palaeostress analysis in metallogenic areas: the case of the Nagano area, southern Kyushu, Japan. J. Geol. Soc. Japan 114, 540–545. doi:10.5575/geosoc.114.540

Hobbs, B.., Zhang, Y., Ord, A., Zhao, C., 2000. Application of coupled deformation, fluid flow, thermal and chemical modelling to predictive mineral exploration. J. Geochemical Explor. 69–70, 505–509. doi:10.1016/S0375-6742(00)00099-6

Honza, E., Fujioka, K., 2004. Formation of arcs and backarc basins inferred from the tectonic evolution of Southeast Asia since the Late Cretaceous. Tectonophysics 384, 23–53. doi:10.1016/j.tecto.2004.02.006

Hosono, T., Nakano, T., 2003. Petrochemistry of volcanic rocks in the Hishikari mining area of southern Japan, with implications for the relative contribution of lower crust and mantle-derived basalt. Resour. Geol. 53, 239–259. doi:10.1111/j.1751-3928.2003.tb00174.x

Ibaraki, K., Suzuki, R., 1993. Gold-silver quartz-adularia veins of the Main, Yamada

and Sanjin deposits, Hishikari Gold Mine; a comparative study of their geology and ore deposits, in: Shikazono, N., Izawa, E., Naito, K. (Eds.), High Grade Epithermal Gold Mineralization : The Hishikari Deposit. The Society of Resource Geology, Tokyo, pp. 1–11.

Imai, A., Uto, T., 2002. Association of Electrum and Calcite and Its Significance to the Genesis of the Hishikari Gold Deposits, Southern Kyushu, Japan. Resour. Geol. 52, 381–394. doi:10.1111/j.1751-3928.2002.tb00148.x

Izawa, E., 2004. The distribution map of volcanic rock and gold deposit in Hokusatsu. Chishitsu News 599.

Izawa, E., Kurihara, M., Itaya, T., 1993a. K-Ar Ages and the initial Ar isotopic ratio of adularia-quartz veins from the Hishikari gold deposit, Japan, in: Shikazono, N., Izawa, E., Naito, K. (Eds.), High Grade Epithermal Gold Mineralization : The Hishikari Deposit. The Society of Resource Geology, Tokyo, pp. 63–69.

Izawa, E., Naito, K., Ibaraki, K., Suzuki, R., 1993b. Mudstones in a Hydrothermal Eruption Crater above the Gold-bearing Vein system of the Yamada Deposit at Hishikari, Japan, in: Shikazono, N., Izawa, E., Naito, K. (Eds.), High Grade Epithermal Gold Mineralization : The Hishikari Deposit. The Society of Resource Geology, Tokyo, pp. 85–92.

Izawa, E., Urashima, Y., Ibaraki, K., Suzuki, R., Yokoyama, T., Kawasaki, K., Koga, A., Taguchi, S., 1990. The Hishikari gold deposit: high-grade epithermal veins in Quaternary volcanics of southern Kyushu, Japan. J. Geochemical Explor. 36, 1–56. doi:10.1016/0375-6742(90)90050-K

Izawa, E., Watanabe, K., 2001. Overview of Epithermal Gold Mineralization in Kyushu, Japan, in: Feebrey, C.A., Hayashi, T., Taguchi, S. (Eds.), Epithermal Gold Mineralization and Modern Analogues, Kyushu, Japan. Society of Economic Geologists, pp. 11–15.

Jolly, R.J.H., Sanderson, D.J., 1997. A Mohr circle construction for the opening of a pre-existing fracture. J. Struct. Geol. 19, 887–892. doi:10.1016/S0191-8141(97)00014-X

Kagiyama, T., 1994. Kirishima Volcanoes-Multi active volcanic group generated in a slightly tensile stress field. J. Geog. 103, 479–487.

Koide, H., Bhattacharji, S., 1975. Formation of fractures around magmatic intrusions and their role in ore localization. Econ. Geol. 70, 781–799. doi:10.2113/gsecongeo.70.4.781

Kolditz, O., Görke, U., Shao, H., Wang, W., Bauer, S., 2015. Thermo-hydro-mechanical- chemical processes in fractured porous media: Modelling and benchmarking. Benchmarking initiatives, Terrestrial Environmental Sciences. doi:10.1007/978-3-319-29224-3

Lahiri, S., Mamtani, M.A., 2016. Scaling the 3-D Mohr circle and quantification of paleostress during fluid pressure fluctuation – Application to understand gold mineralization in quartz veins of Gadag (southern India). J. Struct. Geol. 88, 63–72. doi:10.1016/j.jsg.2016.05.003

Mannington, W., O'Sullivan, M., Bullivant, D., 2004. Computer modelling of the Wairakei–Tauhara geothermal system, New Zealand. Geothermics 33, 401–419. doi:10.1016/j.geothermics.2003.09.009

Matsuhisa, Y., Aoki, M., 1994. Temperature and oxygen isotope variations during formation of the Hishikari epithermal gold-silver veins, southern Kyushu, Japan. Econ. Geol. 89, 1608–1613. doi:10.2113/gsecongeo.89.7.1608

Matsumoto, S., Nakao, S., Ohkura, T., Miyazaki, M., Shimizu, H., Abe, Y., Inoue, H., Nakamoto, M., Yoshikawa, S., Yamashita, Y., 2015. Spatial heterogeneities in tectonic stress in Kyushu, Japan and their relation to a major shear zone. Earth, Planets Sp. 67, 172. doi:10.1186/s40623-015-0342-8

Matsutoya, S., 1967. Structural Features of Kushikino Mine and its Relation to the Regional Geologic Structure of Southwestern Kyushu. Min. Geol. 17, 139–150. doi:10.11456/shigenchishitsu1951.17.139

MITI, 2001. Report on the regional geological structure survey inthe Hokusatsu-Kushikino area in the fiscal year Heisei 12 (in Japanese).

Mogi, K., 1958. Relations between eruptions of various volcanoes and the deformations of the ground surfaces around them. Bull. Earthq. Res. Inst. 36, 99–134.

Morishita, Y., Kodama, K., 1986. Simulation analysis of the gold–quartz vein systems in the Kushikino mine area, southern Kyushu, Japan. Min. Geol. 36.

Morishita, Y., Nakano, T., 2008. Role of basement in epithermal deposits: The Kushikino and Hishikari gold deposits, southwestern Japan. Ore Geol. Rev. 34, 597–609. doi:10.1016/j.oregeorev.2008.09.009

Murakami, H., 2008. Variations in Chemical Composition of Clay Minerals and Magnetic Susceptibility of Hydrothermally Altered Rocks in the Hishikari Epithermal Gold Deposit, SW Kyushu, Japan. Resour. Geol. 58, 1–24. doi:10.1111/j.1751-3928.2007.00041.x

Muto, N., 1952. On the Systematic Arrangement of Veins at the Fuke Gold Mine, Kagoshima Prefecture. Min. Geol. 2, 49–53. doi:10.11456/shigenchishitsu1951.2.49

Nagayama, T., 1993. Precipitation sequence of veins at Hishikari deposits, Kyushu, Japan, in: Shikazono, N., Izawa, E., Naito, K. (Eds.), High Grade Epithermal Gold Mineralization : The Hishikari Deposit. The Society of Resource Geology, Tokyo, pp. 13–27.

Naito, K., 1993. Occurrences of quartz veins in the Hishikari gold deposits, southern Kyushu, Japan, in: Shikazono, N., Izawa, E., Naito, K. (Eds.), High Grade Epithermal Gold Mineralization : The Hishikari Deposit. The Society of Resource Geology, Tokyo, pp. 37–46.

Nakamura, K., 1977. Volcanoes as possible indicators of tectonic stress orientation — principle and proposal. J. Volcanol. Geotherm. Res. 2, 1–16. doi:10.1016/0377-0273(77)90012-9

NEDO, 1991. Geothermal development promotion research report No25-Hikoshi area (In Japanese).

Neuzil, C.E., 1994. How permeable are clays and shales? Water Resour. Res. 30, 145–150. doi:10.1029/93WR02930

Otsubo, M., Yamaji, A., 2006. Improved resolution of the multiple inverse method by eliminating erroneous solutions. Comput. Geosci. 32, 1221–1227. doi:10.1016/j.cageo.2005.10.022

Pan, E., Amadei, B., Savage, W.Z., 1994. Gravitational stresses in long symmetric ridges and valleys in anisotropic rock. Int. J. Rock Mech. Min. Sci. 31, 293–312. doi:10.1016/0148-9062(94)90899-0

Pollard, D.D., Muller, O.H., Dockstader, D.R., 1975. The Form and Growth of Fingered Sheet Intrusions. Geol. Soc. Am. Bull. 86, 351. doi:10.1130/0016-7606(1975)86<351:TFAGOF>2.0.CO;2

Revil, A., Cathles, L.M., Shosa, J.D., Pezard, P.A., de Larouzière, F.D., 1998. Capillary sealing in sedimentary basins: A clear field example. Geophys. Res. Lett. 25, 389–392. doi:10.1029/97GL03775

Sanematsu, K., 2007. Geochronological and Mineralogical Studies on Adularia-Quartz Veins in the Hishikari Epithermal Gold Deposit, Japan. Kyushu University.

Sanematsu, K., Duncan, R., Imai, A., Watanabe, K., 2005. Geochronological Constraints Using 40 Ar/ 39 Ar Dating on the Mineralization of the Hishikari Epithermal Gold Deposit, Japan. Resour. Geol. 55, 249–266. doi:10.1111/j.1751-3928.2005.tb00246.x

Sanematsu, K., Watanabe, K., Duncan, R.A., Izawa, E., 2006. The History of vein formation determined by 40Ar/39Ar dating of adularia inthe Hosen-1 vein at the Hishikari epithermal gold deposit, Japan. Econ. Geol. 101, 685–698. doi:10.2113/gsecongeo.101.3.685

Sasada, M., 2000. Igneous-related active geothermal system versus porphyry copper hydrothermal system. Proc. World Geotherm. Congr. 6, 1691–1693.

Sato, K., Yamaji, A., 2006. Uniform distribution of points on a hypersphere for

improving the resolution of stress tensor inversion. J. Struct. Geol. 28, 972–979. doi:10.1016/j.jsg.2006.03.007

Sato, K., Yamaji, A., Tonai, S., 2013. Parametric and non-parametric statistical approaches to the determination of paleostress from dilatant fractures: Application to an Early Miocene dike swarm in central Japan. Tectonophysics 588, 69–81. doi:10.1016/j.tecto.2012.12.008

Sekine, R., 2002. Timing of fracture formation and duration of hydrothermal activity at the Hishikari gold deposit, southern Kyushu, Japan. Kyushu University.

Sekine, R., Izawa, E., Watanabe, K., 2002. Timing of Fracture Formation and Duration of Mineralization at the Hishikari Deposit, Southern Kyushu, Japan. Resour. Geol. 52, 395–404. doi:10.1111/j.1751-3928.2002.tb00149.x

Sibuet, J.-C., Hsu, S.-K., Shyu, C.-T., Liu, C.-S., 1995. Structural and Kinematic Evolutions of the Okinawa Trough Backarc Basin, in: Backarc Basins. Springer US, Boston, MA, pp. 343–379. doi:10.1007/978-1-4615-1843-3_9

Sillitoe, R.H., 2015. Epithermal paleosurfaces. Miner. Depos. 50, 767–793. doi:10.1007/s00126-015-0614-z

Sillitoe, R.H., Hedenquist, J.W., 2003. Linkages between Volcanotectonic Settings , Ore-Fluid Compositions , and Epithermal Precious Metal Deposits. Soc. Econ. Geol. - Spec. Publ. 10, 315–343. doi:10:315-343

Simmons, S.F., White, N.C., John, D., 2005. Geological characteristics of epithermal precious and base metal deposits. Econ. Geol. 100th Anniv. Vol. 485–522.

Takahashi, R., Tagiri, R., Blamey, N.J.F., Imai, A., Watanabe, Y., Takeuchi, A., 2017. Characteristics and Behavior of Hydrothermal Fluids for Gold Mineralization at the Hishikari Deposits, Kyushu, Japan. Resour. Geol. 67, 279–299. doi:10.1111/rge.12136

Tanaka, H., 1999. Circular asymmetry of the paleomagnetic directions observed at low latitude volcanic sites. Earth, Planets Sp. 51, 1279–1286. doi:10.1186/BF03351601

Tohma, Y., Imai, A., Sanematsu, K., Yonezu, K., Takahashi, R., Koyama, M., Sekine, R., Duncan, R., Watanabe, K., 2010. Characteristics and Mineralization Age of the Fukusen No. 1 Vein, Hishikari Epithermal Gold Deposits, Southern Kyushu, Japan. Resour. Geol. 60, 348–358. doi:10.1111/j.1751-3928.2010.00140.x

Turcotte, D.L., Schubert, G., 2014. Geodynamics, Third. ed. Cambridge University Press, Cambridge.

Uchimura, K., Kano, K., Oki, K., 2014. Quaternary deposits in Kagoshima Rift. J. Geol. Soc. Japan 120, S127–S153. doi:10.5575/geosoc.2014.0017

Urashima, Y., Ikeda, T., 1987. K-Ar ages for adularia from the Fuke, Okuchi, Hishikari, Kuronita, and Hanakago gold-silver deposits, Kagoshima Prefecture, Japan. Min. Geol. 37, 205–213 (in Japanese with English abstract).

Urashima, Y., Saito, M., Sato, E., 1981. The Iwato gold ore deposits, Kagoshima Prefecture, Japan. Min. Geol. Spec. Issue No 10. 1–14 (In Japanese with english abstract).

Uto, T., Imai, A., Yamato, Y., 2001. Horizontal Strain Rate in Relation to Vein Formation of the Hishikari Gold Deposits, Southern Kyushu, Japan. Resour. Geol. 51, 7–18. doi:10.1111/j.1751-3928.2001.tb00077.x

Wallace, R.E., 1951. Geometry of Shearing Stress and Relation to Faulting. J. Geol. 59, 118–130. doi:10.1086/625831

Waples, D.W., Waples, J.S., 2004. A Review and Evaluation of Specific Heat Capacities of Rocks, Minerals, and Subsurface Fluids. Part 1: Minerals and Nonporous Rocks. Nat. Resour. Res. 13, 97–122. doi:10.1023/B:NARR.0000032647.41046.e7

Watanabe, N., Kunz, H., Kolditz, O., 2012. Hydrothermal modeling of a deep geothermal reservoir including a hydraulic fracture.

Yamaji, A., 2016. Genetic algorithm for fitting a mixed Bingham distribution to 3D orientations: a tool for the statistical and paleostress analyses of fracture orientations. Isl. Arc 25, 72–83. doi:10.1111/iar.12135

Yamaji, A., 2003. Slab rollback suggested by latest Miocene to Pliocene forearc stress and migration of volcanic front in southern Kyushu, northern Ryukyu Arc. Tectonophysics 364, 9–24. doi:10.1016/S0040-1951(03)00047-7

Yamaji, A., 2000. The multiple inverse method: a new technique to separate stresses from heterogeneous fault-slip data. J. Struct. Geol. 22, 441–452. doi:10.1016/S0191-8141(99)00163-7

Yamaji, A., Hase, Y., Torii, M., 2003. Paleostresses inferred from mesoscale faults in the Late Pliocene Hitoyoshi Formation; implications for the formation of vein-type ore deposits in southern Kyushu. Shigen-Chishitsu 53, 217–225. doi:10.11456/shigenchishitsu1992.53.217

Yamaji, A., Sato, K., 2011. Clustering of fracture orientations using a mixed Bingham distribution and its application to paleostress analysis from dike or vein orientations. J. Struct. Geol. 33, 1148–1157. doi:10.1016/j.jsg.2011.05.006

Yamaji, A., Sato, K., 2006. Distances for the solutions of stress tensor inversion in relation to misfit angles that accompany the solutions. Geophys. J. Int. 167, 933–942. doi:10.1111/j.1365-246X.2006.03188.x

Yamaji, A., Sato, K., n.d. Stress inversion meets plasticity theory: a review of the theory of the inversion with emphasis on the coordinate invariance of its formulation. J. Struct. Geol.

Yamaji, A., Sato, K., Tonai, S., 2010. Stochastic modeling for the stress inversion of vein orientations: Paleostress analysis of Pliocene epithermal veins in southwestern Kyushu, Japan. J. Struct. Geol. 32, 1137–1146. doi:10.1016/j.jsg.2010.07.001

Zachariáš, J., 2016. Structural evolution of the Mokrsko-West, Mokrsko-East and Čelina gold deposits, Bohemian Massif, Czech Republic: Role of fluid overpressure. Ore Geol. Rev. 74, 170–195. doi:10.1016/j.oregeorev.2015.11.027

Žalohar, J., Vrabec, M., 2007. Paleostress analysis of heterogeneous fault-slip data: The Gauss method. J. Struct. Geol. 29, 1798–1810.doi:10.1016/j.jsg.2007.06.009